Creep Fatigue Crack Growth Behavior of Wrought and Additive Manufactured IN718 at Elevated Temperature

A Thesis

Presented in Partial Fulfillment of the Requirements for the

Degree of Master of Science

with a

Major in Mechanical Engineering

in the

College of Graduate Studies

University of Idaho

By

Cody J. Gibson

Approved by:

Major Professor: Robert Stephens, Ph.D.

Committee Members: Gabriel Potirniche, Ph.D.; Michael Maughan, Ph.D.

Department Chair: Gabriel Potirniche, Ph.D.

December 2021

ABSTRACT

This study focuses on the fatigue crack growth, creep fatigue crack growth, and creep crack growth behavior of wrought and additive manufactured IN718 at 600^{o}C. Task Group on Elevated Temperature Crack Growth (E08.06.05) initiated a round robin, ASTM Interlaboratory Study Program (ILS) assigned program number 1679, in validation of ASTM Standard E2760 using wrought IN718 compact tension specimens which were tested under fatigue crack growth and creep fatigue crack growth conditions with hold times of 0, 60 and 600 seconds. The study showed that for a hold time of 60s to an infinite hold time crack growth rate was independent of number of applied cycles and dependent on time. Additive manufactured (AM) compact tension specimens were also tested under similar conditions. The AM specimens were machined in three different orientations with respect to build direction and the results showed anisotropic behavior. Wrought and AM IN718 crack growth rates were compared and showed that for lower values of stress intensity the AM IN718 had lower crack growth rates but at higher values of stress intensity the AM IN718 material exhibited higher crack growth rates than the wrought IN718. Fracture surface analysis of wrought IN718 shows a transition from transgranular to intergranular fracture mode from the pre-crack to the creep fatigue crack growth region. The fracture surface of the various AM IN718 orientations did not resemble the fracture surface of the wrought IN718.

ACKNOWLEDGEMENTS

Throughout the writing of this thesis, I have received a great deal of support and assistance. I would first like to thank my major professor Dr. Robert Stephens for all of the help and guidance as a mentor. I couldn't have asked for a better professor to help guide me during my time at the University of Idaho. I would also like to extend my appreciation to my other committee members, Dr. Gabriel Potirniche and Dr. Michael Maughan for their support during my master's program.

I would also like to acknowledge my colleagues, Anthony DeSantis, and Michael Myers, who assisted me during the research process. The time spent with them both inside and outside of the lab has made my time at the University of Idaho a phenomenal experience.

The author is grateful to the ASTM Task Group on Elevated Temperature Crack Growth (E08.06.05) for allowing me to participate in the ILS 1679 round robin. A special thanks to Dr. Santosh Narasimhachary with the Siemens Corporation for his insight and expertise as I was testing IN718.

Finally, I would like to thank my father Byron and grandfather Harold for their guidance and wisdom as I worked my way through my undergraduate and graduate programs. I truly wouldn't have made it as far as I have without them.

TABLE OF CONTENTS

LIST OF FIGURES

LIST OF TABLES

NOMENCLATURE

a	crack length
AM	Additive manufacturing
B	Specimen thickness
B_n	Net specimen thickness
COD	Crack opening displacement
ASTM	American Society of Testing Materials
CCG	Creep crack growth
CFCG	Creep fatigue crack growth
C(T)	Compact tension specimen
da/dN	Fatigue crack growth rate
da/dt	Time rate of crack growth
DCPD	Direct current potential drop
DE	Dynamic Embrittlement
EPD	Electric potential difference
FCG	Fatigue crack growth
ILS	Interlaboratory Study Program
IN718	Inconel-718
LEFM	Linear elastic fracture mechanics
LLD	Load line displacement
K	Stress intensity
K_{max}	Maximum stress intensity
K_{min}	Minimum stress intensity
ΔK	Stress intensity range
N	Number of applied cycles
P	Applied load
P_{max}	Maximum applied load
P_{min}	Maximum applied load
R	Stress ratio (ratio of minimum to maximum load)
SAGBO	Stress accelerated grain boundary oxidation

SEN	Single edge notch specimen
SEM	Scanning electron microscope
SLM	Selective laser melting
t	specimen thickness
ΔV_c	Change in load line displacement
W	specimen width
σ_{ys}	Yield strength

1. INTRODUCTION

Components used in high temperature environments such as disks in gas turbine engines can begin to develop cracks in high stress areas over time. To better understand the response of a crack in a high stress and temperature environment the American Society for Testing Materials (ASTM) Task Group on Elevated Temperature Crack Growth (E08.06.05) initiated a round robin, ASTM Interlaboratory Study Program (ILS) assigned program number 1679, to test a creep brittle material, Inconel-718 (IN718), in validation of Standard Test Method for Creep-Fatigue Crack Growth E2760. Compact tension C(T) specimens machined from disk forgings were used to conduct tests under fatigue crack growth (FCG) and creep fatigue crack growth (CFCG) conditions with hold times of 0, 60 and 600 seconds. After completion of the ILS 1679 round robin single edge notch (SEN) specimens were machined from the broken halves of C(T) specimens and tested under the same temperature and hold times but at a different initial stress intensity range.

An additional study was conducted using additive manufactured (AM) IN718 in partnership with Dr. Santosh Narasimhachary from Siemens Corporation, Technology Division. Selective laser melted IN718 blocks were manufactured in two different print orientations. C(T) specimens were machined from the AM blocks with the notches oriented parallel to and normal to the build direction respectively. Print orientation and C(T) machining orientation is covered in more detail in Section 3. The AM IN718 specimens were tested under FCG and CFCG conditions with hold times of 0, 60 and 600 seconds. The same temperature and load ratio used in ILS 1679 were used in testing of the AM IN718 specimens for direct comparison with the wrought IN718 specimens. After completion of testing, crack growth rates with respect to cycle and with respect to time were compared between the different AM print orientations. Comparison was also made between the wrought and AM IN718. Fractographic analysis was conducted using a scanning electron microscope to determine the different modes of crack growth (transgranular or intergranular) during the different hold times.

2. LITERATURE REVIEW

2.1 Fracture Mechanics

Linear elastic fracture mechanics (LEFM) is a method used to determine crack growth in a component assuming that the component material has linear elastic behavior while being fatigued [1]. To better understand crack growth under fatigue three modes of loading are shown in Figure 2.1. Mode I is the opening mode and is the most common mode where the crack plane is perpendicular to the direction of loading. Mode II and Mode III are shearing modes where Mode II is in-plane and Mode III is anti-plane [1]. A combination of modes (I, II, III) fall under mixed mode cracking but will not be discussed in this paper. Mode I is the most common and most studied, and it will be the primary focus in this study.

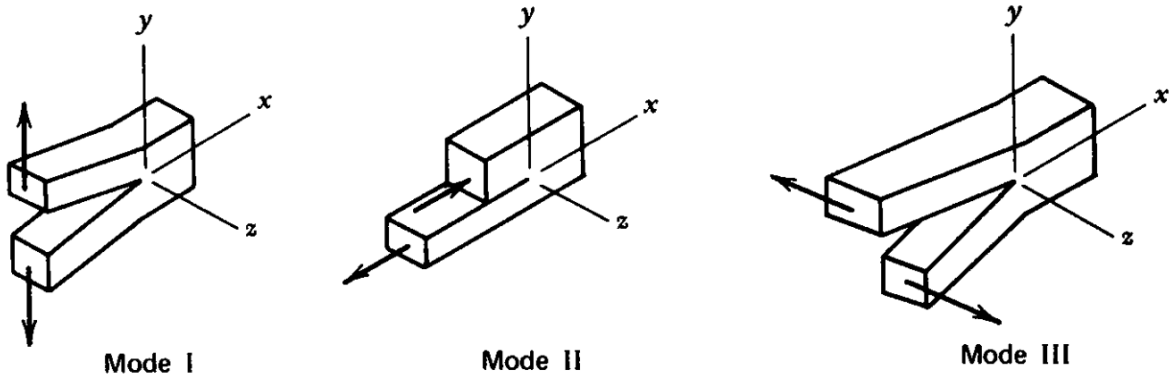

Figure 2. 1: Three basic modes of loading [1].

Under a given loading mode LEFM can be used to evaluate the strength of a structural component in the presence of a crack or flaw. In the early 1900's Griffith conducted tensile strength experiments with glass specimens and observed a large difference between the theoretical strength and experimental values which he attributed to small flaws in the material [12]. To test the theory Griffith conducted several experiments using glass which behaves as an elastic material up until the point of failure. Griffith was able to develop an equation to determine crack growth by relating the square root of crack length to the far field stress and material properties of glass [1]. Griffith's equation was later modified by Irwin who related the energy release rate, G, to stress intensity factor, K, which he used to quantify the driving force

at the tip of a crack in metals. The general form of the stress intensity factor K for mode I is shown in equation 2.1

$$K = S\sqrt{\pi a}F(a/W) \tag{2.1}$$

For the compact tension C(T) specimen geometry used in this study, the stress intensity factor K is represented by equation 2.2.

$$K = \frac{P}{(BB_N)^{1/2}W^{1/2}}F(a/W) \tag{2.2}$$

$F(a/W)$, is given by

$$F\left(a/W\right) = \left[\frac{2+a/W}{\left(1-a/W\right)^{3/2}}\right]\left(0.886 + 4.64\left(a/W\right) - 13.32\left(a/W\right)^2 + 14.72\left(a/W\right)^3 - 5.6\left(a/W\right)^4\right) \tag{2.3}$$

where a is the crack length, W is the specimen width, B = B_n which is the thickness when no side grooving is performed, and P is the applied load. To report FCG data the standard method used compares the change in crack length per cycle (da/dN) where N is cycles, to the change in stress intensity, ΔK, where ΔK = (K_{max} - K_{min}). K_{max} is the maximum stress intensity and K_{min} is minimum stress intensity during a given cycle.

For testing at room temperature or at elevated temperature, crack length measurements are most often determined using electric potential difference (EPD) in either AC or DC, crack opening displacement (COD) compliance, or visual measurements. By method of EPD, the known initial and final crack length are used to determine instantaneous crack extensions using equation 2.5 [3].

$$a = a_0 + \left(a_f - a_0\right) \times \frac{V - V_0}{V_f - V_0} \tag{2.5}$$

Where a_f , a_0 , a are the final, initial, and instantaneous crack lengths, respectively and V_f , V_0 and V are the corresponding final, initial and instantaneous value of the DCPD voltage. Due to

noise in the DCPD system, the secant method or polynomial method data reduction techniques are recommended for reporting data [4].

Another mode of crack growth at elevated temperature can be seen under varying hold times. This time-dependent crack growth phenomenon is known as creep. Under creep crack growth (CCG) and creep fatigue crack growth (CFCG) conditions, a complex interaction of deformation due to creep and/or plasticity, oxygen diffusion rates, oxidation reactions at grain boundaries and the influence of loading history and/or geometry result in crack propagation [5-6]. CCG is purely time dependent where CFCG has a combination of time dependence and cycle dependence. There can be a point however that when a hold time becomes long enough, the effects of fatigue become negligible, and the primary mode of crack propagation is time dependent [6]. Under CFCG and CCG vs. FCG, the crack growth mechanism often transitions from transgranular (through grain) to intergranular (along the grain boundary).

2.2 Wrought IN718

Nickel base super alloys like IN718 exhibit excellent mechanical properties at elevated temperatures which is why they have often been the material of choice for gas turbine engine applications [5]. Like other superalloys IN718 is precipitation hardened and because of the high amount of iron content it contains both coherent γ' and γ'' particles in the γ matrix. The γ phase is the matrix phase and has a face-centered cubic crystal structure while the γ' is usually the main strengthening precipitate and can make up more than 50% of the volume of the material [7]. A δ phase which is a non-hardening precipitate can also be found in IN718 at the grain boundaries and is typically composed of Ti, Nb, and Ni [11].

When used in gas turbine engine applications the main load cycle begins during startup of the engine, and the cycle ends when the engine is shut down. Because of the long hold times at high temperature during the engine cycle the crack growth rate is increased and is often not related to number of engine cycles. This translates to two different fracture modes during a given cycle as suggested previously. For purely cyclic tests the fracture mode is usually transgranular and for the hold time tests the fracture mode is usually intergranular [7]. To better understand the crack growth behavior during hold times at elevated temperatures, Gustafsson *et al.* conducted experiments at 550^{o}C and 650^{o}C under CCG and CFCG conditions with 90s and 2160s hold times. In Figure 2.2 Gustafsson *et al.* shows the da/dt vs K_{hold} behavior of IN718

for given hold times at 550ºC and 650ºC [8]. da/dt is the time rate of crack growth where da/dt is the change in crack length per change in time.

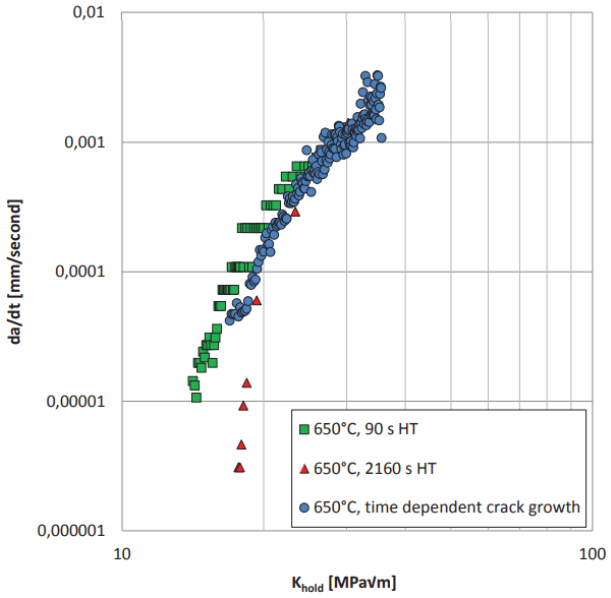

Figure 2. 2: da/dt vs K_{hold} for HT tests at 650ºC [8]

Gustafsson *et al.* showed in Figure 2.2 that when plotting the hold time tests as da/dt vs K_{hold} the pure time dependent tests and hold time tests converged on the same level of da/dt. Thus, crack growth is primarily time dependent and can be described by a creep crack growth model. He proposed two mechanisms to explain crack propagation under hold times; stress accelerated grain boundary oxidation (SAGBO) and dynamic embrittlement (DE).

SAGBO is the combination of high tensile stress and high temperature which facilitate the ingress of oxygen by grain boundary diffusion and can be followed by grain boundary oxidation leading to intergranular fracture at formed oxides at the crack tip exposing new surfaces to oxygen [5,7]. The second theory also explains oxygen induced intergranular fracture but differs by not requiring the formation of oxides. The theory of DE involves diffusion of an absorbed element into a grain boundary when under a tensile stress which can lower the cohesion of the atomic bonds causing failure due to the tensile load [5,7]. In Figure 2.3 the theory of DE is shown and explained with a schematic.

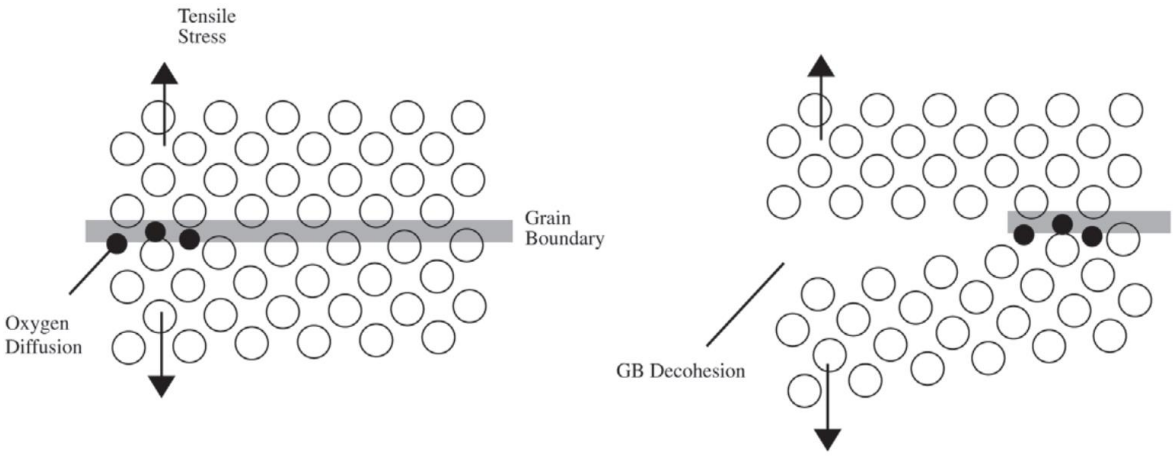

Figure 2. 3: Schematic representation of the dynamic embrittlement mechanism [5].

To better understand time dependent oxygen induced intergranular fracture, Krupp conducted fixed displacement loading tests using IN718 SENB specimens at 650^{o}C inside a high vacuum chamber. During fast cracking, Krupp pumped the chamber for a short time to a high vacuum of $<10^{-4}$ Torr then back filled the chamber with oxygen. By doing this, Krupp was able to stop crack growth during the vacuum period and then start crack growth again with the addition of oxygen. The resultant load vs time curve with vacuum period is shown in Figure 2.4. The change in the load vs time curve shows the effect of oxygen on crack growth rate at elevated temperature. When fracturing at room temperature Krupp observed a preserved portion of the crack tip that had not yet been covered by oxidation products like the grain boundaries further back on the fracture surface. This showed that the crack growth was independent of oxides and that DE was the main driver of intergranular crack growth. Though Krupp showed that DE was the primary mechanism for intergranular crack growth, other research shows that in a different environment with different nominal grain sizes, the mode of intergranular crack growth can be a combination of both oxygen induced intergranular fracture theories [7].

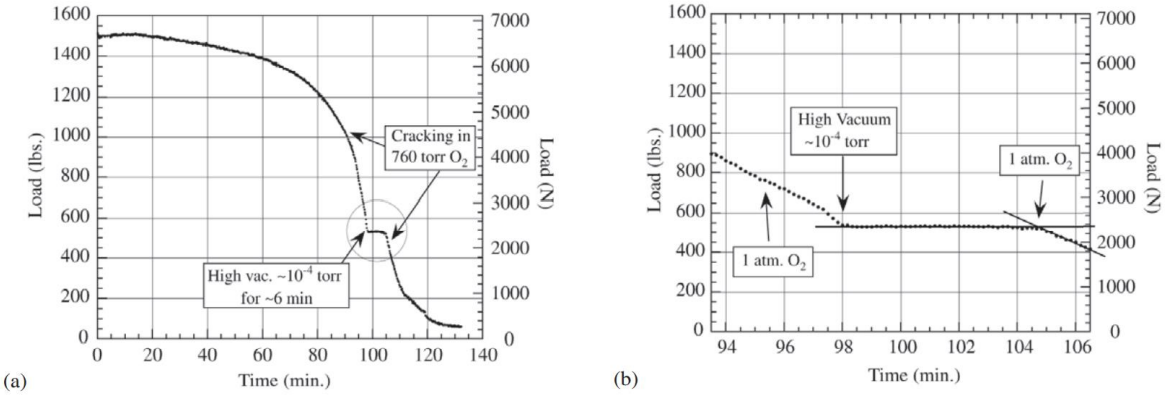

Figure 2. 4: a) Cracking of an IN718 4point-bending specimen (with fatigue pre-crack) under fixed displacement loading at 650°C interrupted by evacuating the chamber, b) shows detail of a) [5].

2.3 Additive Manufactured (AM) IN718

From ASTM Standard F2792, additive manufacturing (AM) processes are separated into seven categories [9]. In these seven categories material is either selectively dispensed, deposited, fused, or bonded to join layers of material to create a desired geometry, part, or component. Direct energy deposition (DED), powder bed fusion (PBF), and selective laser melting (SLM) are some of the common AM processes used in creating parts and components. As the technology regarding AM has improved significantly over the last 30 years, its use and application have expanded the restrictions of design engineers compared to traditional methods. AM has allowed a greater range of components to be produced as a single part, often reducing the material required and the need for joining through methods such as welding, fasteners, etc. For example, the RS-25 Pogo Z-Baffle using AM reduced the number of welds from 127 to just 4 [10].

Where IN718 is a common material used in gas turbine engines as stated in Section 2.1, understanding the FCG, CFCG, and CCG behavior of AM IN718 at elevated temperatures is critical. To better understand the material characteristics of AM IN718, Deng *et al.* conducted CFCG tests under a 2160s hold time at 550°C and compared two different specimen orientations with respect to build direction and three different heat treatments [11]. The specimen orientations with respect to build direction and microstructures post heat treatments from Deng *et al*. are shown in Figure 2.5 and Figure 2.6 and heat treatment details are shown in Table 2.1.

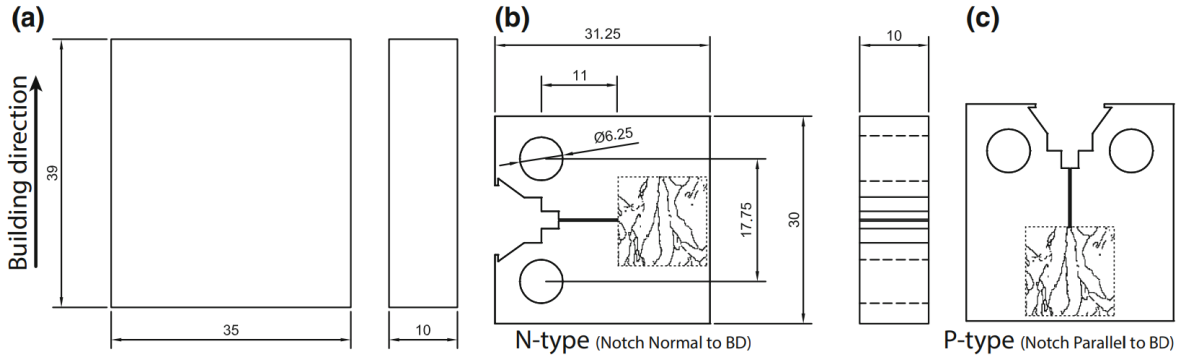

Figure 2. 5: a) Geometry of the as-built SLM IN718 block, b and c) Compact tensile (CT) geometry with the notch normal and parallel to the building direction (BD), respectively. The insets in (b) and (c) indicate how the notch orientates to the grain boundary [11].

Table 2. 1: Designations of Specimens and the Corresponding Heat Treatment Details [11].

	Homogenization	Solution	Aging
SA	None	1253 K (980 °C)/1 h/WC	993 K (720 °C)/8 h
HA	1353 K (1080 °C)/1 h/WC	None	50 K/h FC to 893 K (620 °C)
HSA	1353 K (1080 °C)/1 h/WC	1253 K (980 °C)/1 h/WC	893 K (620 °C)/8 h/AC

FC, AC and WC denotes furnace cooling, air cooling and water cooling, respectively. SA is the standard heat treatment for wrought IN718 (AMS 5662). HSA is the standard heat treatment for cast IN718 (AMS 5383).

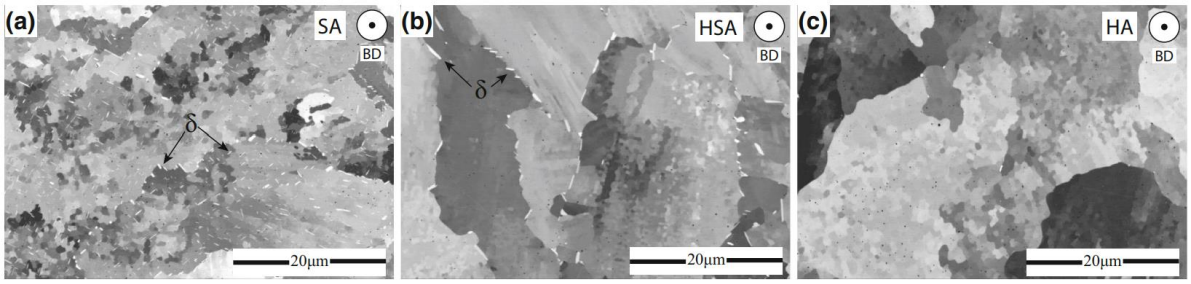

Figure 2. 6: Typical microstructures of (a) SA, (b) HAS and (c) HA characterized by cross sections perpendicular to BD [11].

In the Deng *et al*. study, the N-type specimens where the notch was perpendicular to the build direction exhibited off plane crack growth after the room temperature pre-crack. This violated the parameters of mode I crack growth. Also, in both the N-type and P-type specimens secondary cracking was observed where cracks were perpendicular to the loading direction and did not branch off the main crack path. Deng *et al*. attributed this to creep damage rather than DE and SAGBO which was observed by Gustafsson *et al.* and Krupp regarding their wrought

IN718 tests [5,7,8,11]. An additional observation made by Deng *et al*. was that when comparing the three separate heat treatments, the δ precipitates in the SA and HSA heat treatments aided in reducing the crack propagation rate when compared to the HA heat treatment without noticeable δ precipitates. The observations made by Deng *et al*. with the AM IN718 differ than the observations made by Gustafsson *et al.* and Krupp with Wrought IN718 and require further study.

3. EXPERIMENTAL DETAILS

3.1 Material and Specimen Geometries

Inconel 718 (IN718) was the material of interest for this research. Two different manufacturing processes were used to create the IN718 blanks: forged and additive manufactured (AM). The first set of specimens were machined from forged disk sections. These sections were provided by Rolls-Royce for use in ILS 1679 round robin and are shown in Figure 3.1. The forgings were precipitation heat treated according to AMS 5663 [15]. This post processing resulted in a very fine grain microstructure with average grain sizes of 7 – 12 μm, which can be seen later in fractography images in Section 4. The approximate chemical composition and tensile properties are shown in Tables 3.1 and 3.2.

(a)

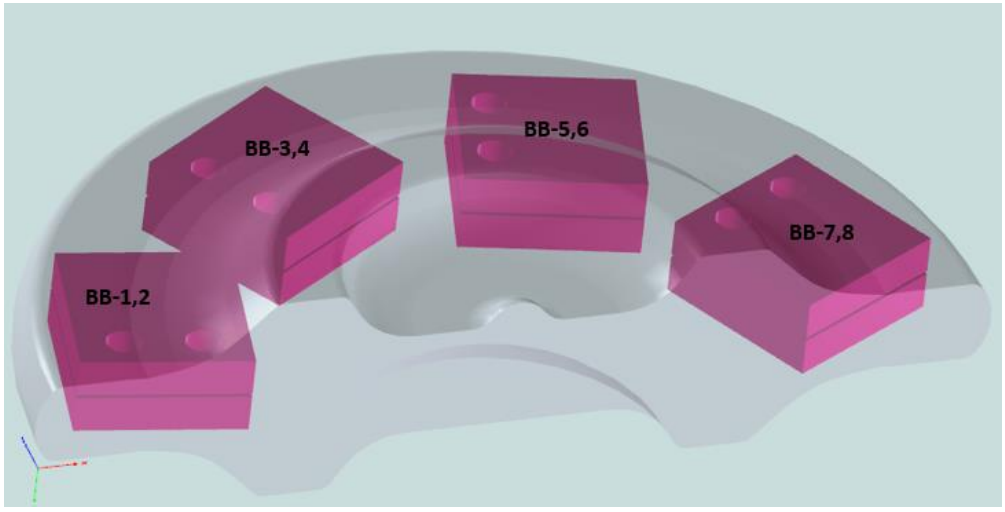

(b)

Figure 3. 1: (a) IN718 forgings provided by Rolls Royce Corporation for use in the ASTM ILS 1679, (b) Typical C(T) specimen layout.

Table 3. 1: Typical composition limits of IN718

Element	Ni	Cr	Mo	Al	Ti	Nb+Ta	Fe	Co
(wt.%)	50-55	17-21	2.80-3.30	0.20-0.80	0.65-1.15	4.75-5.50	Balance	1.00 max
Element	C	Mn	Si	P	S	B	Cu	
(wt.%)	0.08 max	0.35 max	0.35 max	0.015 max	0.015 max	0.006 max	0.30 max	

Table 3. 2: IN718 tensile properties at test temperatures

Material Properties	24°C	600°C
Yield Strength, σ_{ys}, MPa	1100	860
Tensile Strength, σ_{uts}, MPa	1375	1000
Young's modulus, E, GPa	200	166
% elongation	20.1	20.6

The primary specimen geometry used in this research was a compact tension C(T) type specimen. C(T) Specimens were machined from the disk sections such that loading would be in the Radial (R) direction and the notch in the circumferential (C) direction. The dimensions of the C(T) specimens are as follows; W = 50.7 mm, B = 12.7 mm, and a_n = 10 mm. The same specimen type and geometry was used for both the wrought and the AM IN718. A detailed view of the C(T) specimen geometry is shown in Figure 3.2.

Additive Manufacturing was the other process used to create the IN718 blocks from which C(T) specimens were machined. Specifically, Selective Laser Melting (SLM) was used to create blocks in two different orientations and are shown in Figure 3.3. These two print orientations will be denoted as the vertical (VER) and horizontal (HOR) orientations. The deposition layer thickness of powdered IN718 for creating the blocks was 40μm. Additional information regarding the AM process is limited due to proprietary information.

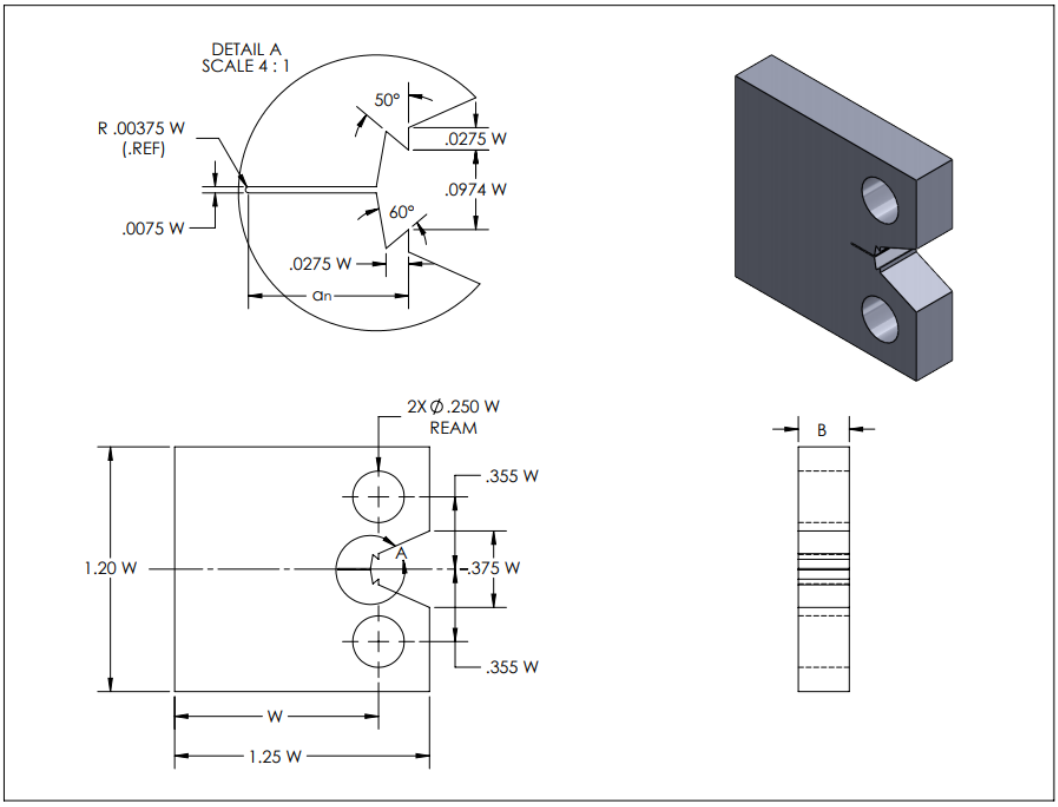

Figure 3. 2: C(T) specimen geometry used for testing wrought and AM IN718.

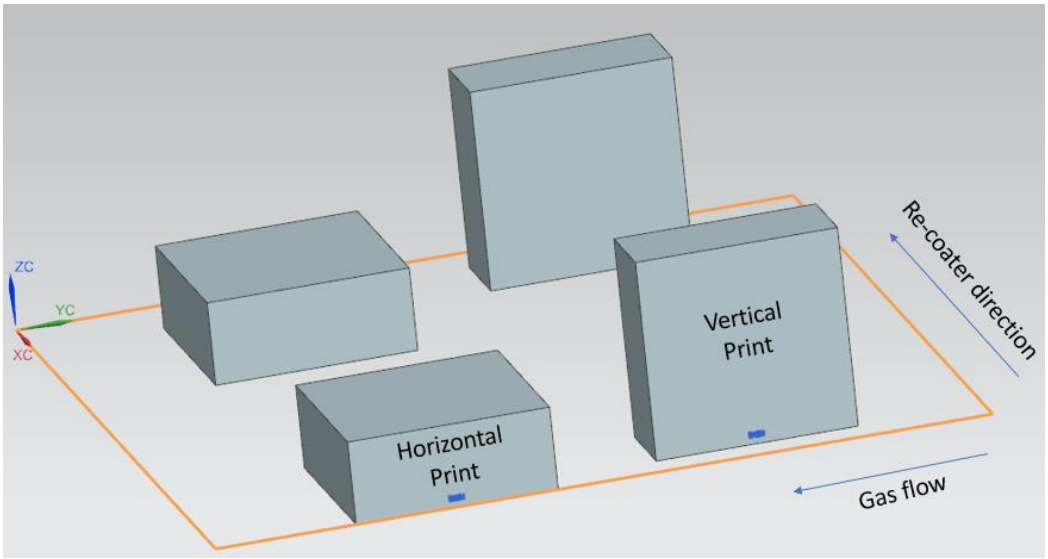

Figure 3. 3: Print orientations for AM IN718 blocks.

Two blocks in each orientation (vertical and horizontal) were printed and each block was printed large enough for two C(T) specimens to be machined for a total of eight specimens.

Where two specimens would be machined from each block, it was decided that C(T) specimens would be machined in a way that the crack plane would be rotated 90 degrees from the previous machined specimen. For example, in the vertical orientation, two specimens were machined with the crack plane normal to the build direction and the other two specimens were machined with the crack plane parallel to the build direction. These specimens will be referred to as P-type and N-type and are labeled in Figure 3.4 as blocks 1 and 2. This allowed the effect of orientation to be evaluated and compared with the other AM specimens as well as with the wrought specimens.

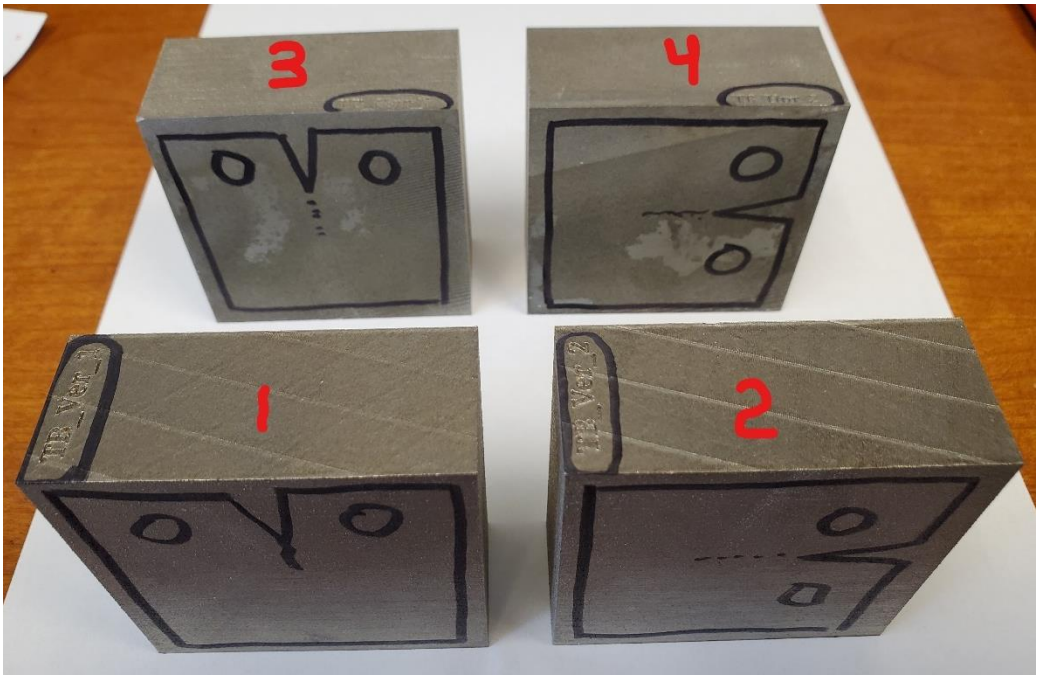

Figure 3. 4: AM IN718 blocks showing C(T) specimen orientation.

When the pilot tests for the round robin program were completed, another specimen geometry was tested: single edge notch (SEN). The fractured halves of the C(T) specimens were machined into (SEN) specimens and are shown in Figure 3.5. Since specimens and material were limited, the purpose of machining the SEN specimens out of the broken (CT) specimen halves was to collect additional data at a lower stress intensity range and to perform a crack profile evaluation.

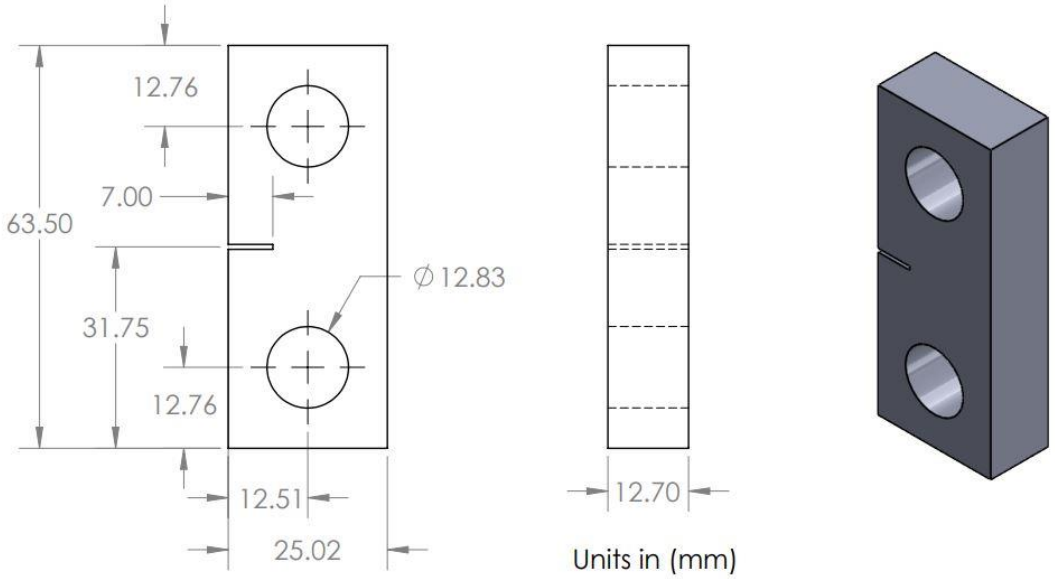

Figure 3. 5: SEN specimen geometry used in testing the fractured wrought IN718 C(T) halves.

3.2 Experimental Testing Equipment

All tests were performed using an MTS 312.11 servo-hydraulic load frame with a maximum load capacity of 44kN (10kip). The load frame was controlled by an MTS 458.20 MicroConsole, and the desired loading wave forms were generated by an MTS 458.91 MicroProfiler. To conduct tests at elevated temperatures an Applied Test Systems (ATS) split case furnace was used. The furnace was controlled by a Watlow EZ-Zone® PID temperature controller and utilized a K-type thermocouple spot welded to the specimen for temperature feedback control. Placement of the spot-welded thermocouple was consistent for all C(T) specimens and is shown in Figure 3.7. During testing a second K-type thermocouple with a separate temperature reading unit was used to probe the test specimens through a slot in the furnace to verify the test temperature. The load frame and other testing equipment is shown in Figure 3.6.

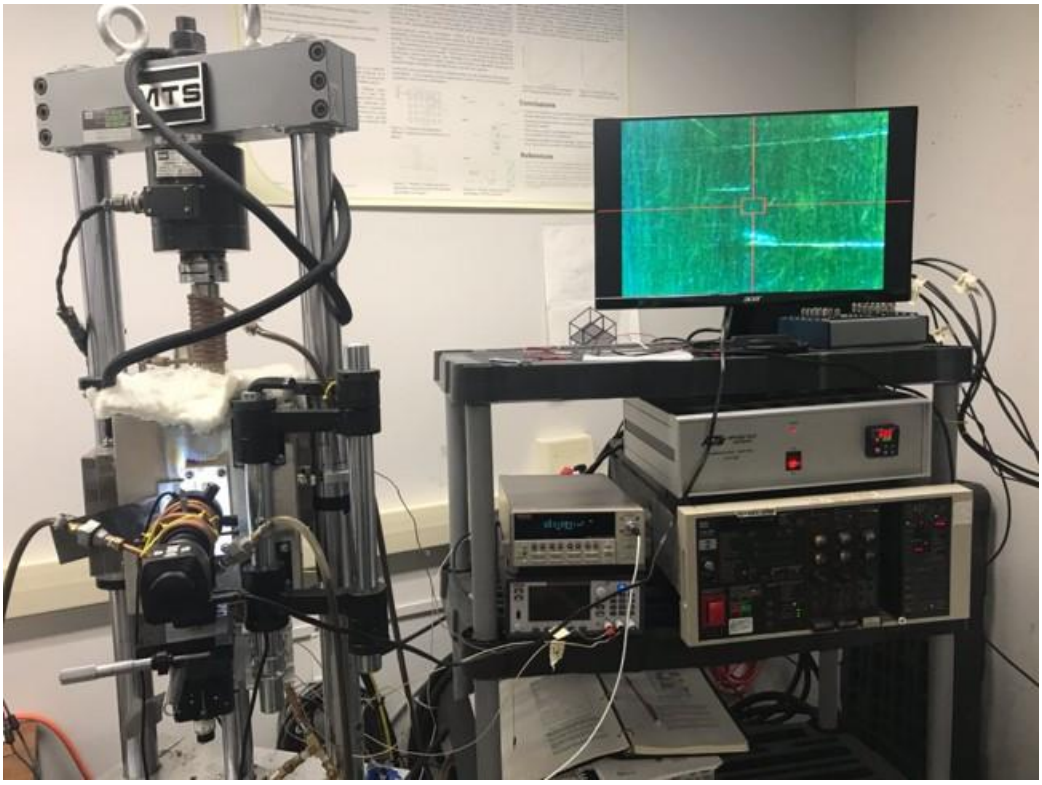

Figure 3. 6: Servo hydraulic load frame and other testing equipment.

Two methods were used to monitor crack length during testing. The primary method used was direct current potential drop (DCPD). For the DCPD method a constant current was applied to the specimen for the duration of the experiment and a voltage across the crack plane was measured. As the crack propagates resistance increases and the measured increase in voltage was later correlated to a specific crack length. To create a constant current, a Keithley 2280S-32-6 Precision Measurement DC Power Supply was used. To measure the potential drop across the crack plane, a Keithley 2182A Nanovoltmeter was used. A constant current of 2 Amps was used for all tests including wrought, AM, as well as C(T) and SEN specimens. The DC power supply and nanovoltmeter were connected to the specimens via spot welded 22-gauge and 26-gauge Nichrome 60 wires. For the C(T) specimen, placement of these wires are shown in Figure 3.7, and for the SEN specimen, are shown in Figure 3.8. In both Figure 3.7 and Figure 3.8, A+/A- are the spot weld locations for the power supply and B+/B- are the spot weld locations for the nanovoltmeter.

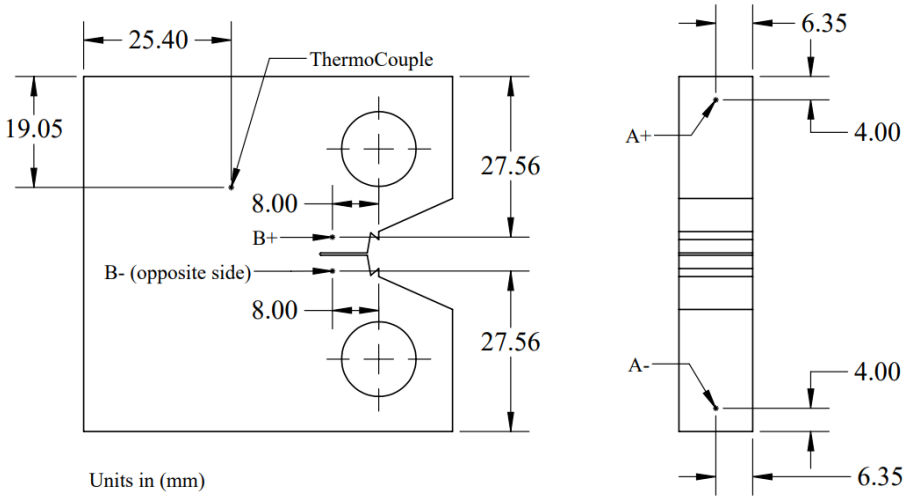

Figure 3. 7: Spot weld location for Thermocouple, Power Supply, and Nanovoltmeter on C(T).

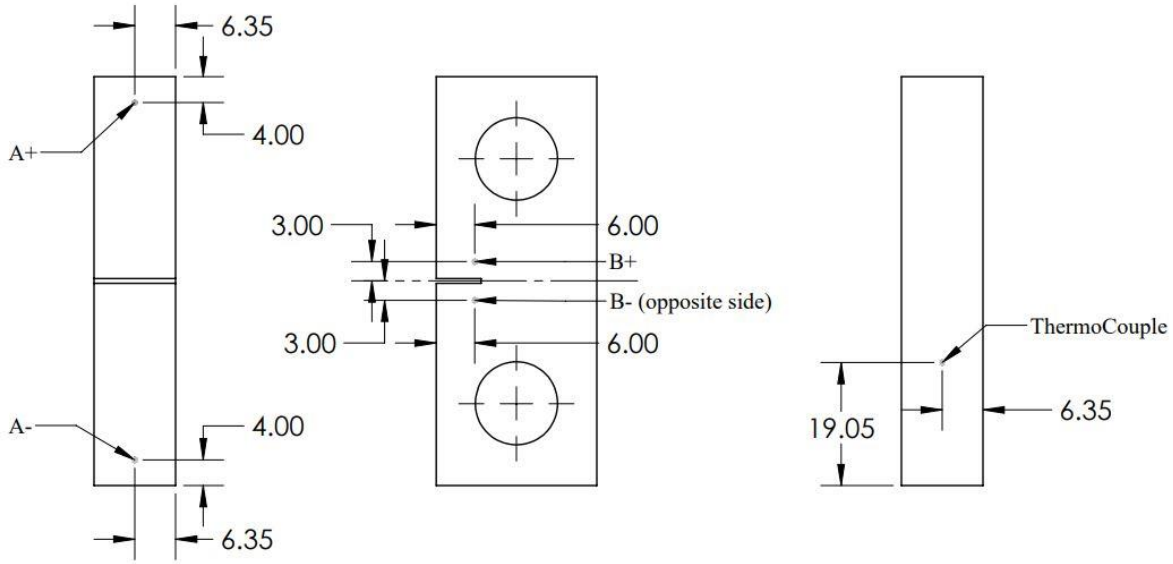

Figure 3. 8: Spot weld location for Thermocouple, Power Supply, and Nanovoltmeter on SEN.

The second method used for monitoring crack length was visual where a traveling microscope was mounted on the outside of the furnace. Using the traveling microscope, the surface crack length was monitored throughout the duration of the test. Visual crack length data

was also collected at specific intervals and was later used for comparison and validation of the DCPD measurements. The traveling microscope is shown in Figure 3.6.

For the C(T) specimens, crack opening displacement (COD) measurements were made during the CFCG and CCG tests. These measurements were made using an MTS model 632.11B-20 extensometer fitted with a set of ceramic rods for use in the furnace. The extensometer is shown in Figure 3.9. The extensometer used was calibrated before testing and has a resolution of 0.5 μm. These COD measurements were later used in determining the load line displacement during each cycle and were compared for different hold times and stress intensity values.

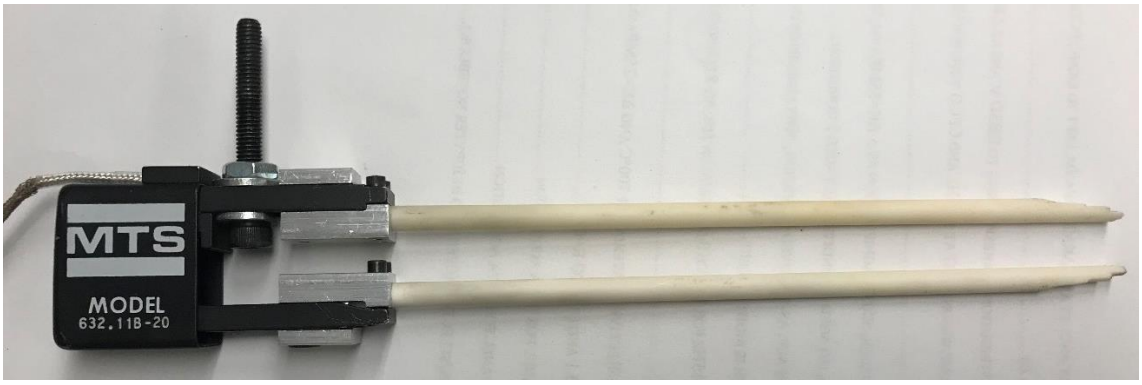

Figure 3. 9: Extensometer used in measuring COD of C(T) specimens.

After tests were completed, fracture surfaces were removed from the broken C(T) halves and were observed under a scanning electron microscope (SEM). The SEM used was a Zeiss Supra 35 VP. Fractography images shown in Section 4 were taken using the secondary detector. A 30 mm aperture size was used in all images.

3.3 Testing Procedure

The primary test specimens used were C(T) type, and the same pre-cracking procedure was used for both wrought and AM specimens. Prior to pre-cracking all specimens were mechanically polished to a 1μm finish. Pre-cracking was conducted at room temperature at a frequency of 15 Hz (sinusoidal waveform). A stress-ratio (R) of 0.1 was maintained throughout the procedure. A load shedding procedure was developed and was in accordance with ASTM E-647. Starting and final crack lengths corresponded to a_o = 10 mm and a_f = 20 mm with starting

and final stress intensity range ΔK_i = 29.5 MPa√m and ΔK_f = 20 MPa√m. The load shedding procedure is located in Appendix B.1. The SEN pre-cracking procedure was similar to the C(T) but had different starting and ending conditions. The purpose of the SEN specimen was to generate additional data at a lower stress intensity range than with the C(T) specimens. The starting and final pre-crack lengths corresponded to a_o = 7 mm and a_f = 13 mm with starting and final stress intensity range ΔK_i = 15 MPa√m and ΔK_f = 9 MPa√m.

A baseline FCG test was required as part of the pilot testing for the round robin, so a 2 Hz triangular wave form was used. One additional FCG test was also conducted with an SEN specimen. It was decided to use a frequency of 15 Hz sinusoidal waveform to reduce test time since the starting stress intensity was near the threshold value. To keep the FCG test consistent with the CFCG testing, a loading and unloading time of 0.25s was used for both the 60s hold time tests and 600s hold time tests which corresponds to the same loading and unloading times used in the 2 Hz FCG test. The majority of experiments conducted were either trapezoidal waveform CFCG with 60s and 600s hold times, or CCG tests. The loading waveforms used are shown in Figure 3.10, and the specimen testing matrix is shown in Table 3.3. It is important to note that all testing, including the room temperature pre-cracking was conducted with an R-ratio of 0.1.

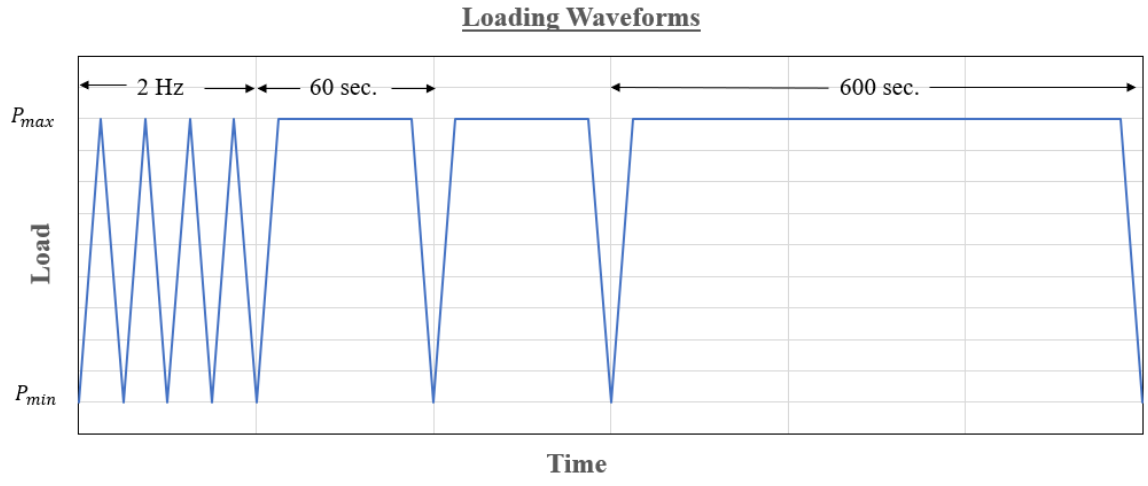

Figure 3. 10: Loading waveforms for FCG and CFCG testing.

When each elevated temperature test reached the point of unstable crack propagation and fracture was imminent the test was stopped, and the specimens were cooled to room

temperature. The room temperature specimens were then cyclically loaded at the same minimum and maximum load levels used during testing until fracture. Each fracture surface was observed using an optical microscope and the pre-crack and final crack lengths were determined by taking the average of 5 equally spaced measurements on each of the crack fronts in relation to the load line. These measurements were used to correlate the DCPD voltage values to physical crack lengths. The data was then reduced using a seven-point secant method as recommended by ASTM E-647.

One variation of this procedure was used with the SEN specimens. SEN specimens prior to testing were polished to a 1μm finish and etched using a Kalling's Reagent. This allowed the grain boundaries to be seen using the SEM secondary detector. After cooling the specimen and prior to fracture, SEN specimens were removed from the load frame and observed under the SEM. This allowed the crack path and grain boundary interaction to be observed on the surface of the specimen. When SEM imaging was finished, specimens were returned to the load frame and cyclically loaded until they fractured. The same measurement method was used to determine the initial and final crack lengths.

Table 3. 3: Specimen Testing Matrix

Material	**Specimen Type**	**RT, Pre-Cracking**	**Temperature ºC**	**Loading Waveform**	**Hold Time/ Frequency**	**Starting a (mm)**	**Starting ΔK (MPa√m)**
Wrought IN718	CT	R=0.1, 15 Hz	600	Triangular	2 Hz	20	20
	CT		600	Trapezoidal	60s	20	20
	CT		600			20	20
	CT		600		600s	20	20
	CT		600			20	20
	CT		600	CCG	N/A	20	20
Wrought IN718	SEN	R=0.1, 15 Hz	600	Sinusoidal	15 Hz	13	9
	SEN		600	Trapezoidal	60s	13	9
	SEN		600		600s	13	9
	SEN		600	CCG	N/A	13	9
AM IN718	Vertical P-type	R=0.1, 15 Hz	600	Trapezoidal	600s	20	20
			600	CCG	N/A	20	20
	Vertical N-type		600	Trapezoidal	600s	20	20
			600	CCG	N/A	20	20
	Horizontal		600	Triangular	2 Hz	20	20
			600	Trapezoidal	60s	20	20
			600		600s	20	20
			600	CCG	N/A	20	20

4. RESULTS AND DISCUSSION

4.1 Wrought IN718 C(T)

As a participant in the ASTM ILS 1679 round robin, five wrought IN718 C(T) specimens were provided and tested under FCG and CFCG conditions at 600°C with a stress ratio (R) of 0.1. One additional specimen was provided and tested at 600°C under CCG conditions but not reported in the final submission of experimental findings for ILS 1679. The first test was a baseline 2 Hz FCG test with an initial crack length of a_i = 20 mm and an initial stress intensity range ΔK_i = 20 MPa√m. The next four tests were CFCG tests with hold times of 60s and 600s. A summary of the results are shown in Table 4.1.

Table 4. 1: Summary of wrought C(T) FCG, CFCG, and CCG results.

Fatigue Crack Growth/Creep Fatigue Crack Growth/Creep Crack Growth								
Specimen ID	Waveform	a_i (mm)	a_f (mm)	P_{max} (kN)	ΔK_i (MPa √m)	ΔK_f (MPa √m)	# Cycles	Hours
BB5-CT-4	2 Hz	20.3	40.0	8.9	20.4	105.9	37407	5.2
BB5-CT-7	60 s-1	20.0	39.4	8.9	20.1	97.1	1891	31.5
AW1-CT-8	60 s-2	20.6	39.1	8.9	20.7	93.1	2376	39.6
AD1-CT-4	600 s-1	20.3	40.0	8.9	20.4	105.9	211	35.2
DD-1	600 s-1	20.7	41.4	8.9	20.8	132.3	248	41.3
DD-6	CCG	21.4	40.3	8.9	K_{max} = 24.0	K_{max} = 123.1	N/A	39.8

Fatigue crack growth rates, da/dN, as a function of ΔK are shown in Figure 4.1(a). When comparing 2 Hz, 60s, and 600s results, there is a noticeable increase in crack growth rate with respect to ΔK for the 60s and 600s hold times compared to the 2 Hz test. The 60s and 600s hold tests showed good repeatability with the 60s hold having an approximate 30% difference in crack growth rate. Comparing the 60s and 600s hold tests, a 10x increase in hold time resulted in approximately a 10x increase in crack growth rate with respect to ΔK.

Additional comparison was made by evaluating time rate of crack growth, da/dt, as a function of K_{max} shown in Figure 4.1(b). da/dt is the time rate of crack growth where t_h is hold time. The relation of da/dt to da/dN is shown in equation 4.1:

$$da/dt = \frac{1}{t_h}\left(\frac{da}{dN}\right) \tag{4.1}$$

When plotting hold time data from Figure 4.1(a) as (da/dt vs $K_{max,}$) shown in Figure 4.1(b), the 60s and 600s hold tests collapse onto each other to form a single scatter band. The single CCG test data is also plotted in Figure 4.1(b) and falls within the same scatter band. The relationship between data sets shows that for a hold time of 60s to an infinite hold time (CCG), the primary mode of crack growth is independent of number of cycles but dependent on time. This demonstrates that for a creep brittle material, wrought IN718, the stress intensity parameter, K, is sufficient for characterizing creep fatigue crack growth rates for fixed hold times [6].

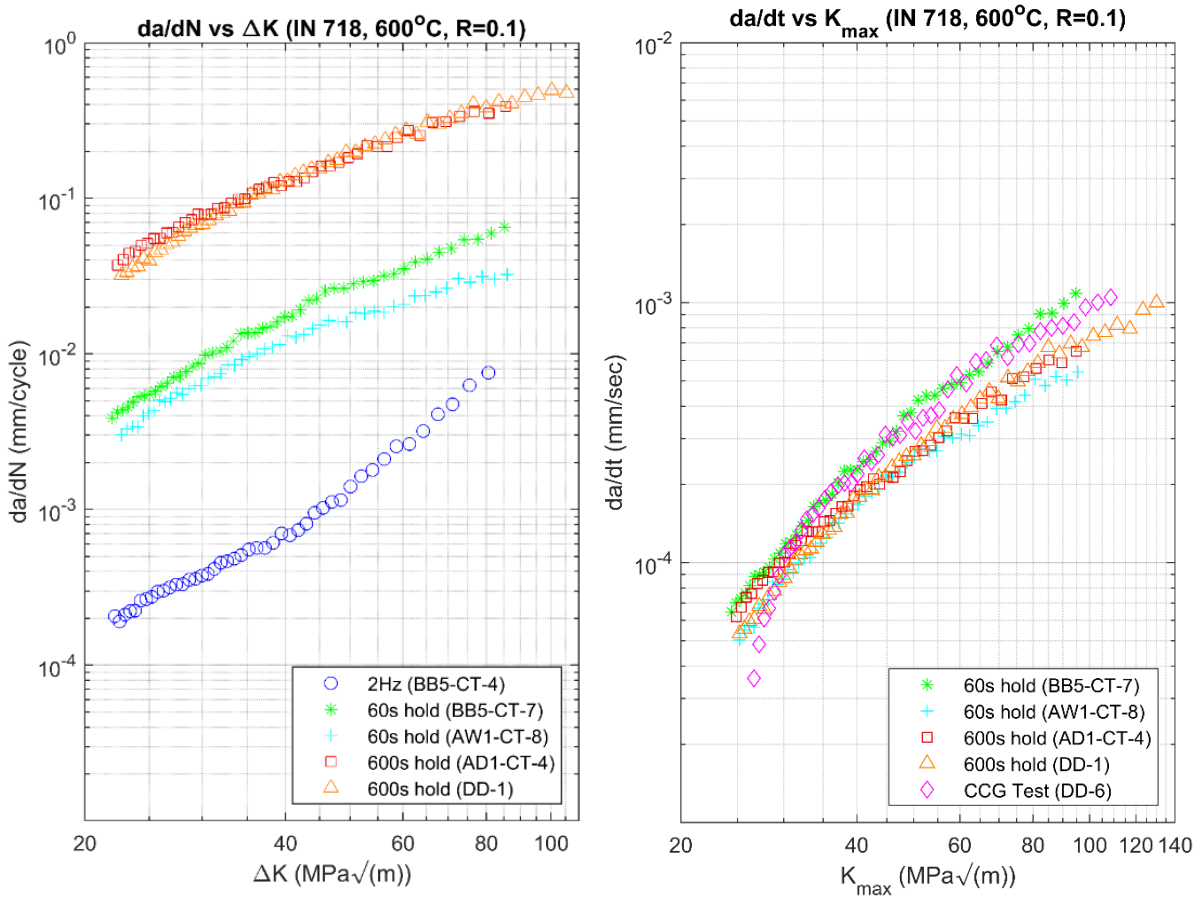

(a) (b)

Figure 4. 1: Crack growth rates for wrought IN718, (a) fatigue crack growth rate, (b) time rate of crack growth.

Regarding the fatigue crack growth rate data in Figure 4.1(a), two creep fatigue crack growth rate models were applied. These models are associated with combining hold time effects due to creep and effects of continuous cycling. The purpose of these models is to predict longer hold times by combining known FCG and CFCG data. The first model applied is typically used with materials that have creep brittle characteristics which are primarily time dependent modes of crack growth. This model is represented in equation 4.2 and comes from ASTM E2760 equation (A1.5) [13].

$$\frac{da}{dN} = C_o(\Delta K)^{n_o} + C_2(\Delta K)^{n_2}\sqrt{t_h} \tag{4.2}$$

Values of n and C are found by fitting a power curve to a data set and determining the slope and intercept. For equation 4.2, n_o and C_o are the slope and intercept values found by fitting a curve to the 2 Hz data in Figure 4.1(a). In the second term of equation 4.2, n_2 and C_2 were found by fitting a curve to the second 60s hold time test (AD1-CT-8). The second model applied is typically used with materials that have creep ductile characteristics that are primarily cycle dependent modes of crack growth. This model is represented in equation 4.3 and comes from ASTM E2760 equation (A1.4). The second term was modified to use K_{max} instead of $(C_t)_{avg}$.

$$\frac{da}{dN} = C_o(\Delta K)^{n_o} + C_1(K_{max})^{n_1} t_h \tag{4.3}$$

In equation 4.3, n_o and C_o are represented by the same values found from the 2 Hz data. In the second term of equation 4.3, n_1 and C_1 were found by fitting a curve to the second 60s hold time data (AD1-CT-8) in Figure 4.1(b). In both models t_h is the desired hold time prediction. Both models are shown in Figure 4.2 and the values of n and C used are shown in Table 4.2.

In Figure 4.2, the model derived from equation 4.2 is represented by a dashed line and the model derived from equation 4.3 is represented by a solid line. Though the model from equation 4.2 is primarily used for creep ductile materials, it best aligns with the 600s hold time data. Where IN718 is a creep brittle material, this model may be a better fit due to the lack of creep resistance under hold time and the abundance of grain boundary oxidation [6].

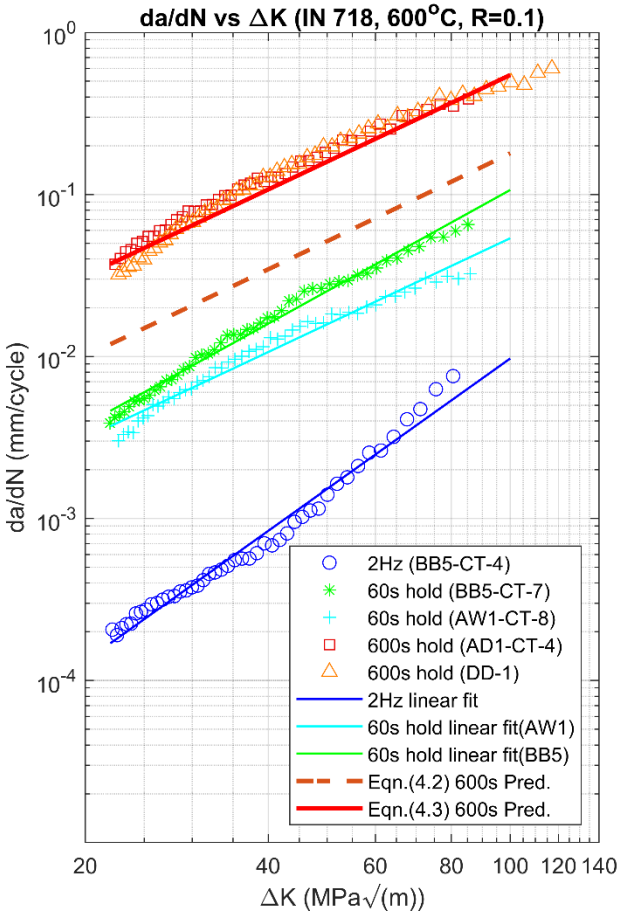

Figure 4. 2: Fatigue crack growth of IN718 with predictive models applied for 600s hold.

Table 4. 2: Slope and intercept constants used in predictive models for 600s hold.

2 Hz FCG (da/dN) (mm/cycle)	C_o	4.365E-8
	n_o	2.674
60s CFCG (da/dt) (mm/s)	C_1	2.193E-7
	n_1	1.765
60s CFCG (da/dN) (mm/cycle)	C_2	1.585E-5
	n_2	1.765

During all testing COD data was collected using an MTS extensometer referenced in Section 3.2. The COD data collected was used to analyze LLD during individual cycle hold times. The change in LLD during a given cycle, or load line displacement difference, ΔV_c, was later plotted as a function of ΔK. The magnitude of ΔV_c is a function of the amount of creep deformation during the hold period of a cycle and is independent of the crack growth during loading and unloading of the fatigue cycle. In Figure 4.3, single cycles from 60s hold and 600s hold time tests are shown at corresponding ΔK values of 80 MPa$\sqrt{m}$. In Figure 4.3(a), for the 60s hold, there is less than 5µm change in LLD (from 280-284 µm) where in Figure 4.3(b) for the 600s hold, there is aproximately 25-30µm of change in LLD (from 360-385 µm). Due to the small change in ΔV_c for the 60s hold tests, only one 60s hold test was plotted in Figure 4.4. From Figure 4.4, it can be seen that ΔV_c for the two 600s hold tests were very similar. This is consistent with the similar 600s hold CFCG curves shown in Figure 4.1(a).

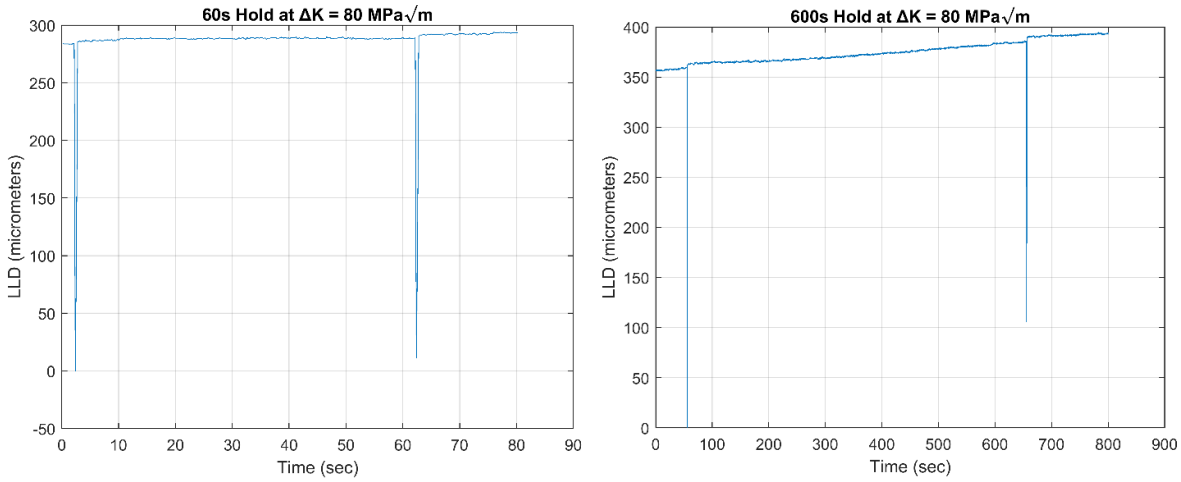

(a) (b)

Figure 4. 3: Single cycle LLD at ΔK = 80 MPa$\sqrt{m}$: (a) 60s hold, (b) 600s hold.

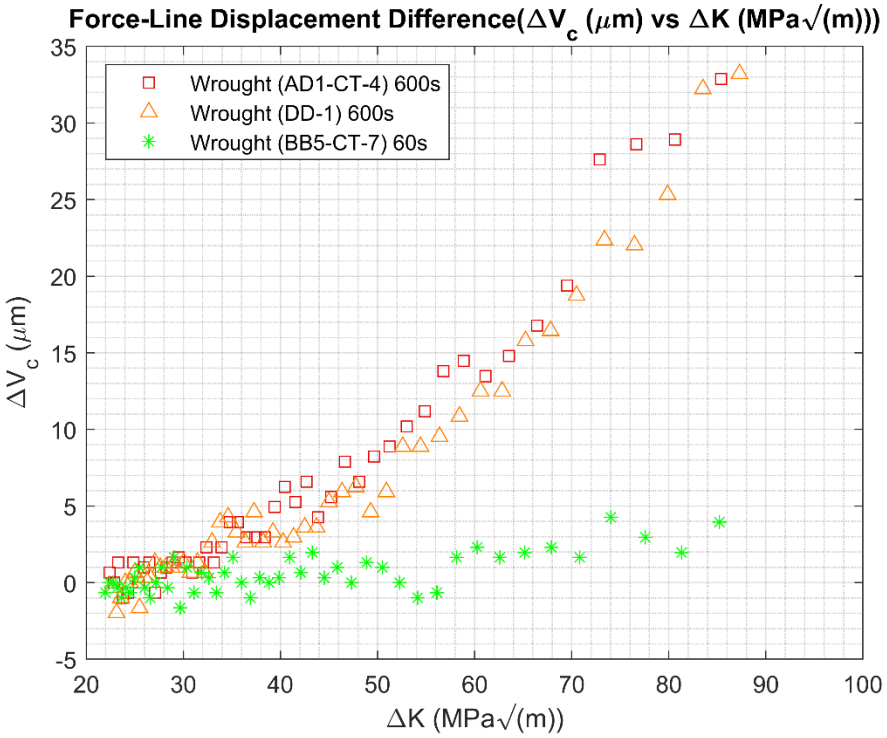

Figure 4. 4: Force-line displacement difference (ΔV_c) vs. ΔK for wrought 60s and 600s hold time.

To relate initial and final crack lengths to DCPD voltages, fracture surfaces were measured under an optical microscope using the procedure presented in Section 3.3. The fracture surfaces of all six specimens are shown in Figure 4.5 with the direction of crack growth from right to left. Fractography was later performed using a SEM. Figure 4.6 shows SEM imaging of the fracture surfaces for the 2 Hz FCG test and the 600s hold CFCG test at an initial ΔK_i = 20 MPa√m. In both figures the surface on the right half labeled 1 denote the end of the room temperature pre-crack. In the pre-crack region of both specimens the surface shows that mode of crack growth was transgranular. On the left half of Figure 4.6(a) labeled 2, the mode of crack growth is still primarily transgranular with some secondary cracking. However, on the left half of Figure 4.6(b) the primary mode of crack growth was intergranular and exhibits extensive secondary cracking. Observations of the 60s hold time fracture surface at the same initial ΔK_i = 20 MPa√m also showed the same intergranular cracking as seen in Figure 4.6(b). Additional fractography with wrought IN718 will be discussed in Section 4.6.

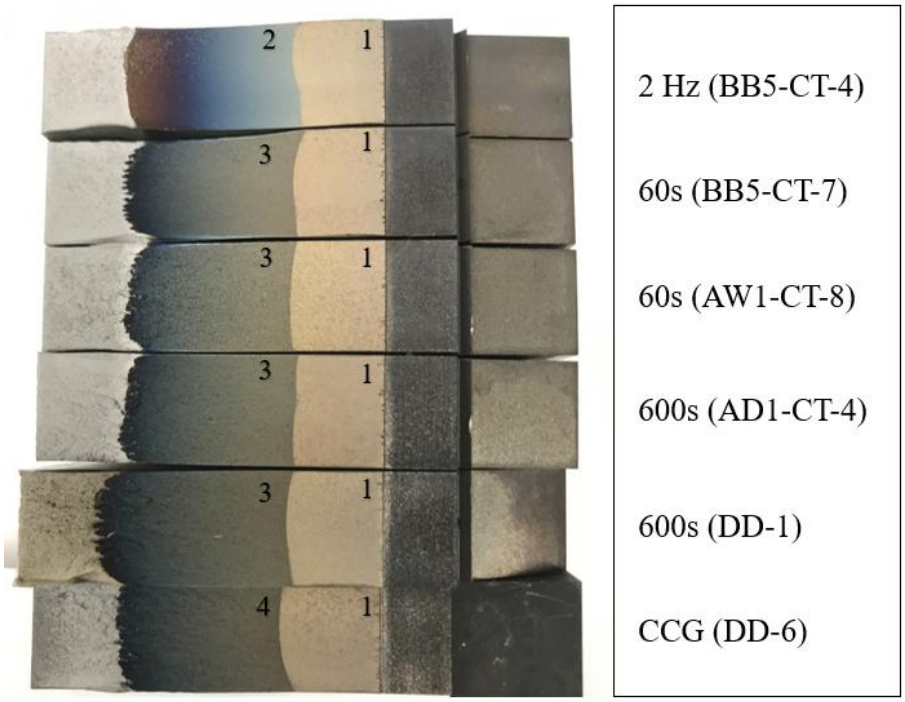

Figure 4. 5: Fracture surfaces of wrought C(T) specimens. 1) Pre-crack region, 2) FCG region,
3) CFCG region, 4) CCG region.

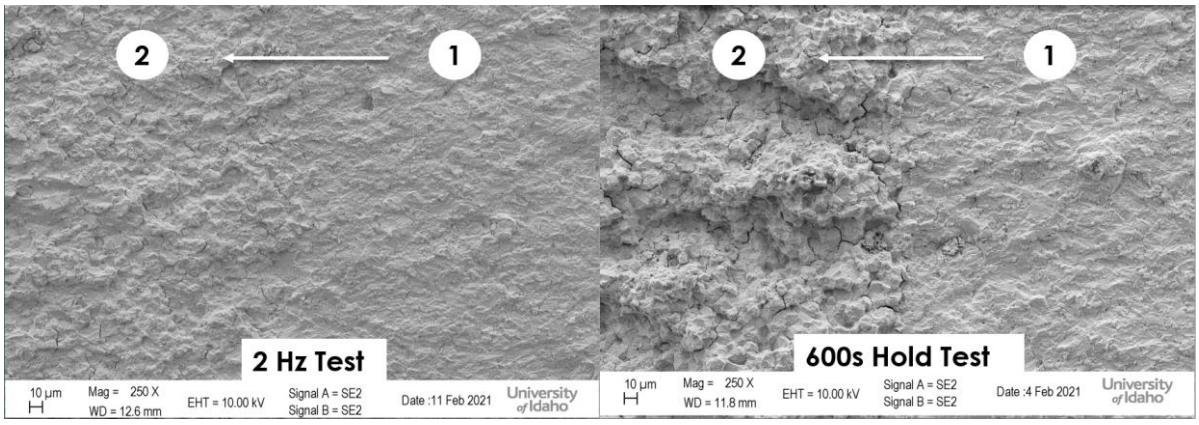

(a) (b)

Figure 4. 6: Fracture surfaces at initial ΔK_i = 20 MPa√m, a) 2 Hz FCG labeled 1-pre-crack, 2-FCG, b) 600s hold CFCG labeled 1-pre-crack, 2-CFCG.

4.2 Wrought IN718 SEN

As a participant of ILS 1679 round robin, it was required that tests began at a specific stress intensity range of ΔK_i = 20 MPa√m. To gather additional data at lower stress intensity ranges, SEN specimens were machined from broken halves of C(T) specimens. The SEN specimens were tested under FCG, CFCG and CCG conditions consistent with the original tests conducted with the C(T) geometry. The first test with the SEN geometry was a FCG test at 15 Hz, temperature of 600°C, R = 0.1, and ΔK_i = 9 MPa√m. Because the FCG test started at a lower ΔK, a cycling frequency of 15 Hz was chosen to decrease the total test time vs conducting the test at 2 Hz. The next two tests were CFCG tests with hold times of 60s and 600s. The last test was a CCG test with the same starting crack length and maximum load as the previous tests. A summary of FCG, CFCG, and CCG results for the SEN geometry are shown in Table 4.3.

Table 4. 3: Summary of wrought SEN FCG, CFCG, and CCG results.

Fatigue Crack Growth/Creep Fatigue Crack Growth/Creep Crack Growth								
Specimen ID	Waveform	a_i (mm)	a_f (mm)	P_{max} (kN)	ΔK_i (MPa √m)	ΔK_f (MPa √m)	# Cycles	Hours
SEN-DD-6	15 Hz	12.7	20.6	5.8	10.3	43.1	152024	2.8
SEN-BB5-7	60 s	13.1	19.7	5.8	11.0	36.5	4414	73.6
SEN-AD1-4	600 s	12.6	20.1	6.7	11.7	45.4	267	44.5
SEN-DD-6-2	CCG	14.1	20.2	8.0	K_{max}=20.1	K_{max}=61.5	N/A	35.4

Fatigue crack growth rates, da/dN, as a function of ΔK are shown in Figure 4.7(a). It is important to note that for all SEN specimens, crack growth at the initial conditions did not occur so additional steps were taken to initiate crack growth. These steps are shown in Appendix A.7-A.10. The 15 Hz FCG test and 60s hold CFCG test required P_{max} to be increased by 20% before a change in DCPD volage was observed which indicated crack growth. The 600s hold CFCG test required P_{max} to be increased by 40% before a change in DCPD volage was observed which indicated crack growth. The CCG test was the final test conducted and P_{max} was increased by 60% before crack growth was observed by a change in DCPD voltage. The cycling and holding patterns used to initiate crack growth found in Appendix A.7-A.10 can be seen on the fracture

surfaces of the SEN specimens in Figure 4.8. The region labeled 3 on the fracture surfaces is the area of crack growth during the cycling and holding periods. The difficulty in initiating crack growth at low ΔK_i = 9 MPa√m was attributed to the threshold ΔK value of IN718 lying between 8-10 MPa√m [7].

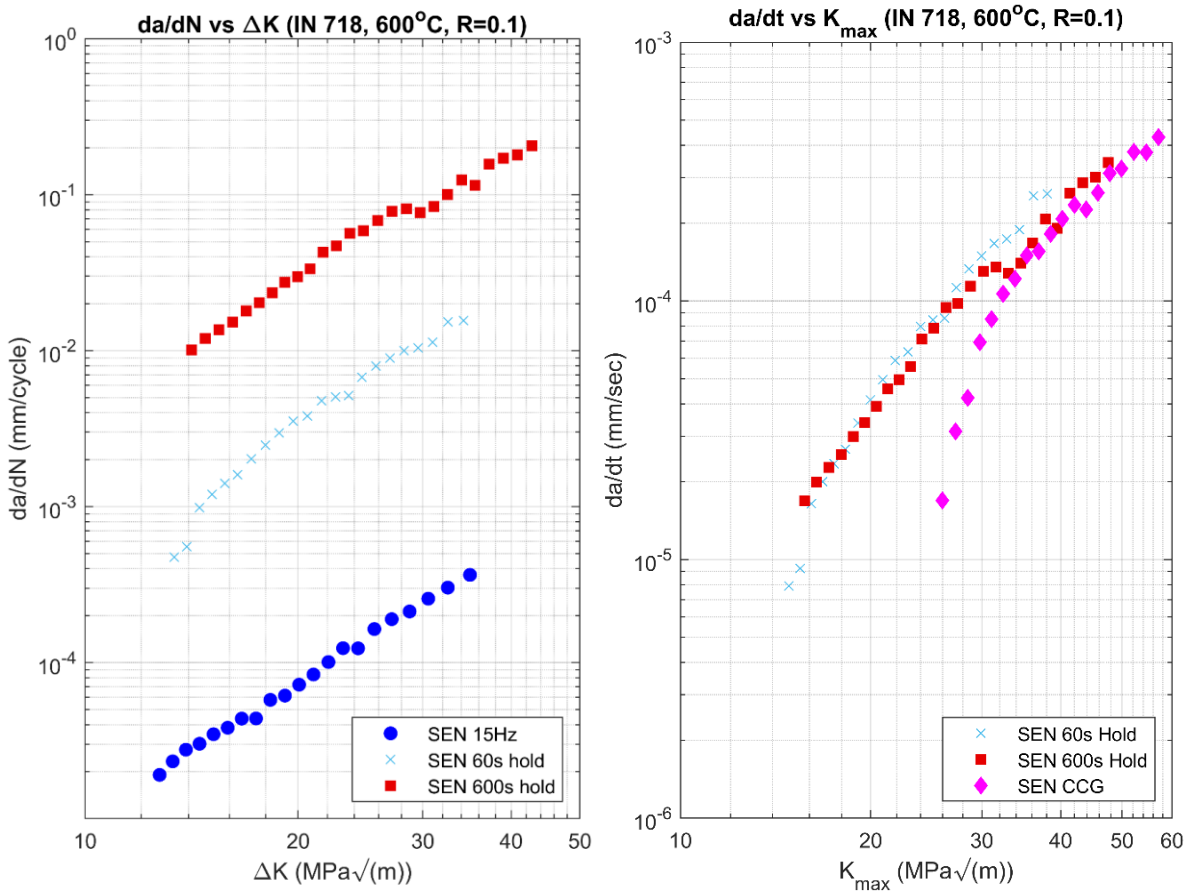

(a) (b)

Figure 4. 7: SEN crack growth rates for wrought IN718, (a) fatigue crack growth rate, (b) time rate of crack growth.

When comparing 15 Hz, 60s, and 600s hold data in Figure 4.7(a), there is noticeable increase of crack growth rate with respect to ΔK for the 60s and 600s hold tests compared to the 15 Hz FCG test. Similar to the wrought C(T) specimens, comparing SEN 60s and 600s hold time tests showed a 10x increase in crack growth rate with respect to ΔK. When plotting the hold time data seen in Figure 4.7(a) as (da/dt vs $K_{max,}$), the 60s and 600s hold tests collapse onto each other to form a single scatter band and are shown in Figure 4.7(b). The CCG test was also

plotted in Figure 4.7(b). The lower portion of the CCG test showed lower crack growth rates but merged at a K_{max} = 35 MPa√m with the 60s and 600s hold tests.

Fracture surfaces were measured using the same method as with the C(T) specimens. The fracture surfaces are shown in Figure 4.8 where the direction of crack growth is from right to left. It is important to note that the notch shape is different for the 15 Hz test than the other tests. The 15 Hz test has a straight notch while the 60s, 600s and CCG tests have a chevron notch. It was decided after pre-cracking the 15 Hz test that a chevron notch would be cut into the other specimens to aide in crack initiation and help reduce the total time required for pre-cracking.

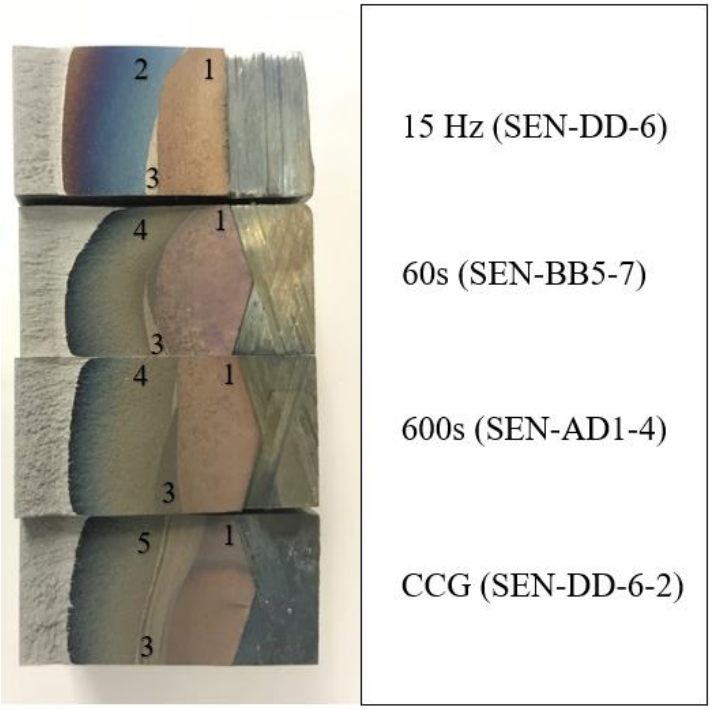

Figure 4. 8: Fracture surfaces of wrought SEN specimens. 1) Pre-crack region, 2) FCG region, 3) cycling and holding pattern in Appendix A.7-A.10, 4) CFCG region, 5) CCG region.

After each test was stopped, and prior to fracture, the specimens were cooled to room temperature. Before fracturing each specimen at room temperature, specimens were removed from the load frame and the crack profiles were observed under a SEM. The surfaces had been polished and etched prior to testing as described in Section 3.3. Figure 4.9(a) shows the crack

opening of an unloaded (60s hold) SEN specimen prior to fracture at a ΔK = 12 MPa√m with the direction of crack growth from right to left denoted by the white arrow. Individual grains and grain boundaries can be seen on the surface. The purpose of etching the surface was to observe the interaction between the crack path, grain/grain boundaries, and precipitates. In Figure 4.9(a) the bottom portion of the crack opening indicates that crack propagation was along the grain boundary and the primary mode of crack growth was intergranular. This mode of crack propagation is consistent with the observations made on the fracture surfaces of the C(T) specimens during hold times.

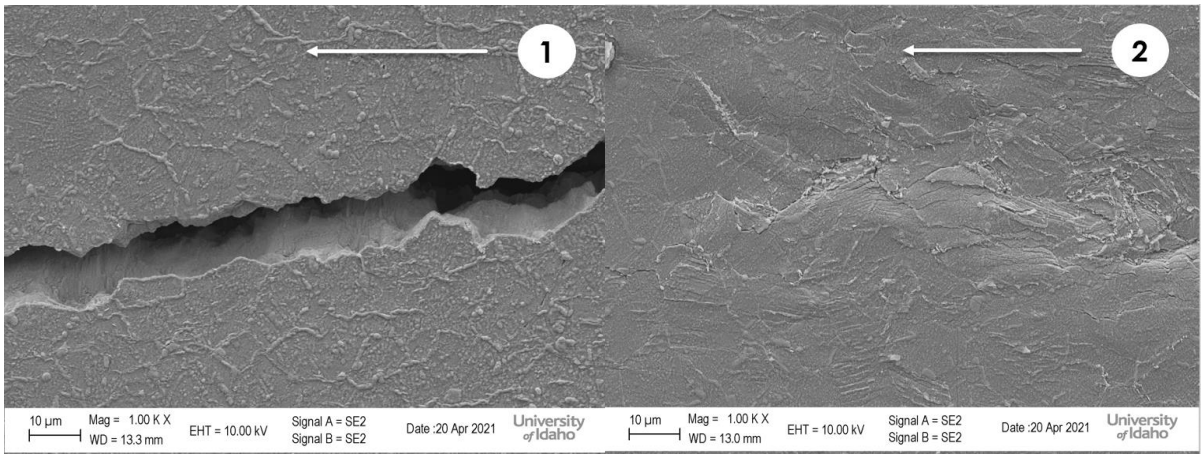

(a) (b)

Figure 4. 9: Crack profile of unloaded (60s hold) SEN prior to fracture, a) ΔK = 12 MPa√m, b) ΔK = 35 MPa√m (near the crack tip – mostly closed).

Figure 4.9(b) shows the crack tip of the unloaded (60s hold) SEN specimen prior to fracture at a ΔK = 35 MPa√m with the direction of crack growth from right to left denoted by a white arrow. Extensive plastic deformation can be seen at the tip of the crack as well as slip bands within individual grains. For the 600s hold and CCG test, similar crack path and grain/grain boundary interactions were observed.

4.3 Wrought IN718 C(T) and SEN Comparison

In Figure 4.10(a) fatigue crack growth rates for C(T) and SEN geometries are compared. Though the FCG growth tests (2 Hz and 15 Hz) were conducted at different frequencies, the curves were very similar. Had the 15 Hz SEN FCG test finished at a ΔK = 40 MPa√m, this data

would have aligned with the 2 Hz C(T) test. Comparing SEN and C(T) 60s hold tests the SEN data aligned reasonably well with the 60s C(T) tests and had only a 5% to 10% increase in da/dN for a given ΔK. The 600s hold SEN data showed a slight increase in da/dN for a given ΔK but was very comparable to the 600s hold C(T) tests. With only one SEN specimen tested at each loading cycle, the repeatability of the SEN data is unknown, but the overlap shows good consistency between the two specimen geometries. While loading for the C(T) specimens was in the radial (R) direction and for the SEN specimens in the circumferential (C) direction with respect to the forgings in Figure 3.1, the comparison shows that differences in specimen geometries and orientation are negligible. Comparing the two specimen geometries as time rate of crack growth, da/dt, as a function of K_{max} shown in Figure 4.10 (b), both C(T) and SEN hold data fall within a single scatter band.

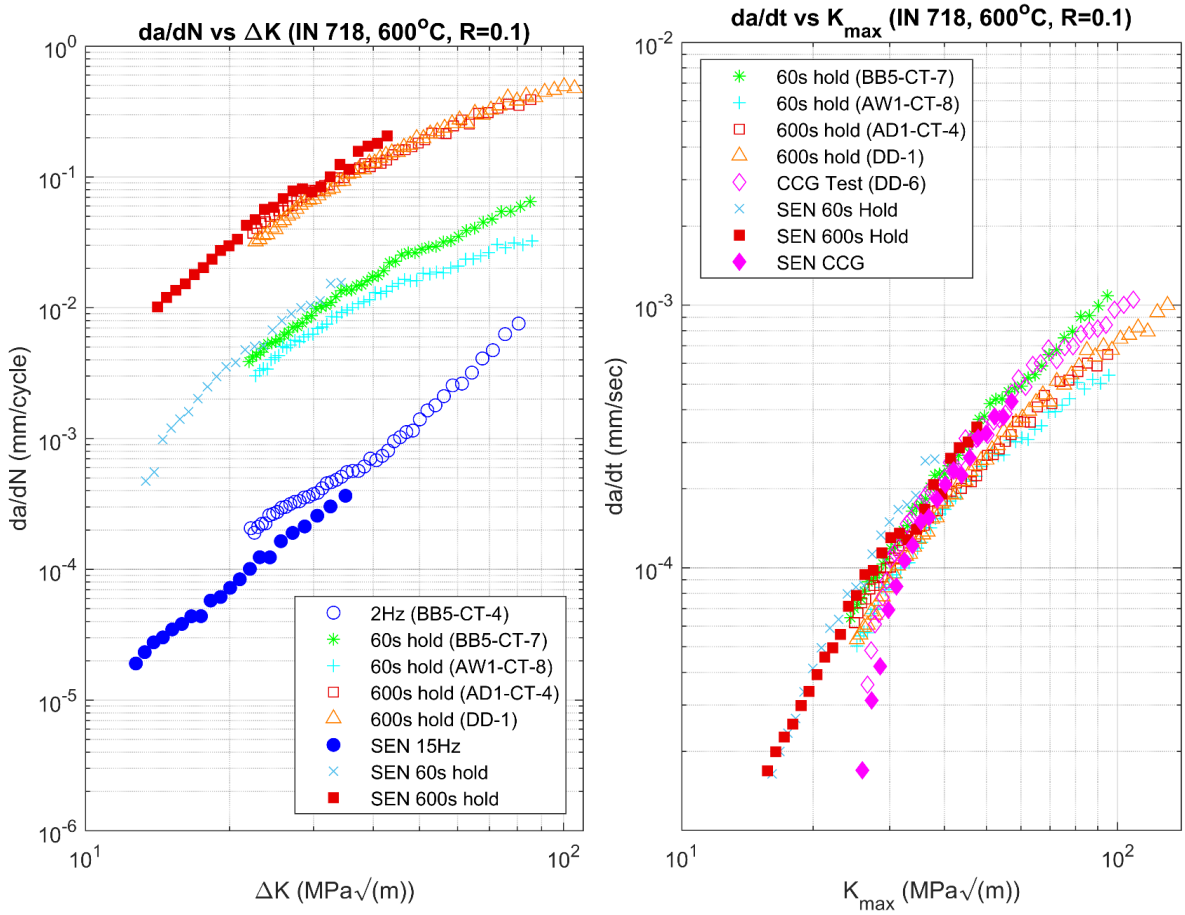

(a) (b)

Figure 4. 10: C(T) and SEN crack growth rates for wrought IN718, (a) fatigue crack growth rate, (b) time rate of crack growth.

4.4 AM IN718 C(T)

Eight AM IN718 C(T) specimens were machined from blocks printed in two different orientations. The print orientations are shown in Figure 3.3. In the vertical print orientation two specimens were machined with the notch parallel to the build direction (P-type) and the other two specimens were machined with the notch normal to the build direction (N-type). Both P-type and N-type specimens were tested under CFCG conditions at 600^{o}C with R = 0.1, and ΔK_i = 20 MPa√m to match the loading conditions used with the wrought C(T) specimens. The P-type and N-type specimens were also tested under CCG conditions with the same initial crack length and P_{max} as the CFCG tests. For the horizontal print orientation two specimens were machined from each block where the notch for the first two specimens was rotated 90 degrees from the next two machined specimens. The machining orientation for the horizontal specimens (H-type) are numbered 3 and 4 in Figure 3.4.

The first test conducted was an N-type specimen loaded under CFCG conditions with a 600s hold time. Crack growth could not be initiated at the starting condition so the hold time test was stopped, and the specimen was cycled at 15 Hz under the same initial P_{max} until a change in DCPD voltage could be seen, indicating crack growth. The 600s hold test was started again with the same initial P_{max} but again crack growth could not be initiated. The specimen was cycled again at 15 Hz under the same initial P_{max} until a change in DCPD voltage could be seen, and then the hold time test was started after an increase in P_{max} of 10%. Crack growth under increased P_{max} for the 600s hold time could not be initiated so the same cycling and holding pattern was conducted until P_{max} was finally increased by 38%, and a change in DCPD voltage indicated crack growth.

A P-type specimen was tested next and loaded under CFCG conditions with a 600s hold time and no additional steps were required to initiate crack growth. Tests three through six were H-type specimens and were tested under FCG, CFCG, and CCG conditions at 600^{o}C with the same initial P_{max} as the P-type and N-type specimens. The first H-type specimen was tested at a frequency of 2 Hz to match the first wrought IN718 FCG test. The next two H-type specimens were tested under CFCG conditions with a 60s and 600s hold and the last H-type specimen was

tested under CCG conditions. For the H-type CCG test crack growth was not observed under the same initial P_{max} as the FCG and CFCG tests so the same cycling and holding pattern used with the N-type 600s hold test was used until P_{max} was increased by 20% and a change in DCPD voltage indicated crack growth. The seventh test was a P-type specimen tested under CCG conditions. The P-type CCG test had the same issue with crack growth under the initial loading conditions so the cycling and holding pattern was used until P_{max} was increased by 20%. The last test was also conducted under CCG conditions with an N-type specimen. Crack growth did not occur at the initial loading condition so the cycling and holding pattern was used until P_{max} was increased 38%. The crack growth rates for AM IN718 are shown in Figure 4.11 and a summary of AM C(T) FCG, CFCG, and CCG results are shown in Table 4.4.

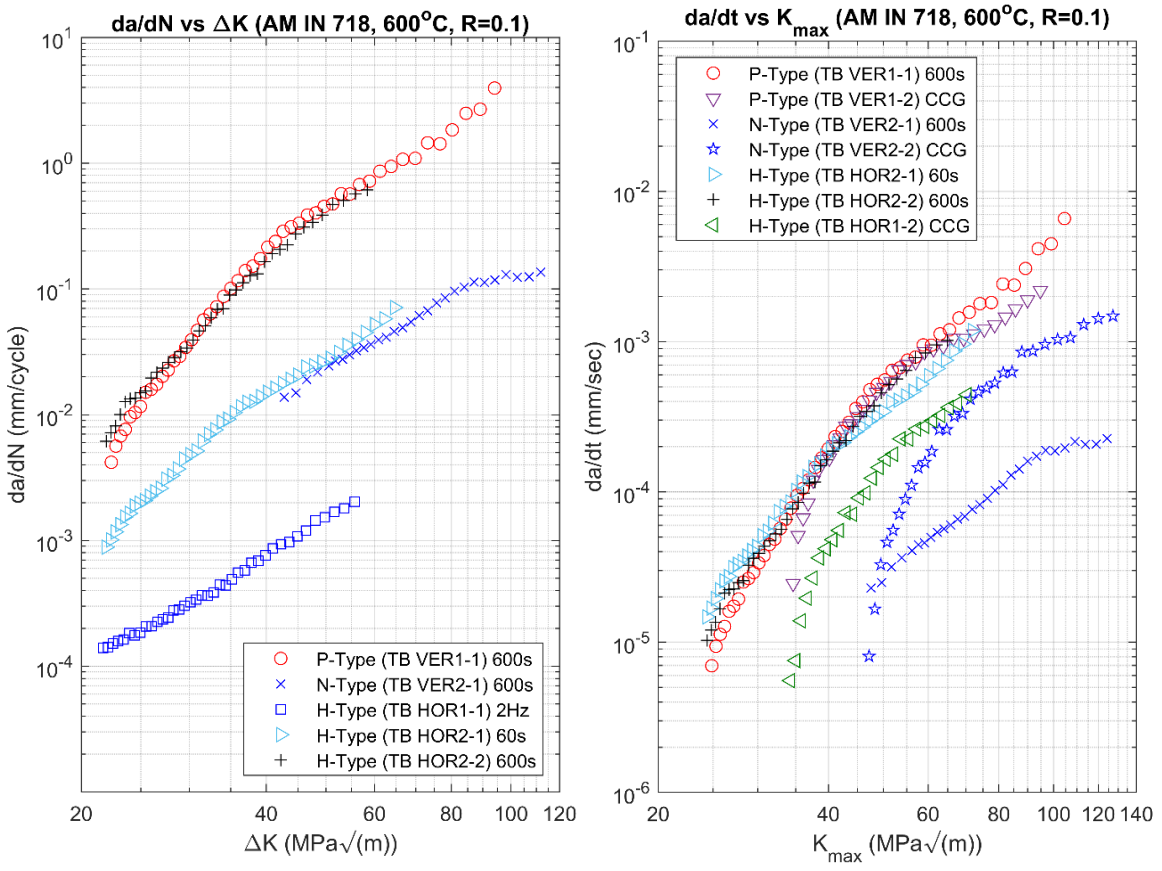

(a) (b)

Figure 4. 11: Crack growth rates for AM IN718, (a) fatigue crack growth rate, (b) time rate of crack growth.

When comparing 2 Hz, 60s, and 600s results for the three different print orientations in Figure 4.11(a), there is an increase in crack growth rate with respect to ΔK for the H-type 60s and 600s hold and P-type 600s hold compared to the H-type 2 Hz test. The P-type and H-type 600s hold tests showed similar crack growth behavior. Where only one 60s hold test was conducted with an H-type specimen, no comparison was available. Comparing the 60s and 600s hold tests, a 10x increase in time from a 60s hold to 600s hold resulted in approximately a 10x increase in crack growth rate with respect to ΔK for the H-type and P-type specimens. The N-type 600s hold specimen is also shown in Figure 4.11, but due to off plane crack growth shown in Figure 4.13 this data cannot be directly compared to the other orientations. Due to an equipment malfunction, DCPD and COD data was not collected during the first portion of the N-type 600s hold test, but visual crack length data was collected. The N-type 600s curve in Figure 4.11 represents a combination of the visual data points taken during the beginning of the test and the last portion of the test where DCPD data was collected.

When plotting hold time data shown in Figure 4.11(a) as (da/dt vs $K_{max,}$) in Figure 4.11(b), the H-type 60s and 600s hold and P-type 600s hold tests collapse to form a single scatter band. P-type and H-type CCG tests are also plotted in Figure 4.11(b) and fall within the same scatter band as the 60s and 600s hold tests except for the H-type CCG test which had a roughly 30% lower crack growth rate for a given K_{max}. The P-type and H-type CCG tests showed lower da/dt values for a given K_{max} vs. the CFCG tests at initial values of K_{max}. There was also a significant shift to the right of the initial K_{max} values due to the higher initial values of P_{max} required as discussed above. It is unclear why there was a need to increase the initial values of P_{max} to generate crack growth under CCG conditions, but it might be related to reduced effects of grain boundary oxidation and dynamic embrittlement for the AM material. This was also suggested by Deng *et al*. regarding the AM material. As a result, the primary mode of crack growth regarding the AM CCG tests is attributed to some other form of time dependent crack growth. The N-type CCG tests is also shown in Figure 4.11(b). Though starting and ending conditions of the N-type 600s hold and CCG tests are very similar, the CCG test has a 5x greater crack growth rate for a given K_{max}. It is unclear why these two data sets are dissimilar. It is obvious that the AM material, mostly the N-type, exhibited anisotropic behavior as the various orientations produce different crack growth behavior.

Table 4. 4: Summary of AM C(T) FCG, CFCG, and CCG results.

Fatigue Crack Growth/Creep Fatigue Crack Growth/Creep Crack Growth								
Specimen ID	Waveform	a_i (mm)	a_f (mm)	P_{max} (kN)	ΔK_i (MPa $\sqrt{m}$)	ΔK_f (MPa $\sqrt{m}$)	# Cycles	Hours
TB-VER1-1	600s	20.5	40.5	8.9	20.6	114.3	843	140.5
TB-VER1-2	CCG	23.0	38.2	10.7	K_{max}=31.5	K_{max}=110.2	N/A	37.5
TB-VER2-1	600s	26.3	39.1	12.2	39.4	128	481	80.2
TB-VER2-2	CCG	25.7	39.6	12.2	K_{max}=42.2	K_{max}=152.6	N/A	106.6
TB-HOR1-1	2 Hz	19.9	35.6	8.9	20	61	49540	6.9
TB-HOR1-2	CCG	22.8	35.2	10.7	K_{max}=31.1	K_{max}=78.1	N/A	190.4
TB-HOR2-1	60 s	20.2	37.18	8.9	20.3	72.9	5306	88.4
TB-HOR2-2	600s	20.2	36.5	8.9	20.3	67.4	717	119.5

Fracture surfaces were measured using the same method as the wrought C(T) specimens. The fracture surfaces of all AM C(T) specimens are shown in Figure 4.12 with the direction of crack growth from right to left. On the fracture surfaces of the P-type CCG, N-type 600s hold and CCG, and H-type CCG test, the crack growth during the cycling and holding patterns are labeled 3. An additional difference can be seen on the fracture surface of the P-type 600s hold test that is different than the others. In the room temperature fracture region of this test on the far left of the fracture surface, the surface is discolored and not light gray like the others. The reason for discoloration is exposure to air while under temperature due to fracturing while in the furnace. Fracture in the furnace was caused by improper interlock settings on the

controller. To determine final crack length of the specimen before fracture, the specimen had to be analyzed under and optical microscope to locate the point of failure due to yielding.

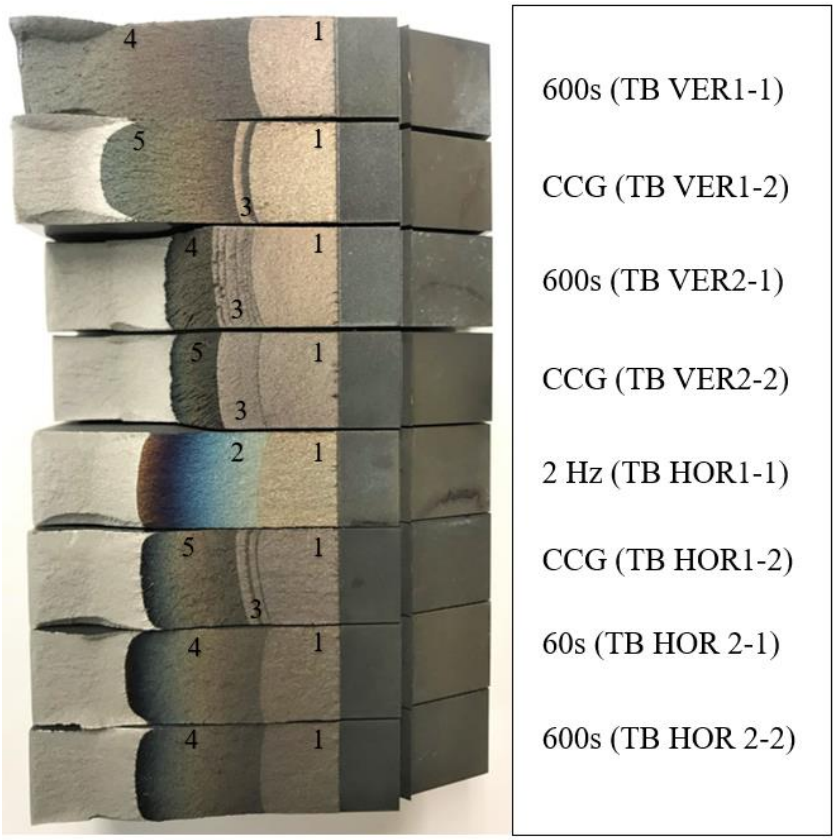

Figure 4. 12: Fracture surface of AM C(T) specimens. 1) Pre-crack region, 2) FCG region, 3) cycling and holding pattern in Appendix A. (12-14,16), 4) CFCG region, 5) CCG region.

Another fracture surface observation can be made with the N-type 600s hold and CCG specimens. In Figure 4.13 the fractured halves of both N-type C(T) specimens are shown. The 600s hold specimen in the rear had an initial crack length of 26.3 mm and the CCG specimen had an initial crack length of 25.7 mm. After each test started the cracks in both specimens began to grow off plane at an angle approximately 55^{o} from horizontal. The same N-type tests were studied by Deng *et al*. with a hold time of 2160s and showed similar off plane crack growth [11]. This off plane crack growth is attributed to crack propagation along the grain boundaries of long columnar vertically oriented grains with respect to the horizontally oriented notch.

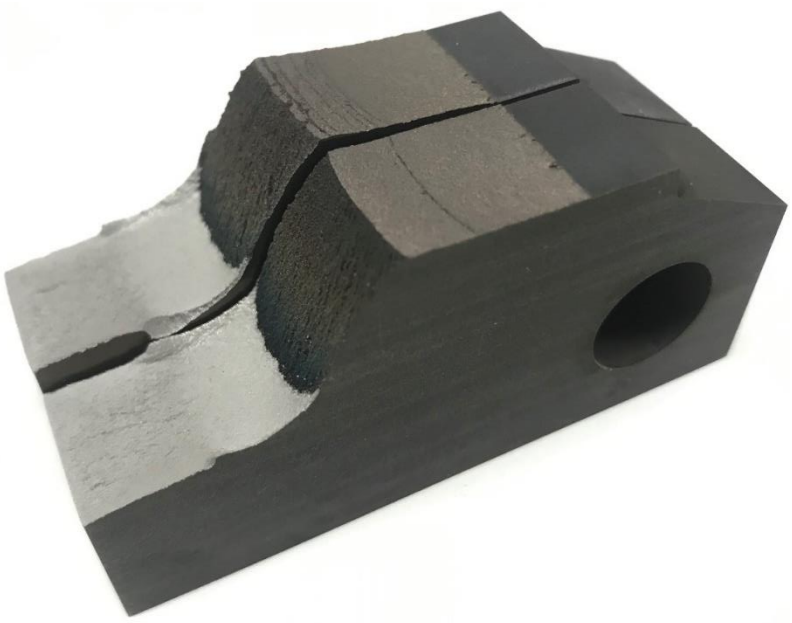

Figure 4. 13: Fractured halves of N-type C(T) specimens.

As with the wrought C(T) tests, COD data was collected for all AM C(T) specimens using the same MTS extensometer referenced in Section 3.2. The COD data collected was used to analyze LLD during individual cycle hold times for comparison with wrought C(T) specimens. In Figure 4.14 change in LLD (ΔV_c) during the 600s hold tests are plotted as a function of ΔK for the three different specimen orientations. As with the wrought 60s hold test, small displacements were observed with the H-type 60s hold test, so this data is not represented in Figure 4.14. The P-type and H-type 600s hold show similar ΔV_c for given values of ΔK and are significantly larger than the ΔV_c for the 600s hold N-type specimen. It is important to note that ΔK values of N-type data are representative of the actual crack length seen on the angled surface of Figure 4.13 and not the projected crack length. Regardless of the value of ΔK, the N-type specimen experienced a ΔV_c less than 5μm during the duration of the test.

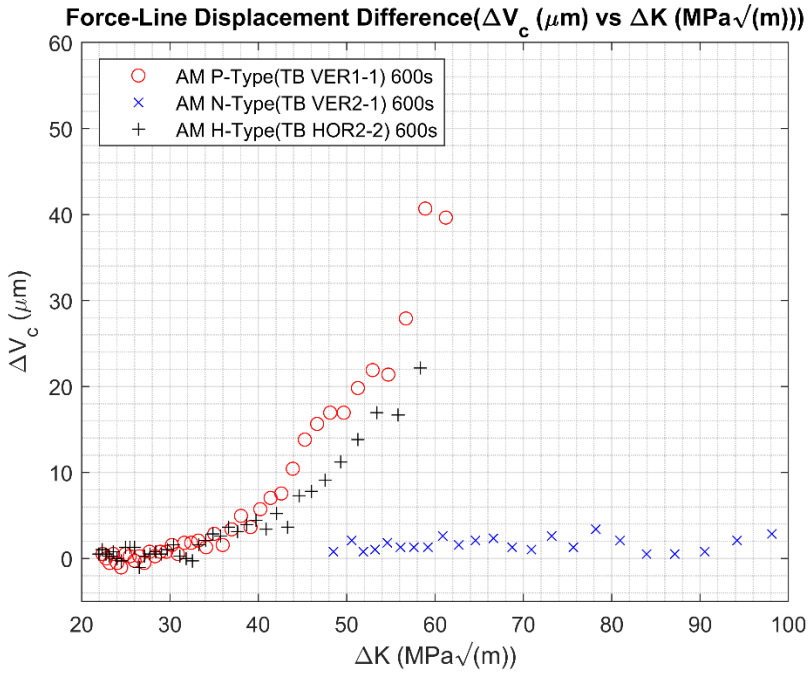

Figure 4. 14: Force-line displacement difference (ΔV_c) vs. ΔK for AM 600s hold time.

4.5 Wrought and AM IN718 Comparison: FCG, CFCG, CCG

In Figure 4.15 fatigue crack growth rates (2 Hz–15 Hz) for wrought C(T) and SEN geometries and AM C(T) specimens are compared. The wrought and AM 2 Hz tests align well and show the same crack growth rate for a given ΔK. The SEN 15 Hz curve is also very similar, and appears that it would have merged with the other curves if the test had continued beyond a ΔK = 40 MPa√m. In Figure 4.16 crack growth rates for wrought and AM 60s hold C(T) specimens are compared. Due to limited AM specimens, only one 60s hold test was conducted with an H-type orientation. In Figure 4.16, the AM specimen starts at a lower crack growth rate for a given ΔK than the wrought specimens. The curve of the AM specimen also has a steeper slope, so it intersects the wrought data at approximately ΔK = 40 MPa√m. While the slope of the AM data is steeper than the wrought, it shows better resistance to crack growth for a given ΔK less than 40 MPa√m.

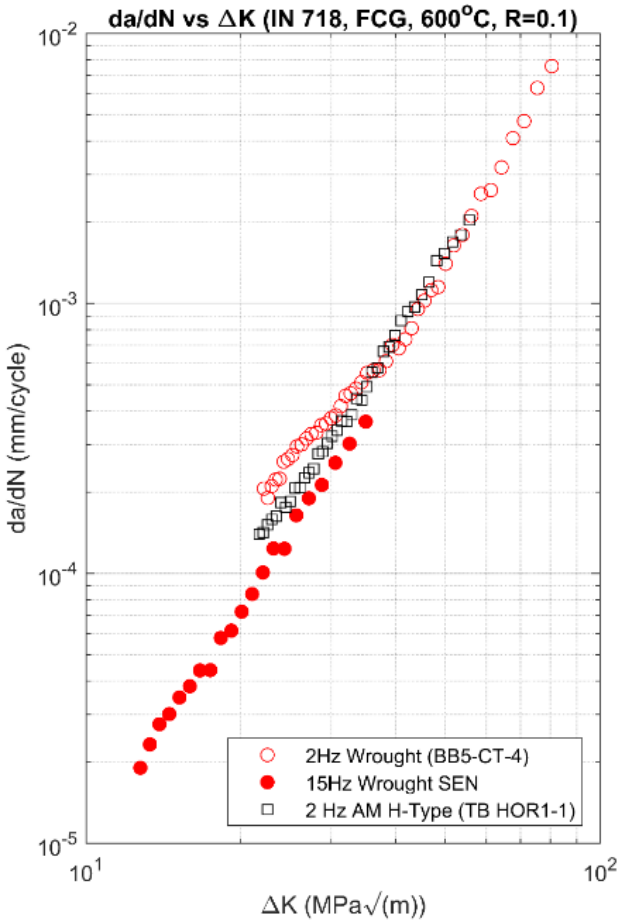

Figure 4. 15: Fatigue crack growth rates for AM and wrought IN718.

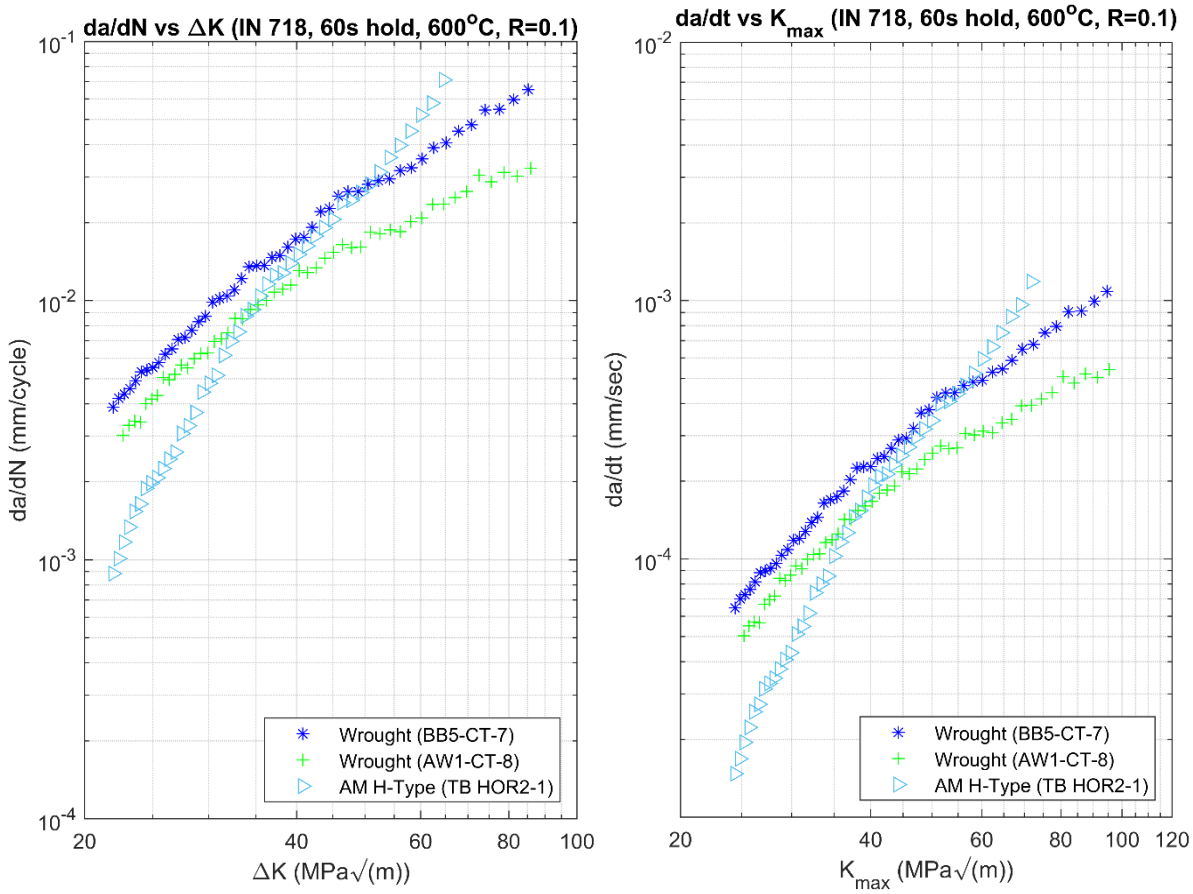

(a) (b)

Figure 4. 16: Crack growth rates for 60s hold time of AM and wrought IN718, (a) fatigue crack growth rate, (b) time rate of crack growth.

In Figure 4.17 crack growth rates for wrought and AM 600s hold C(T) specimens are compared. In Figure 4.17(a), the AM P-type and H-type specimens start at a lower crack growth rate for a given ΔK than the wrought specimens. The curve of the AM specimens also has a steeper slope, so it intersects the wrought data at approximately ΔK = 35 MPa√m. Though the slope of the AM data is steeper than the wrought, it shows better resistance to crack growth for a given ΔK less than 35 MPa√m. This behavior is similar to that observed in Figure 4.16 for the AM and wrought 60s hold tests. To better quantify how crack growth resistance effects total life or time until failure a comparison between the wrought and AM 600s hold tests from Figure 4.17 are made using data from Tables 4.1 and 4.4. It is important to note that in this comparison the pre-cracking procedure and the starting loads were the same for the wrought and AM

specimens. From Table 4.1 the two wrought 600s hold tests started at ΔK = 20.4 and 20.8 MPa$\sqrt{m}$ and cycled 35 and 41 hours until failure. From Table 4.4 the H-type and P-type AM 600s hold tests started at ΔK = 20.3 and 20.6 MPa$\sqrt{m}$ and cycled 119.5 and 140 hours until failure. A lower starting crack growth rate for the AM IN718 resulted in the 600s hold tests running an average of 92 hours or roughly 3x longer than the wrought 600s hold tests. Although there is a crossover in CFCG data for the wrought vs. AM IN718, the comparison shows the significance of a lower initial crack growth rate on the total time cycled until failure. The N-type specimen also started at a lower crack growth rate for a given ΔK compared to the wrought, H-type, and P-type specimens. It is important to note however that for the N-type specimen, the crack lengths used in determining da/dN and ΔK are the actual crack lengths seen in Figure 4.13 and not the projected (horizontal or mode I) crack length. Where crack growth was off plane, the N-type specimen cannot truly be compared to the other specimens because it falls outside the parameters of mode I crack growth.

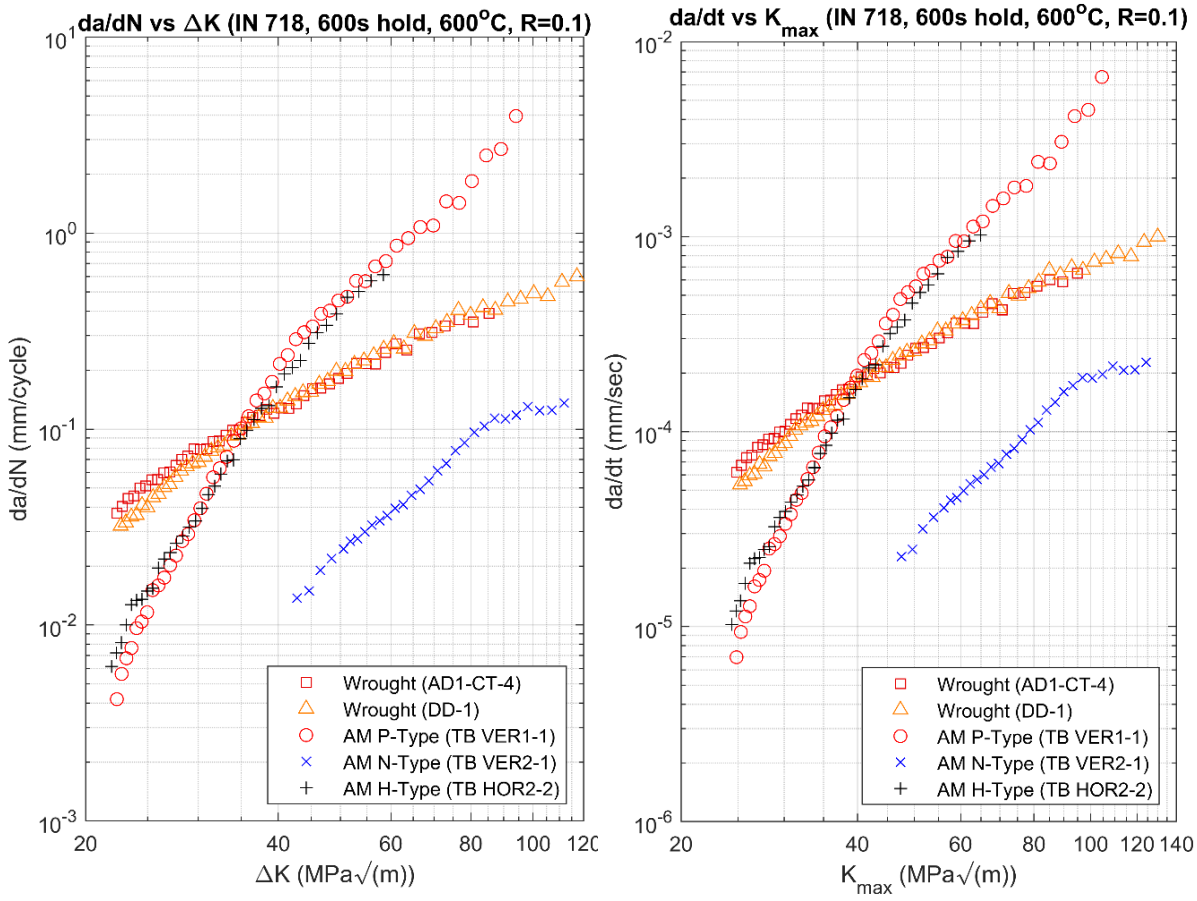

(a) (b)

Figure 4. 17: Crack growth rates for 600s hold time of AM and wrought IN718, (a) fatigue crack growth rate, (b) time rate of crack growth.

In Figure 4.18, creep crack growth rates for wrought and AM C(T) specimens are compared. Similar to the 60s and 600s hold, the AM specimens start at a lower crack growth rate for a given K_{max} compared to the wrought specimen. The P-type CCG test intersects the wrought CCG tests at a K_{max} = 40 MPa√m which is consistent with the intersection points of the 60s and 600s hold tests. It is important to note again that the N-type CCG test was evaluated using the actual crack length, so this data cannot be truly compared to the other CCG data.

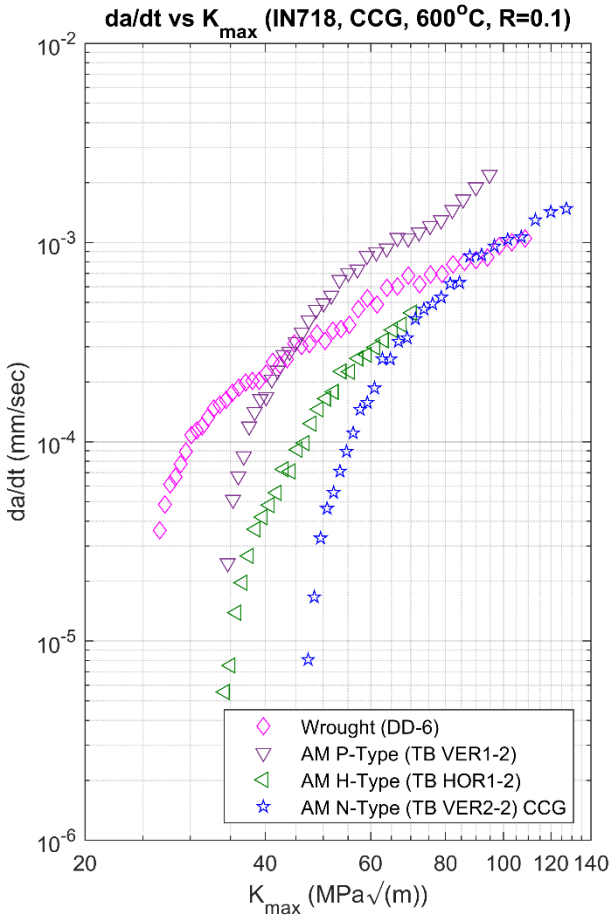

Figure 4. 18: Time rate of crack growth for AM and wrought IN718 CCG tests.

A combination of all wrought and AM hold time and CCG tests are shown in Figure 4.19. A trend can be seen in Figure 4.19(b) where the AM P-type and H-type tests intersect the wrought tests at approximately K_{max} = 40 MPa√m. At a K_{max} less than 40 MPa√m, the AM hold time and CCG specimens show better resistance to crack growth at a given K_{max} than the wrought hold time and CCG tests.

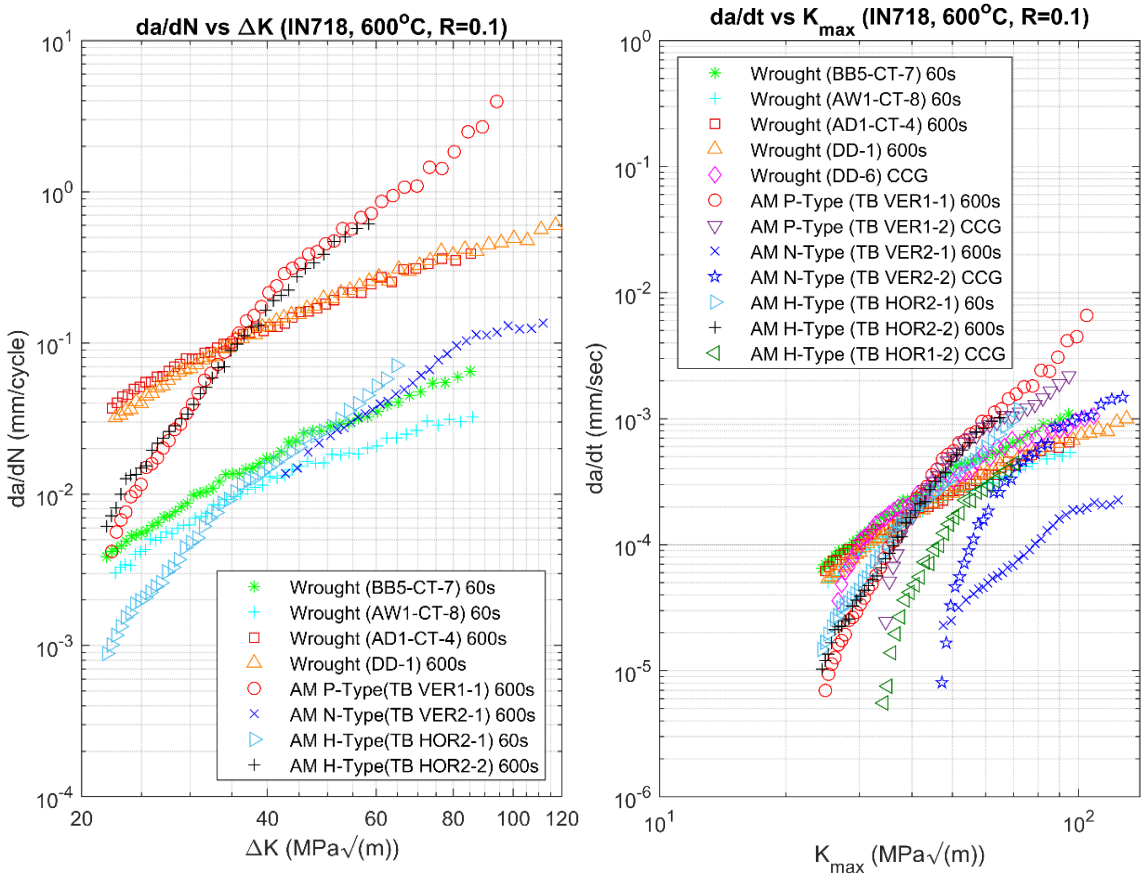

(a) (b)

Figure 4. 19: Crack growth rates of AM and wrought IN718, (a) fatigue crack growth rate, (b) time rate of crack growth.

In Figure 4.20 the force-line displacement difference (ΔV_c) vs. ΔK for AM and wrought 60s and 600s hold tests are compared. At ΔK values less than 35 MPa$\sqrt{m}$, values of ΔV_c are approximately the same. At a ΔK of approximately 35-40 MPa$\sqrt{m}$, the AM and wrought data begin to diverge. As ΔK increases, ΔV_c for the AM specimens becomes significantly greater than the ΔV_c for the wrought specimens. The increase in ΔV_c for the AM P-type and H-type compared to the wrought occurs very close to the cross over point in the da/dN vs ΔK plots. An increase in ΔV_c indicates a greater creep contribution related to either crack growth or creep damage. For wrought IN718, the primary mode of crack growth has been attributed to SAGBO or DE as shown by Gustafsson *et al.* and Krupp [5,7]. For the AM material, it is possible that additional creep mechanisms are superimposed on the two proposed mechanisms resulting in

higher crack growth rate at high ΔK or K_{max} as seen with the AM P-type and H-type. This is consistent with what Deng *et al*. suggested in his AM IN718 study regarding inferior creep resistance (enhanced creep) with the P-type orientation. Therefore, it is possible to say that lower (ΔV_c) corresponds to a lower crack growth rate when comparing wrought and AM IN718, and as ΔK increases ΔV_c for AM IN718 becomes greater than ΔV_c for wrought IN718 leading to higher crack growth rates for AM IN718 versus wrought IN718.

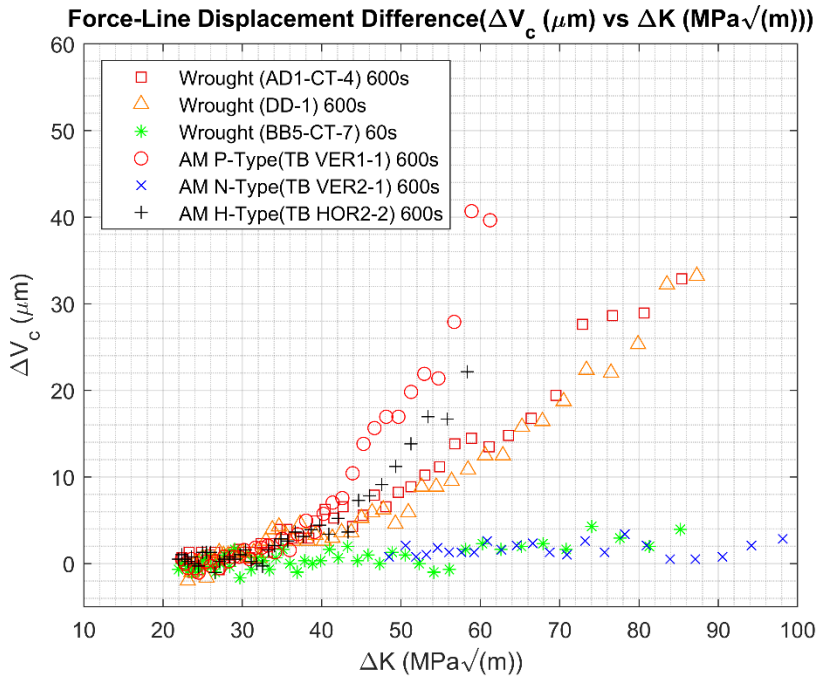

Figure 4. 20: Force-line displacement difference (ΔV_c) vs. ΔK for AM and wrought 60s and 600s hold times.

4.6 Wrought and AM IN718 Fractography

Fracture surfaces of wrought and AM C(T) specimens were observed using the SEM outlined in Section 3.2. In all SEM images the direction of crack growth is from right to left. Figure 4.21 shows the wrought C(T) fracture surfaces of the 2 Hz FCG test, 60s hold, 600s hold, and CCG test at initial conditions. In Figure 4.21 the right half of the SEM images show the end of the pre-crack, and the left half shows the FCG, CFCG, or CCG portions of the test. The fracture surface of the 2 Hz FCG test shows transgranular crack growth where the 60s hold,

600s hold, and CCG tests show intergranular cracking during crack growth. All tests show signs of secondary cracking during crack growth.

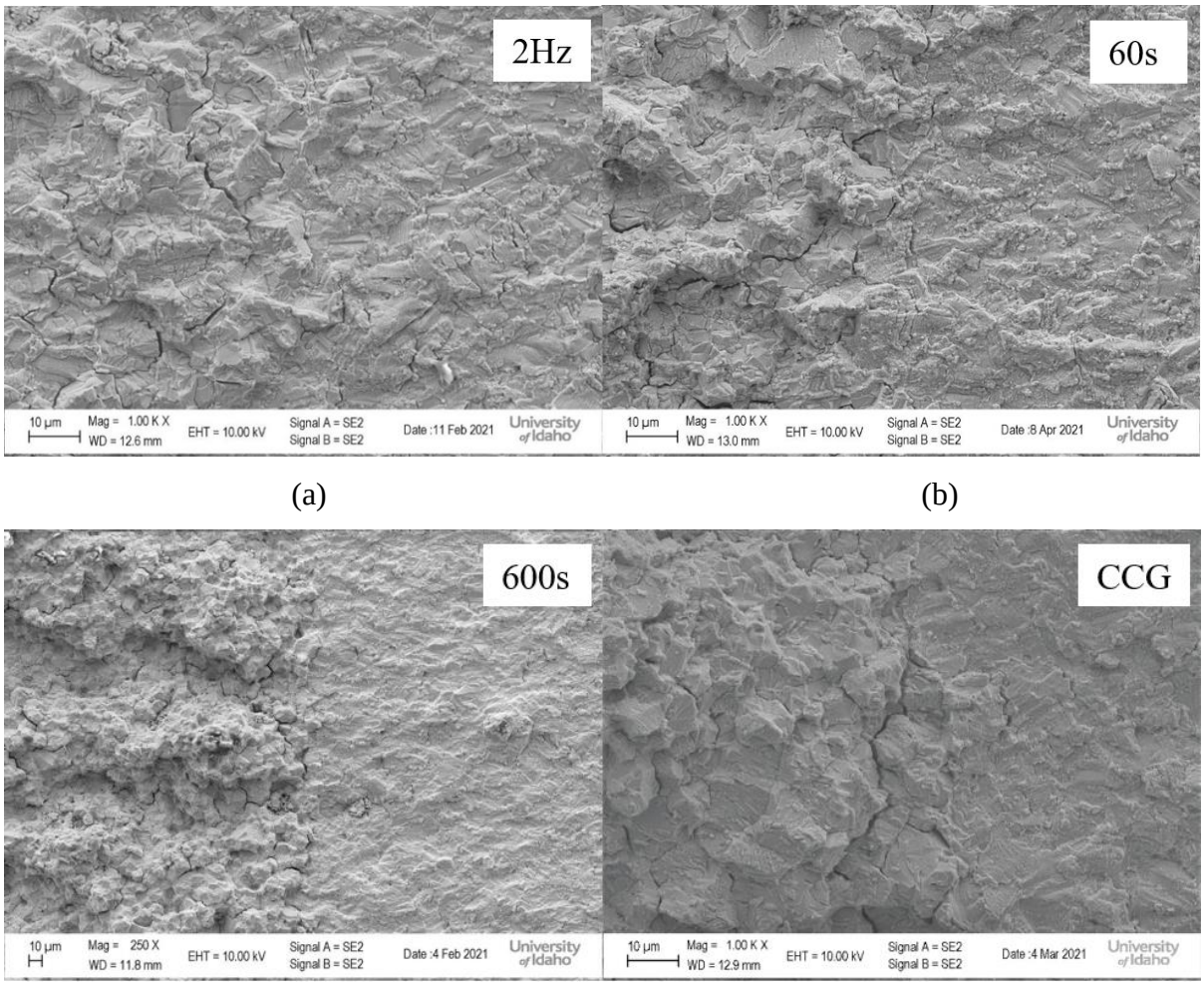

Figure 4. 21: Wrought fracture at initial $\Delta K = 20$ MPa√m, a) 2 Hz FCG, b) 60s hold CFCG, c) 600s hold CFCG, d) CCG – $K_{max} = 24$ MPa√m.

Figure 4.22 show the same fracture surfaces as in Figure 4.21, but at a $\Delta K = 40$ MPa√m. The 2 Hz test in Figure 4.22(a) shows small striations oriented vertically, perpendicular to the direction of crack growth which is from right to left. There is also secondary cracking aligned in the same direction of the striations but with larger openings in the secondary cracks than at $\Delta K = 20$ MPa√m. The 60s hold, 600s hold, and CCG tests fracture surfaces exhibit larger voids in the secondary cracks. The individual grains also appear more defined.

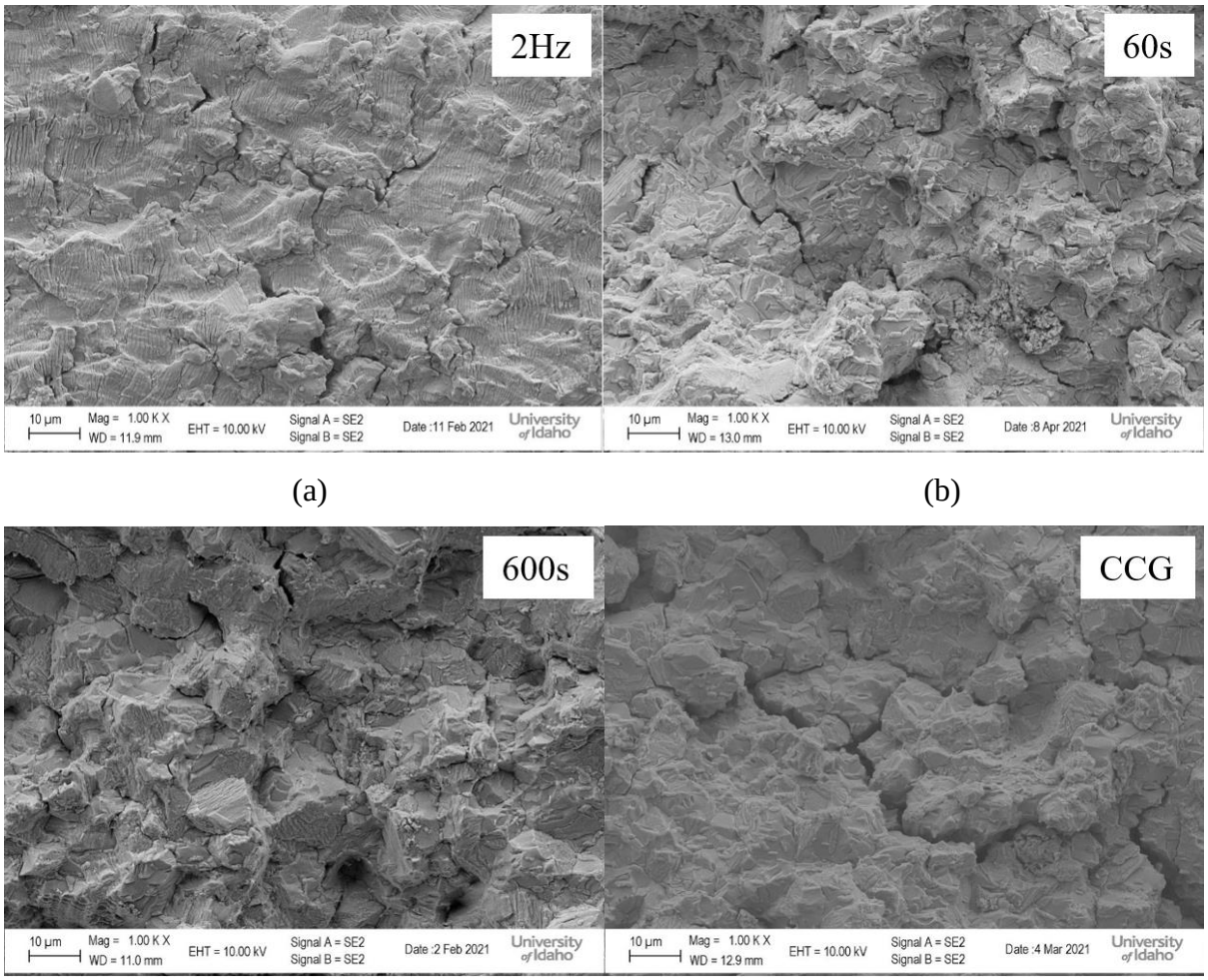

Figure 4. 22: Wrought fracture at ΔK = 40 MPa√m, a) 2 Hz FCG, b) 60s hold CFCG, c) 600s hold CFCG, d) CCG – K_{max} = 44 MPa√m.

At ΔK = 60 MPa√m in Figure 4.23(a), striations are more defined with larger spacing between each striation indicating a greater crack growth rate than at lower ΔK values. The fracture surfaces of the hold time and CCG tests exhibit even larger secondary crack openings which create small voids between clusters of grains.

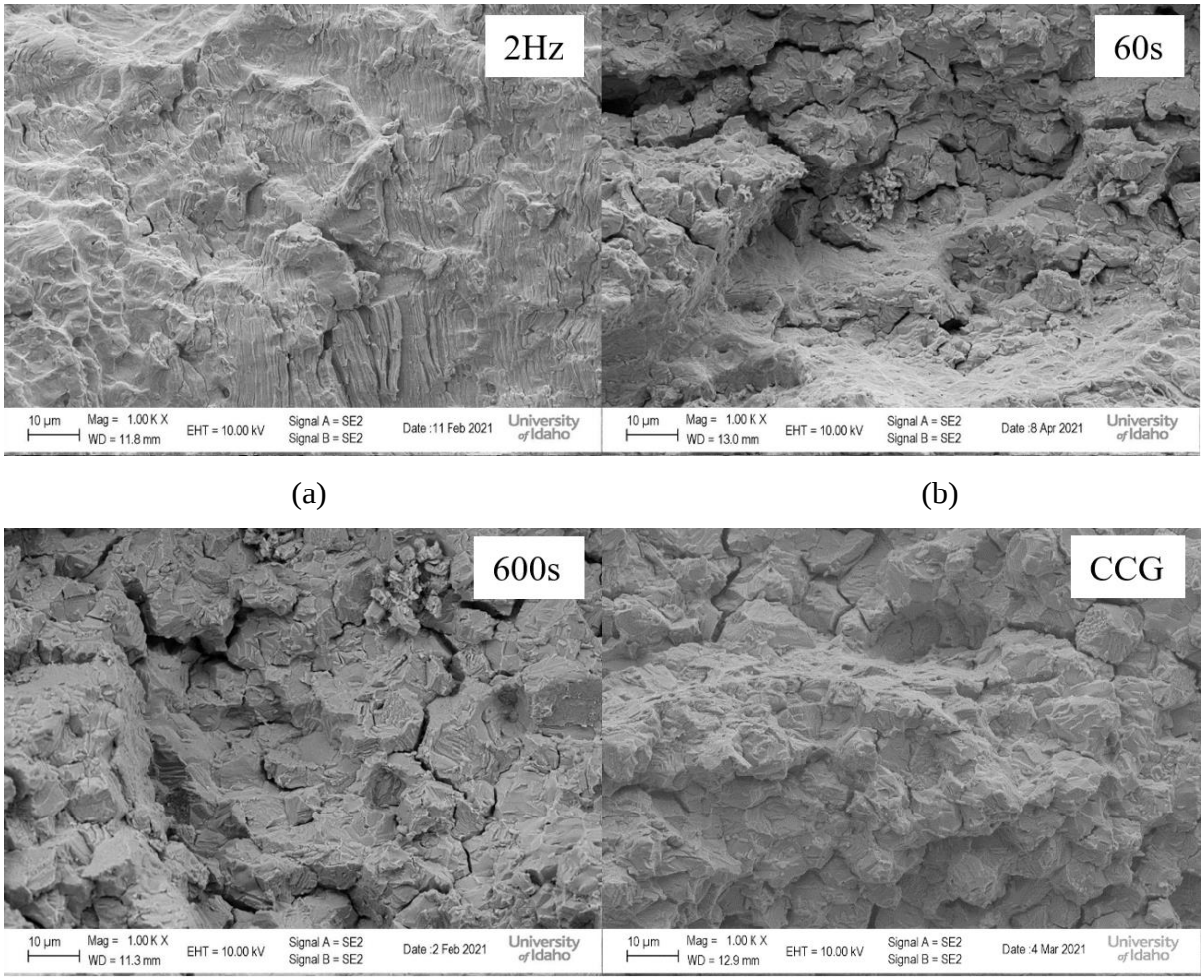

Figure 4. 23: Wrought fracture at ΔK = 60 MPa√m, a) 2 Hz FCG, b) 60s hold CFCG, c) 600s hold CFCG, d) CCG – K_{max} = 67 MPa√m.

At ΔK = 80 MPa√m in Figure 4.24(a), the striation spacing is larger indicating a greater crack growth rate than seen in Figure 4.23(a). At ΔK = 80 MPa√m all surfaces exhibit extensive secondary cracking and the fracture surfaces of the 60s and 600s hold time show very large voids between clusters of grains. At this high stress intensity, crack growth rates are very high and are approaching final fracture.

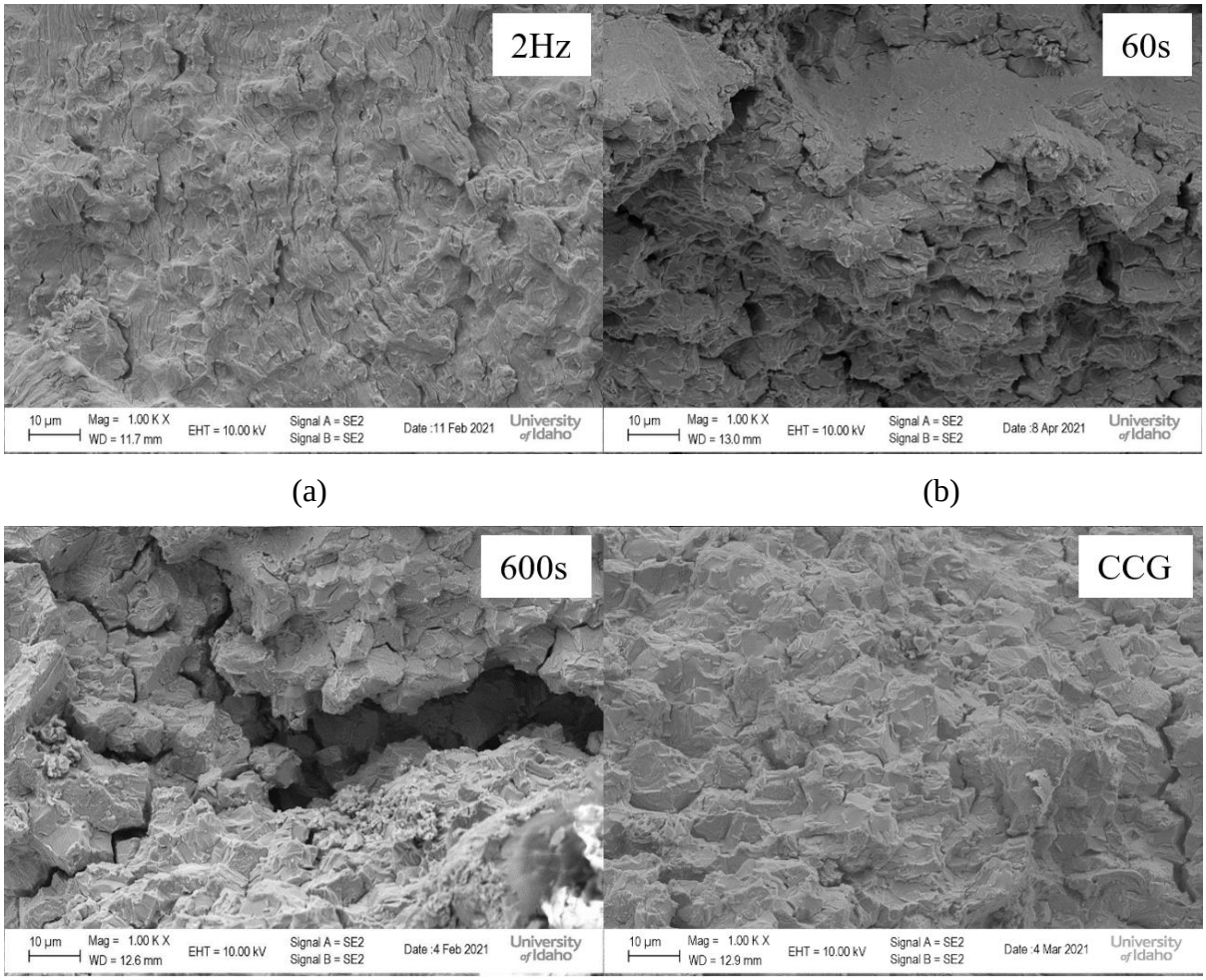

Figure 4. 24: Wrought fracture surfaces at ΔK = 80 MPa√m, a) 2 Hz FCG, b) 60s hold CFCG, c) 600s hold CFCG, d) CCG – K_{max} = 89 MPa√m.

Consistent with the wrought SEM images, the direction of crack growth in all AM SEM images is from right to left. Figure 4.25 shows the AM H-type C(T) fracture surfaces of the 2 Hz FCG test, 60s hold, 600s hold, and CCG test at the initial conditions shown in Table 4.4. Consistent with Figure 4.21, the right half of the SEM images show the end of the pre-crack, and the left half shows the FCG, CFCG, or CCG portions of the test. Unlike with the wrought SEM images in Figure 4.21, it is unclear whether the mode of crack growth remains transgranular from the end of the pre-crack into the high temperature CFCG/CCG portion or if there is a transition from transgranular to intergranular. However, the fracture surfaces on the right and left portions of the CFCG and CCG images in Figure 4.25 are dissimilar.

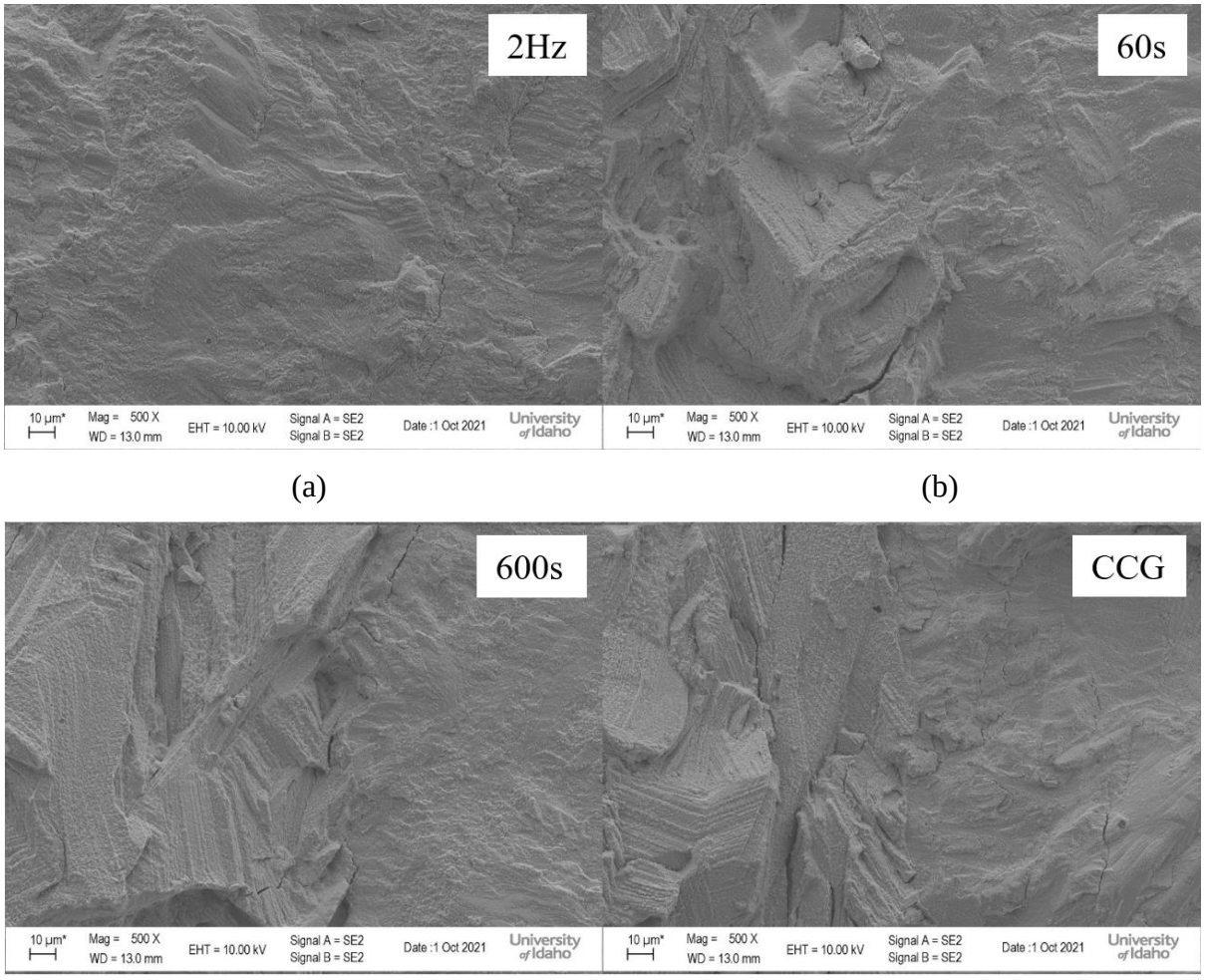

(a) (b)

(c) (d)

Figure 4. 25: AM H-type fracture surfaces at initial ΔK = 20 MPa√m, a) 2 Hz FCG, b) 60s hold CFCG, c) 600s hold CFCG, d) CCG – K_{max} = 31.1 MPa√m.

Figure 4.26 show the same fracture surfaces as in Figure 4.25, but at a ΔK = 40 MPa√m. In Figure 4.26(a) small vertically oriented striations can be seen perpendicular to the direction of crack growth which is from right to left. The 60s hold, 600s hold, and CCG fracture surfaces are much more textured than the FCG surface. They also have small linear ridges at differing angles but are mostly vertical. These linear ridges are different than the striations seen on the fracture surface of the FCG test in Figure 4.26(a) and in the case of the CCG test, are independent of cycles where the CCG test was held under constant load. It is unclear what the linear ridges are, but they are observed on the fracture surfaces of all AM specimens tested under CFCG and CCG. This fracture pattern is most likely associated with the printing or

deposition process where the same pattern was not seen on the fracture surfaces of the wrought specimens.

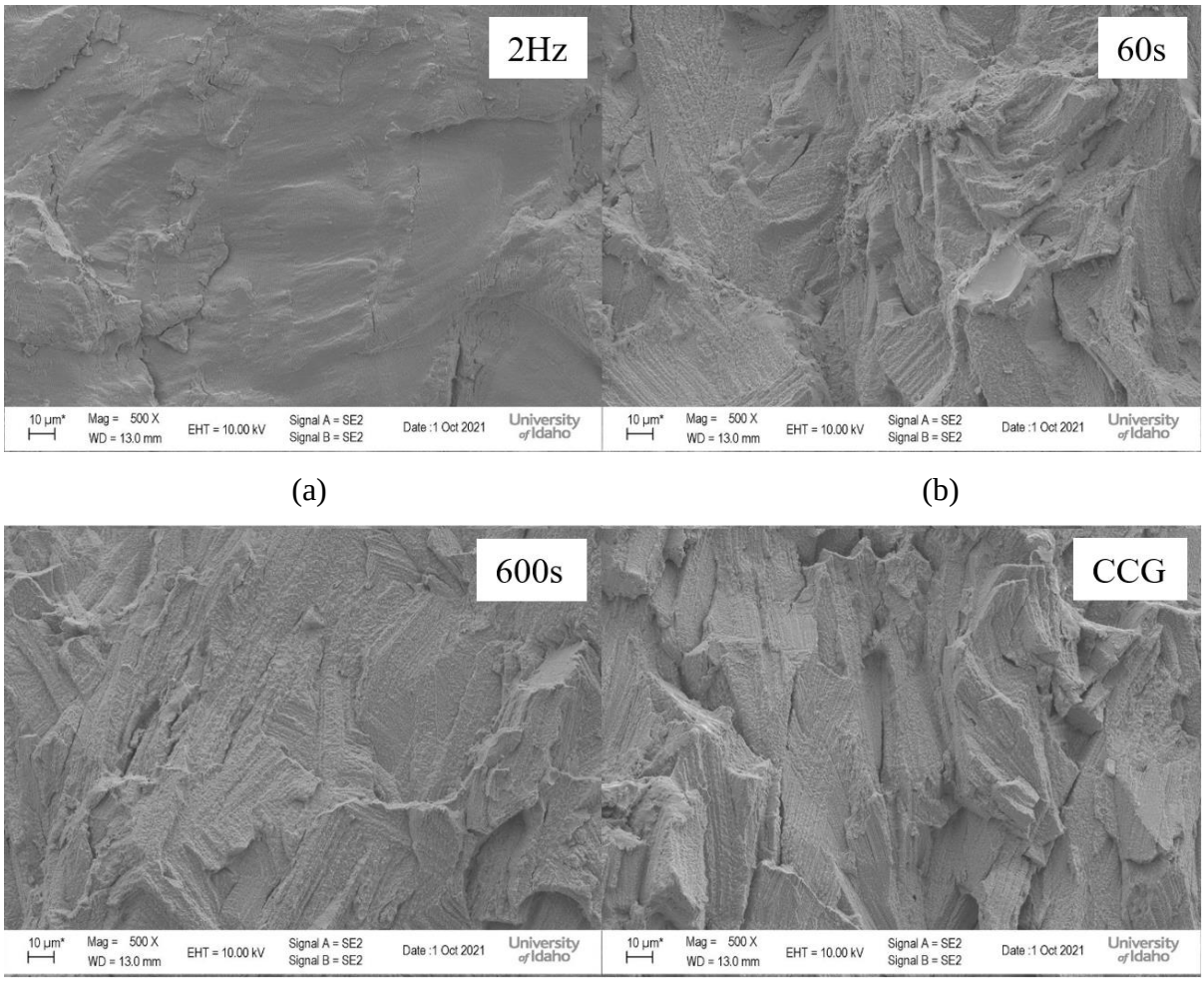

(a) (b)

(c) (d)

Figure 4. 26: AM H-type fracture surfaces at initial ΔK = 40 MPa√m, a) 2 Hz FCG, b) 60s hold CFCG, c) 600s hold CFCG, d) CCG – K_{max} = 44.6 MPa√m.

At ΔK = 60 MPa√m in Figure 4.27(a), striations are more defined with larger spacing between each striation indicating a greater crack growth rate than at lower ΔK values, and there also appears to be some delamination or secondary cracking oriented vertically which is perpendicular to the direction of crack growth. In Figure 4.27 the fracture surfaces of the 60s hold, 600s hold and CCG tests look very similar to the fracture surfaces in Figure 4.26 at a lower ΔK but do show some small vertically oriented secondary cracks.

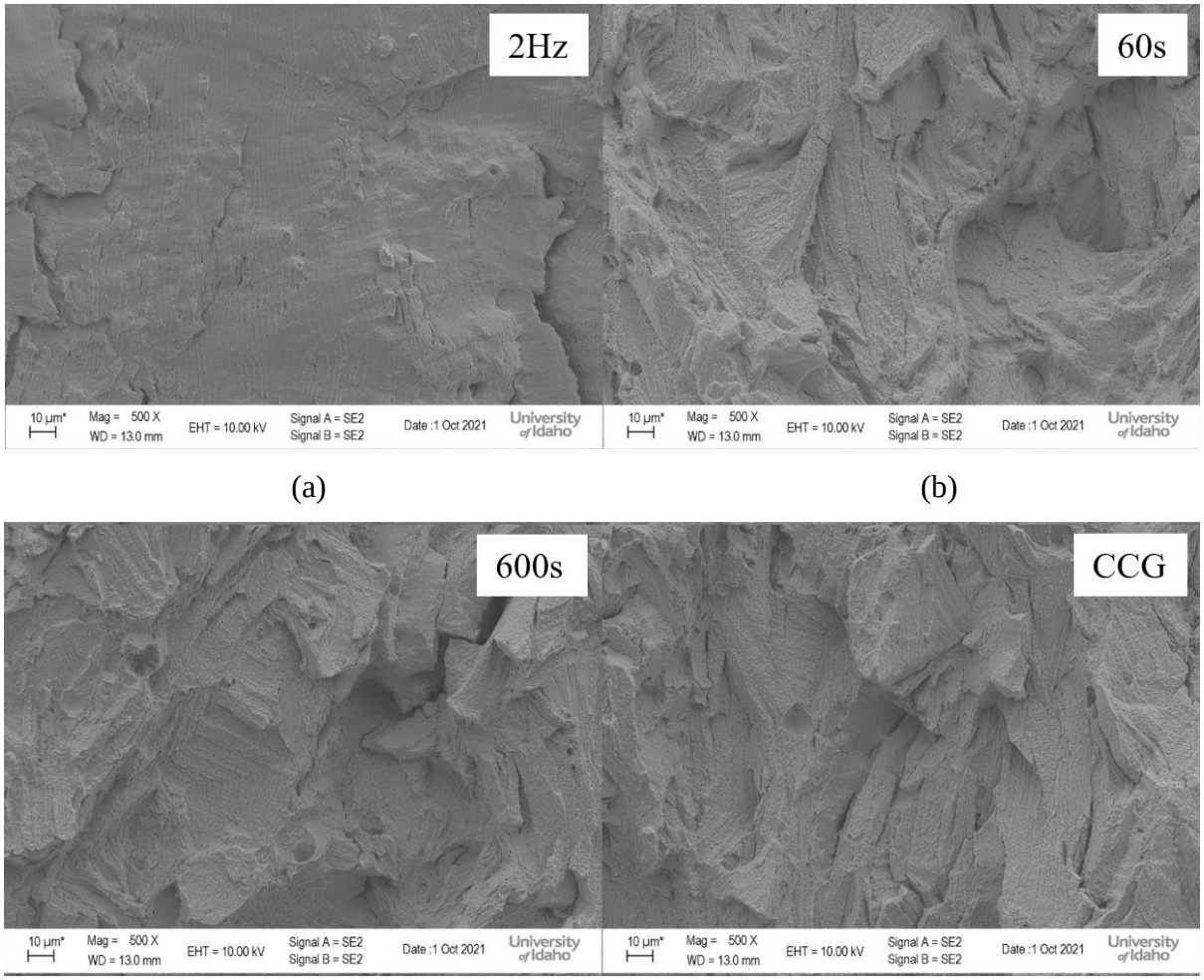

(a) (b)

(c) (d)

Figure 4. 27: AM H-type fracture surfaces at initial ΔK = 60 MPa√m, a) 2 Hz FCG, b) 60s hold CFCG, c) 600s hold CFCG, d) CCG – K_{max} = 66.7 MPa√m.

Figure 4.28 shows the AM P-type C(T) fracture surfaces of the 600s hold and CCG test at the initial conditions shown in Table 4.4. In Figure 4.28 the right half of the SEM images show the end of the pre-crack, and the left half shows the CFCG or CCG portions of the test. Similar to the H-type specimen it is unclear with the P-type specimen whether the mode of crack growth remains transgranular from the end of the pre-crack into the high temperature CFCG/CCG portion or if there is a transition from transgranular to intergranular. The fracture surfaces on the right and left portions of the P-type CFCG and CCG images in Figure 4.28 are dissimilar, however.

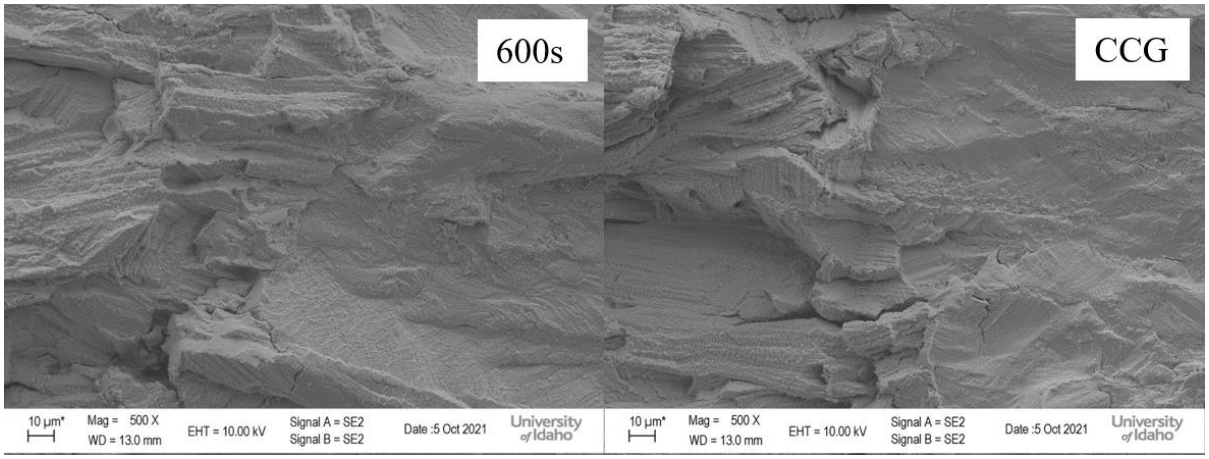

(a) (b)

Figure 4. 28: AM P-type fracture surfaces at initial ΔK = 20 MPa√m, a) P-type 600s hold, b) P-type CCG– K_{max} = 31.5 MPa√m.

In Figure 4.29 the fracture surfaces of the P-type and N-type 600s hold and CCG tests are shown at a ΔK = 40 MPa√m. For the N-type specimens ΔK = 40 MPa√m is near the initial starting conditions shown in Table 4.4, so that is why there was not a comparison with the P-type specimens in Figure 4.28 at a lower ΔK. The fracture surfaces of the P-type and N-type 600s hold and CCG tests in Figure 4.29 are very similar. Both the P-type and N-type fracture surfaces exhibit small linear ridges at differing angles but are mostly horizontal which is parallel to the direction of crack growth. Where the linear ridges are oriented parallel to the direction of crack growth and are observed on both the 600s hold and CCG fracture surfaces, the linear ridges are independent of cycles unlike the striations observed on the fracture surface of the 2 Hz FCG specimen in Figure 4.26(a) and Figure 4.27(a). In Figure 4.29 there is some secondary cracking on all the fracture surfaces and the secondary cracks are also parallel to the direction of crack growth.

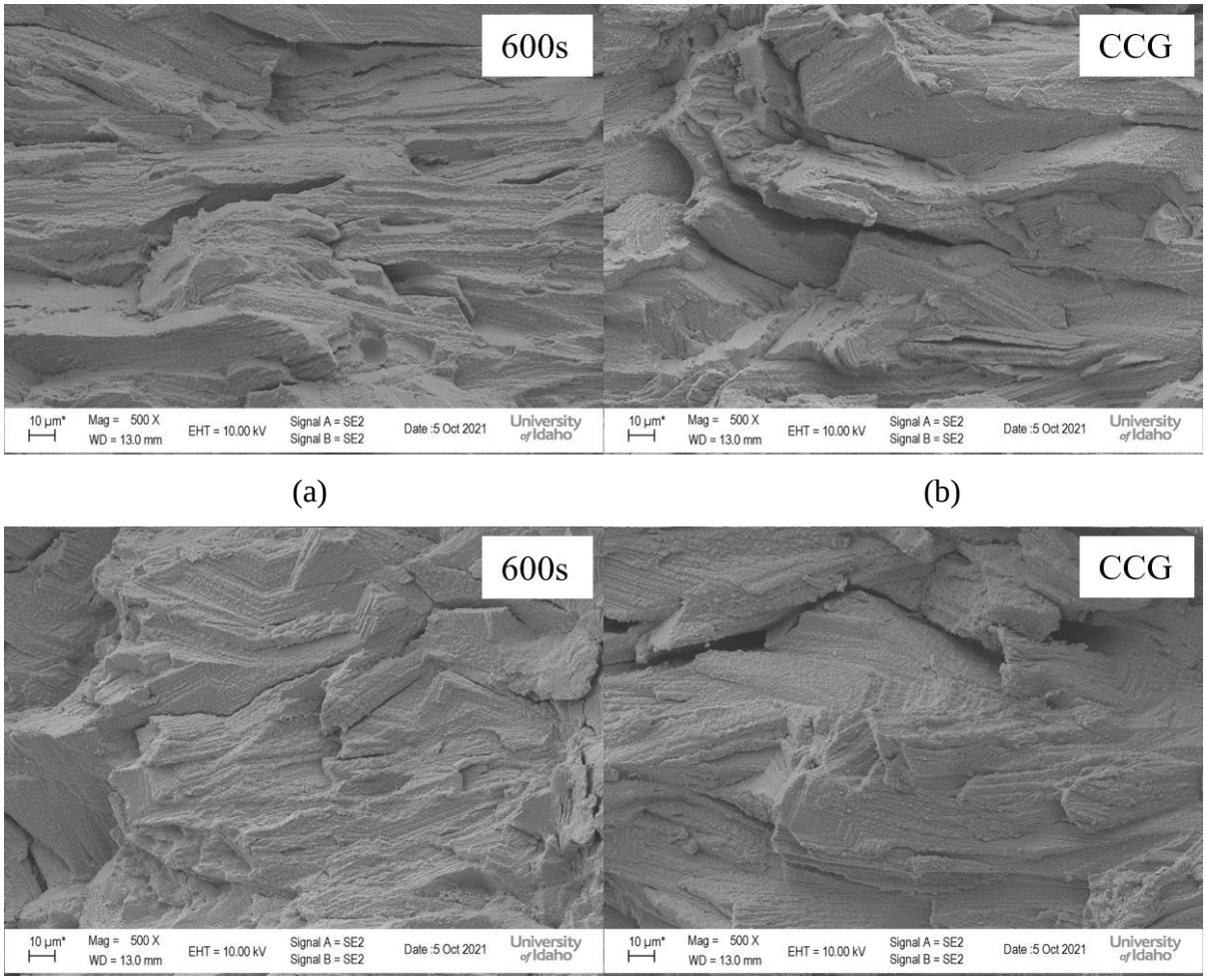

(a) (b)

(c) (d)

Figure 4. 29: AM P-type fracture surfaces at initial ΔK = 40 MPa√m, a) P-type 600s hold, b) P-type CCG– K_{max} = 44.4 MPa√m, c) N-type 600s hold, d) N-type CCG– K_{max} = 44.4 MPa√m.

In Figure 4.30 the fracture surfaces of the P-type and N-type 600s hold and CCG tests look very similar to the fracture surfaces in Figure 4.29 at a lower ΔK. When comparing the fracture surfaces in Figure 4.30 at a ΔK = 60 MPa√m of the P-type and N-type 600s hold and CCG to the H-type 600s hold and CCG in Figure 4.27, the only notable difference is the orientation of linear ridges and secondary cracking. With the P-type and N-type specimens, the linear ridges and secondary cracks are oriented horizontally or parallel to the directions of crack growth and with the H-type specimen the linear ridges and secondary cracks are oriented vertically or perpendicular to the direction of crack growth.

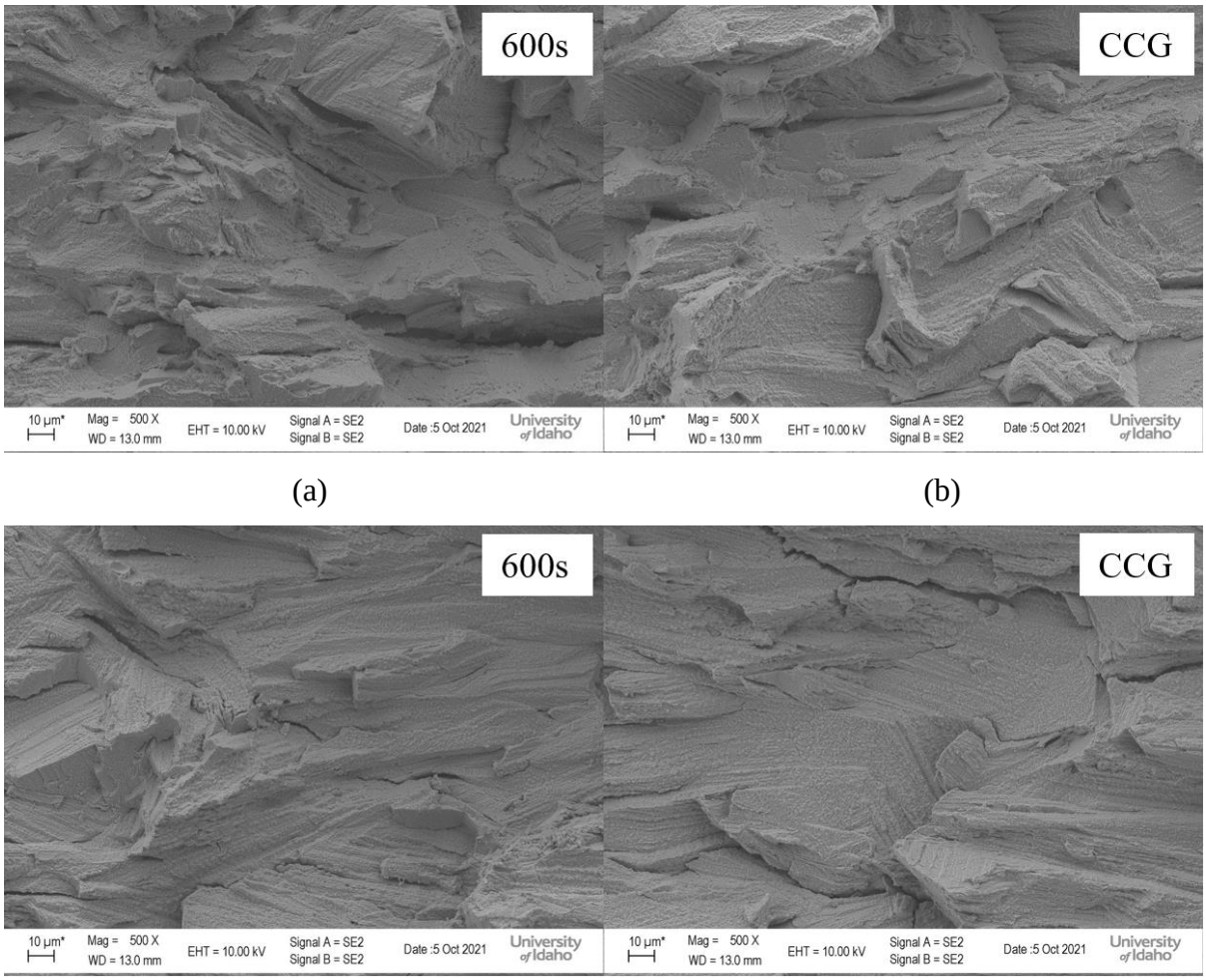

Figure 4. 30: AM P-type fracture surfaces at initial ΔK = 60 MPa√m, a) P-type 600s hold, b) P-type CCG– K_{max} = 66.7 MPa√m, c) N-type 600s hold, d) N-type CCG– K_{max} = 66.7 MPa√m.

The fracture surface observed for all three AM orientations include these linear ridges. It is unclear what the fracture mode is as there is limited literature. The study performed by Deng *et al*. suggested that the mode of fracture was intergranular during CFCG, but fracture surface images were not shown in the Deng *et al*. study so a comparison could not be made. One distinct difference between the three orientations is for both P-type and N-type CFCG and CCG tests the secondary cracks observed are parallel to the direction of crack growth (right to left). This secondary cracking may be some form of delamination or perhaps grain boundary

cavitation. Additional microscopy is suggested which includes EBSD. This technique was not available during this study.

5. CONCLUSIONS, RECOMMENDATIONS, FUTURE WORK

The wrought C(T) specimens showed a noticeable increase in crack growth rate with respect to ΔK for the 60s and 600s hold times compared to the 2 Hz test. When comparing the 60s and 600s hold tests, a 10x increase in hold time resulted in approximately a 10x increase in crack growth rate with respect to ΔK. When comparing the 60s hold, 600s hold, and CCG test as da/dt vs K_{max}, all tests align to form a single scatter band of data. This relationship between CFCG and CCG tests show that for a hold time of 60s to an infinite hold time (CCG), the primary mode of crack growth is independent of number of cycles but dependent on time. This demonstrates that for wrought IN718, K appears sufficient for characterizing creep fatigue crack growth for fixed hold times. Fractographic analysis shows that in the pre-crack region of wrought C(T) specimens the mode of crack growth was transgranular and in the CFCG and CCG regions the primary mode of crack growth was intergranualr. This observation is consistent with the results of Gustafsson *et al.* and Krupp where SAGBO or DE is the casue of intergranular fracture.

Wrought SEN specimens were tested under the same conditions as the C(T) specimens but started at a lower stress intensity range. There was difficulty in initiating crack growth at low ΔK_i = 9 MPa√m so the maximum and minimum loads were increased until a change in DCPD voltage was seen, indicating crack growth. Difficulties at low ΔK = 9 MPa√m regarding crack growth were attributed to ΔK_{th} of IN718 approaching 8-10 MPa√m. Similar to the wrought C(T) specimens, comparing SEN 60s and 600s hold time tests showed a 10x increase in crack growth rate with respect to ΔK. When comparing the 60s and 600s hold tests as da/dt vs K_{max} the tests collapse to form a single scatter band. The SEN CCG test was also plotted as da/dt vs K_{max} and the data fell within the same scatter band as the 60s and 600s hold, but not until a higher ΔK approaching 36 MPa√m. Comparison of the C(T) and SEN specimens showed similar curves for the FCG, CFCG and CCG tests with only a 5-10% difference between the 60s and 600s hold curves. For the SEN specimens, tests were stopped prior to fracture and the specimens were cooled to room temperature and removed from the load frame to observe the

crack profiles under a SEM. The crack profiling showed that the mode of crack growth was intergranular for the 60s, 600s, and CCG tests which was consistent with what was observed on the fracture surfaces of the C(T) specimens.

Comparing the AM FCG and CFCG tests there was a significant increase in crack growth rate with respect to ΔK for the H-type 60s and 600s hold and P-type 600s hold compared to the H-type 2 Hz test. For the 60s and 600s hold tests, a 10x increase in time resulted in approximately a 10x increase in crack growth rate with respect to ΔK for the H-type and P-type specimens. When comparing the three different test orientations, (P-type, H-type, and N-type), the P-type and H-type 600s hold tests showed the most similar crack growth behavior. When plotting the H-type 60s hold, 600s hold, and CCG test and P-type 600s hold and CCG test as da/dt vs K_{max} the tests collapse to form a single scatter band of data apart from the H-type CCG test, which had a 30% lower crack growth rate for a given K_{max}. For the N-type 600s hold and CCG test, the crack grew off plane making the mode I loading assumption invalid so the N-type tests could not be directly compared to the P-type and H-type tests. Although the N-type CFCG and CCG cracks grew off plane, one comparison can be made between the N-type, P-type, and H-type specimens. For both N-type tests, the initial load had to be increased until P_{max} = 12.2 kN corresponding to a K_{max} = 42 MPa√m before crack growth would begin. For the P-type and H-type CCG tests the load also had to be increased to generate crack growth but the maximum load required was only P_{max} = 10.7 kN corresponding to a K_{max} = 31.1 MPa√m. From this, the N-type specimens showed better resistance to crack growth for the same starting K_{max} compared to the P-type and H-type specimens. For CCG tests, the increase in the initial P_{max} necessary to cause crack propagation for all AM orientations is attributed to a lack of grain boundary oxidation and dynamic embrittlement. This statement is consistent with that made by Deng *et al*. In addition, the resistance to CFCG (600s hold) and CCG for the N-type at the initial P_{max} can be attributed to columnar grains oriented near parallel to the loading direction. This resulted in a reduced mode I stress intensity due to off plane crack growth (mode II), thus reducing the driving force at the crack tip.

The wrought and AM 2 Hz FCG tests showed similar fatigue crack growth rates for a given ΔK. The SEN 15 Hz curve was also similar and most likely would have merged with the other curves had the test continued beyond ΔK = 40 MPa√m. Comparing the wrought and AM 60s and 600s hold tests, excluding the AM N-type test, the AM hold tests show steeper slopes

than the wrought hold tests on the da/dN vs ΔK plots. Also, in comparing the 60s and 600s hold tests, the AM tests intersect the wrought tests at a K_{max} = 40 MPa√m. For any given K_{max} < 40 MPa√m, both the P-type and H-type CFCG and CCG test have a lower crack growth rate than the wrought CFCG and CCG tests. Comparison of the force-line displacement difference (ΔV_c) vs. ΔK for AM and wrought 60s and 600s hold tests show that for ΔK values < 35 MPa√m, ΔV_c for the wrought and AM hold time tests are approximately the same. For ΔK greater than 35-40 MPa√m, the AM and wrought data begin to diverge and as ΔK increases, and ΔV_c for the AM specimens becomes significantly greater than ΔV_c for the wrought specimens. The divergence between the wrought and AM data occurs very close to the cross over point in the da/dN vs ΔK plots. Increase in ΔV_c indicates a greater creep contribution to either crack growth or creep damage. As seen with the AM P-type and H-type tests, it is possible that additional creep mechanisms are superimposed on the two proposed mechanisms, (SAGBO and DE), resulting in higher crack growth rates at higher values of ΔK or K_{max}. This is consistent with the AM study by Deng *et al*. suggesting inferior creep resistance (enhanced creep) with the AM P-type orientation. An increase in ΔV_c appears to correspond to an increase in crack growth rate for AM vs. wrought.

In comparison of wrought and AM IN718 fracture surfaces, it is unclear what the exact mode of crack propagation is for the AM specimens. For the wrought specimens it was clear that after the tests began the mode of crack propagation on the CFCG and CCG fracture surfaces was intergranular. For the AM CFCG and CCG surfaces a transition can be seen from the end of the pre-crack region to the beginning of the CFCG and CCG portions of the test but it is unclear what the mode of crack propagation is. The CFCG and CCG fracture surface all three AM orientations did include linear ridges and limited secondary cracking, however. For the AM H-type, the linear ridges and secondary cracks were perpendicular to the direction of crack growth, but on the P-type and N-type fracture surfaces the linear ridges and secondary cracks were parallel to the direction of crack growth.

A more extensive material characterization study regarding the CFCG and CCG behavior of AM IN718 would improve the understanding of failure modes under hold times at elevated temperature. This could include additional testing and microstructure analysis using EBSD, TEM, and specimen sectioning techniques. Where only one test at each hold time was conducted with each specimen geometry in this study, duplicate tests for the three different

specimen orientations would provide additional understanding of the CFCG and CCG characteristics as well as aide in determining test repeatability. TEM analysis could provide insight regarding dislocation behavior and motion at grain boundaries, and specimen sectioning and EBSD would provide additional information regarding crack path and grain/grain boundary interactions as well as any secondary cracking interactions with the main crack and grain/grain boundaries.

6. REFERENCES

1. R. Stephens, A. Fatemi, R. Stephens, and H. Fuchs, Metal Fatigue in Engineering, Second. Wiley-Interscience, 2001.
2. ASTM E647-15e1, Standard Test Method for Measurement of Fatigue Crack Growth Rates, ASTM International, West Conshohocken, PA, 2015, www.astm.org
3. ASTM E647-A.3, Guidelines for Electrical Potential Difference Determination of Crack Size, ASTM International, West Conshohocken, PA, 2015,
4. ASTM E647-X1, Recommended Data Reduction Techniques, ASTM International, West Conshohocken, PA, 2015,
5. U. Krupp, Oxygen-Induced Intergranular Fracture of Nickel-Base Alloys - An Example of Dynamic Embrittlement," University of Pennsylvania, 2009
6. Saxena, A. Creep and creep–fatigue crack growth. *Int J Fract* **191,** 31–51 (2015). https://doi.org/10.1007/s10704-015-9994-4
7. D. Gustafsson, J.J. Moverare, S. Johansson, M. H¨ornqvist, K. Simonsson, S. Sj¨ostr¨om, B. Sharifimajd (2010). Fatigue crack growth behaviour of Inconel 718 with high temperature hold times, Procedia Engineering, Volume 2, pp. 1095-1104.
8. D. Gustafsson, E. Lundstr¨om (2012). High temperature fatigue crack growth behaviour of Inconel 718 under hold time and overload conditions, International Journal of Fatigue, DOI: 10.1016/j.ijfatigue.2012.10.018
9. ASTM Standard F2792, Standard Terminology for Additive Manufacturing Technologies. West Conshohocken, PA.
10. "Introduction to Additive Manufacturing for Propulsion Systems," AIAA Joint Propulsion Conference, July 9-11, 2018. https://ntrs.nasa.gov/archive/nasa/casi.ntrs.nasa.gov/20180006357.pdf
11. Deng, D., Eriksson, R., Peng, R.L. *et al.* On the Dwell-Fatigue Crack Propagation Behavior of a High-Strength Ni-Base Superalloy Manufactured by Selective Laser Melting. *Metall Mater Trans A* **51,** 962–972 (2020). https://doi.org/10.1007/s11661-019-05548-8
12. Hohnbaum, Charles C., "Fracture Toughness and Fatigue Crack Growth Rate Characterization of Inconel 718 Formed by Laser Powder Bed Fusion" (2019). Theses and Dissertations. 2221.
13. ASTM E2760-19e1, Standard Test Method for Creep-Fatigue Crack Growth Testing, ASTM International, West Conshohocken, PA, 2019
14. ASTM E1457-19e1, Standard Test Method for Measurement of Creep Crack Growth Times in Metals, ASTM International, West Conshohocken, PA, 2019
15. AMS5663

7. APPENDICIES

Appendix A. Visual Crack Length Data

A.1 Specimen BB5-CT-4 (2 Hz)

Baseline Test Data: 2 Hz-Triangular Wave Form, 600ºC,						
a (mm)	cycles	Pmax (lbs)	Pmin (lbs)	DP (lbs)	caliper (mm)	time
20	0	2000	200	1800	11.8	10:30
20.5	2400	2000	200	1800	12.3	10:53
21	4700	2000	200	1800	12.8	11:10
21.5	7100	2000	200	1800	13.3	11:32
22	9150	2000	200	1800	13.8	11:48
22.5	12200	2000	200	1800	14.3	12:13
23	13900	2000	200	1800	14.8	12:27
23.5	15800	2000	200	1800	15.3	12:43
24	17500	2000	200	1800	15.8	12:57
24.5	19200	2000	200	1800	16.3	1:11
25	20700	2000	200	1800	16.8	1:23
25.5	21930	2000	200	1800	17.3	1:34
26	23300	2000	200	1800	17.8	1:45
26.5	24450	2000	200	1800	18.3	1:55
27	25700	2000	200	1800	18.8	2:05
27.5	26800	2000	200	1800	19.3	2:14
28	27900	2000	200	1800	19.8	2:23
28.5	28900	2000	200	1800	20.3	2:32
29	29800	2000	200	1800	20.8	2:39
29.5	30725	2000	200	1800	21.3	2:47
30	31550	2000	200	1800	21.8	2:54
30.5	32350	2000	200	1800	22.3	3:00
31	33025	2000	200	1800	22.8	3:06
31.5	33650	2000	200	1800	23.3	3:12
32	34200	2000	200	1800	23.8	3:16
33	35200	2000	200	1800	24.8	3:25
34	36040	2000	200	1800	25.8	3:31
35	36700	2000	200	1800	26.8	3:36
36	37000	2000	200	1800	27.8	3:39

A.2 Specimen BB5-CT-7 (60s hold)

60s hold, 600°C,						
a (mm)	cycles	Pmax (lbs)	Pmin (lbs)	DP (lbs)	caliper (mm)	time
20	0	2000	200	1800	12.8	10:30
20.37	290	2000	200	1800	13.17	3:21
21.43	595	2000	200	1800	14.23	8:27
25.26	1247	2000	200	1800	18.06	7:17
28.84	1577	2000	200	1800	21.64	12:47
29.45	1630	2000	200	1800	22.25	1:41
29.95	1670	2000	200	1800	22.75	2:20
30.4	1697	2000	200	1800	23.2	2:47
30.9	1719	2000	200	1800	23.7	3:12
32.43	1781	2000	200	1800	25.23	4:12
32.95	1797	2000	200	1800	25.75	4:27
33.45	1813	2000	200	1800	26.25	4:43
33.95	1829	2000	200	1800	26.75	4:58
34.45	1838	2000	200	1800	27.25	5:08
34.95	1848	2000	200	1800	27.75	5:19
35.45	1859	2000	200	1800	28.25	5:29
35.95	1867	2000	200	1800	28.75	5:37
	1891					6:02

A.3 Specimen AW1-CT-8 (60s hold)

60sec hold, 600°C,						
a (mm)	cycles	Pmax (lbs)	Pmin (lbs)	DP (lbs)	caliper (mm)	time
20	0	2000	200	1800	11.37	7:20
20.51	209	2000	200	1800	11.88	10:52
20.76	292	2000	200	1800	12.13	12:16
21.41	531	2000	200	1800	12.78	4:16
22.43	754	2000	200	1800	13.8	8:00
25.5	1363	2000	200	1800	16.87	6:08
27.03	1615	2000	200	1800	18.4	10:20

27.56	1694	2000	200	1800	18.93	11:39
28.18	1760	2000	200	1800	19.55	12:45
29.21	1847	2000	200	1800	20.58	2:11
29.51	1902	2000	200	1800	20.94	3:07
30.18	1947	2000	200	1800	21.55	3:51
30.78	1978	2000	200	1800	22.11	4:23
31.03	2010	2000	200	1800	22.4	4:53
31.76	2048	2000	200	1800	23.13	5:33
32.07	2078	2000	200	1800	23.44	6:03
32.91	2130	2000	200	1800	24.28	6:55
33.48	2169	2000	200	1800	24.85	7:34
34.22	2213	2000	200	1800	25.59	8:18
34.26	2247	2000	200	1800	26	8:52
35.13	2275	2000	200	1800	26.5	9:20
35.63	2300	2000	200	1800	27	9:45

A.4 Specimen AD1-CT-4 (600s hold)

60sec hold, 600^{o}C,						
a (mm)	cycles	time	caliper (mm)	Pmax (lbs)	Pmin (lbs)	DP (lbs)
20	0	10:30 AM	12.85	2000	200	1800
22.95	62	8:45 PM	15.8	2000	200	1800
27.35	133	8:33 AM	20.2	2000	200	1800
29.99	163	1:35 PM	22.84	2000	200	1800
32.95	185	5:15	25.8	2000	200	1800
33.45	192	6:25	26.3	2000	200	1800
34.95	200	7:41	27.8	2000	200	1800
35.3	202	8:03	28.15	2000	200	1800
	211	9:03				

A.5 Specimen DD-1 (600s hold)

600s Hold, 600^{o}C,

a (mm)	cycles	Pmax (lbs)	Pmin (lbs)	DP (lbs)	caliper (mm)	time
20	0	2000	200	1800	12.37	9:45
	28	2000	200	1800	12.87	2:22
	45	2000	200	1800	13.45	5:13
	65	2000	200	1800	14.13	8:30
	140	2000	200	1800	17.25	8:57
	164	2000	200	1800	18.75	12:54
	183	2000	200	1800	20.24	4:10
	206	2000	200	1800	22.18	8:03
	229	2000	200	1800	25.58	11:50
	241	2000	200	1800	28.25	1:47
	248					2:56

A.6 Specimen DD-6 (CCG)

Creep Crack Growth Test, 600ºC,						
a (mm)	cycles	Pmax (lbs)	Pmin (lbs)	DP (lbs)	caliper (mm)	time
20	0	2000	N/A	N/A	13.08	9:43
20.5		2000	N/A	N/A	13.58	1:58
20.96		2000	N/A	N/A	14.04	5:16
21.62		2000	N/A	N/A	14.7	9:20
24.58		2000	N/A	N/A	17.66	8:19
25.67		2000	N/A	N/A	18.75	12:30
26.7		2000	N/A	N/A	19.78	2:35
27.27		2000	N/A	N/A	20.35	3:21
27.86		2000	N/A	N/A	20.94	4:47
31.05		2000	N/A	N/A	24.13	8:57
32.4		2000	N/A	N/A	25.48	10:24
33.04		2000	N/A	N/A	26.12	11:03
34.17		2000	N/A	N/A	27.25	11:57
35.25		2000	N/A	N/A	28.32	12:23
40.28						1:33

A.7 Specimen SEN-DD-6 (15 Hz)

15 Hz-Triangular Wave Form, 600°C,						
a (mm)	cycles	time	caliper (mm)	Pmax (lbs)	Pmin (lbs)	DP (lbs)
13	0		7.55	1081	108	973
13.5	58300		8.05	1081	108	973
Went to 500,000 cycles with no crack growth						
Increase load 10 %						
14	0		8.55	1190	119	1071
14	180000		8.55	1190	119	1071
No Crack Growth, Bump load another 10%						
14	0		8.55	1300	130	1170
15	79300		9.55	1300	130	1170
16	108300		10.55	1300	130	1170
17	127900		11.55	1300	130	1170
18	140700		12.55	1300	130	1170
19	147700		13.55	1300	130	1170
	152024		15.16			

A.8 Specimen SEN-BB5-7 (60s hold)

60s hold, 600°C,								
a (mm)	cycles	time	caliper (mm)	DCPD	Pmax (lbs)	Pmin (lbs)	DP (lbs)	Date
13	0	7:26 PM	N/A	0.25	1081	108	973	4/14/2021
13	938	11:00 AM	N/A	0.2509	1082	108	974	4/15/2021
13	1005	12:16 PM	N/A		1083	108	975	4/15/2021
Test was stopped-no crack growth, Begin cycling at 15 Hz								
13	0	12:14 PM	N/A	0.2522	1081	108	973	4/15/2021
13	68196	1:28 PM	N/A	0.2522	1081	108	973	4/15/2021
Test was stopped-no crack growth, 10% increase in load								

13	0	1:30 PM	N/A	0.2522	1188	119	1069	4/15/2021
13	45050	2:20 PM	N/A	0.2522	1188	119	1069	4/15/2021
Test was stopped-no crack growth, 10% increase in load								
13	0	2:26 PM	N/A	0.2529	1300	130	1170	4/15/2021
13	6419	2:31 PM	N/A	0.2555	1300	130	1170	4/15/2021
Starting 60s hold test again								
13	0	2:44 PM	N/A	0.2543	1300	130	1170	4/15/2021
13	182	5:47 PM	N/A	0.2558	1300	130	1170	
13	331	8:16 PM	N/A	0.256	1300	130	1170	
13	1051	8:15 AM	N/A	0.258	1300	130	1170	4/16/2021
13	1393	2:00 PM	N/A	0.258	1300	130	1170	
Test was stopped-no crack growth, Begin cycling at 15 Hz								
12.5	0	2:04 PM	5.45	0.2586	1300	130	1170	4/16/2021
13	66829	3:20 PM	6.5	0.2685	1300	130	1170	
Starting 60s hold test again								
13	0	3:26 PM	6.5	0.2663	1300	130	1170	4/16/2021
N/A	216	7:01 PM	N/A	0.2676	1300	130	1170	
N/A	334	9:00 PM	N/A	0.2683	1300	130	1170	
N/A	817	5:01 AM	N/A	0.2708	1300	130	1170	4/17/2021
N/A	1516	4:40 PM	N/A	0.2753	1300	130	1170	
N/A	1751	8:35 PM	N/A	0.28	1300	130	1170	
N/A	2490	8:54 AM	N/A	0.2907	1300	130	1170	4/18/2021
N/A	3047	6:12 PM	N/A	0.3067	1300	130	1170	

N/A	3153	7:58 PM	N/A	0.3105	1300	130	1170	
N/A	3895	8:19 AM	N/A	0.3572	1300	130	1170	4/19/2021
16.76	4045	10:49	9.59	0.3764	1300	130	1170	
17.67	4202	1:26 PM	10.5	0.4061	1300	130	1170	
18.67	4309	3:14	11.5	0.4399	1300	130	1170	
19.67	4401	4:46	12.5	0.488	1300	130	1170	
20	4414	4:58	12.83	0.4981	1300	130	1170	

A.9 Specimen SEN-AD1-4 (600s hold)

Baseline Test Data: 600s hold, 600°C,								
a (mm)	cycles	time	caliper (mm)	DCPD	Pmax (lbs)	Pmin (lbs)	DP (lbs)	Date
13	0	5:40 PM	N/A	0.2522	1300	130	1170	4/30/2021
13.25	110	12:00 PM	5.76	0.2618	1300	130	1170	5/1/2021
13.47	277	3:46 PM	6.57	0.2707	1300	130	1170	5/2/2021
N/A	424	3:00 PM	N/A	0.2701	1300	130	1170	5/3/2021
N/A	525	9:00 AM	N/A	0.2701	1300	130	1170	5/4/2021
Test was stopped-no crack growth, Begin cycling at 15 Hz								
N/A	0	9:39 AM	6.55	0.2725	1300	130	1170	5/4/2021
N/A	167000	12:43 PM	6.55	0.2726	1300	130	1170	
N/A	184000	1:02	N/A	0.2726	1300	130	1170	
N/A	207000	1:20	N/A	0.275	1300	130	1170	
Starting 600s hold again								
N/A	0	1:26 PM	6.55	0.2745	1500	150	1350	5/4/2021
N/A	140	10:09 AM	7.67	0.3063	1500	150	1350	5/5/2021
15.4	187	6:02 PM	N/A	0.3321	1500	150	1350	

N/A	207	9:21	8.57	0.3478	1500	150	1350	
17.09	236	2:14 AM	10.1	0.3848	1500	150	1350	5/6/2021
N/A	267	2:58 PM	N/A	0.514	1500	150	1350	

A.10 Specimen SEN-DD-6-2 (CCG)

Creep Crack Growth, 600°C,								
a (mm)	cycles	time	caliper (mm)	DCPD	Pmax (lbs)	Pmin (lbs)	DP (lbs)	Date
13	N/A	11:53 AM	5.98	0.231	1400			6/1/2021
		8:09 AM	5.98	0.231	1400			6/2/2021
Cycling at 15 Hz								
13	0			0.2317	1350	135	1215	6/2/2021
				0.2371	1600	160	1440	6/2/2021
				0.2402	1500	150	1350	6/2/2021
	322854			0.244	1500	150	1350	6/2/2021
CCG Test Starting Again								
13	N/A	2:13 PM	N/A	0.242	1500			6/2/2021
13	N/A	4:12		0.2426	1500			6/3/2021
Cycling at 15 Hz								
13.3	0	4:20 PM		0.2447	1550	155	1395	6/3/2021
	49300	8:32		0.2467	1750	175	1575	
	51800	8:35		0.249	1650	165	1485	
	54700	8:38		0.2513	1600	160	1440	
	57700	8:41		0.2535	1550	155	1395	
	59500	8:44	6.26	0.2557	1500	150	1350	
	62600	8:47		0.2584	1400	140	1260	
	66500	8:52	6.46	0.2604	1300	130	1170	
	71000	8:57		0.2624	1200	120	1080	
	82500	9:09	6.77	0.2674	1200	120	1080	
	88278	9:16	6.87	0.27	1200	120	1080	
CCG Test Starting Again								
14	N/A	9:18 PM	6.87	0.2686	1500			6/3/2021
14		8:14 AM	6.87	0.2693	1500			6/4/2021

		9:05 AM	6.87	0.2693	1500			
Cycling at 15 Hz								
14	0	9:08 AM	6.87	0.2705	1300	130	1170	6/4/2021
	10000	9:19	6.87	0.2706	1400	140	1260	
	20000	9:29	6.87	0.2709	1500	150	1350	
	30000	9:40			1600	160	1440	
	50000	10:00			1700	170	1530	
	56800	10:10	7.15	0.2749	1700	170	1530	
	66000	10:22		0.284	1650	165	1485	
CCG Test Starting Again								
14	N/A	10:23 AM	7.15	0.2826	1700			6/4/2021
		11:56	7.3	0.2844	1700			
		7:25 PM	7.3	0.285	1700			6/6/2021
		10:42 AM	7.3	0.2852	1700			
Cycling at 15 Hz								
14	0	10:45 AM	7.3	0.2909	1700	170	1530	6/6/2021
	19200	11:05	7.83	0.2918	1800	180	1620	
	25700	11:13	7.83	0.2975	1800	180	1620	
CCG Test Starting Again								
14	N/A	11:16 AM	8.11	0.297	1800			6/6/2021
16		8:03 AM	8.73	0.3124	1800			6/7/2021
16.5		1:07 PM	9.25	0.3255	1800			
17		3:42	9.75	0.3397	1800			
18.25		8:01	11	0.3944	1800			
19.75		10:43	12.5	0.488	1800			
		10:46		0.4916				

A.11 Specimen TB-VER1-1 (600s hold)

600 sec hold, 600°C,							
a (mm)	cycles	time	caliper (mm)	Pmax (lbs)	Pmin (lbs)	DCPD (mV)	date

20	0	10:07 AM	24.3	2000	200	0.3036	7/13/2021
	39	4:35 PM		2000	200	0.3047	
	143	9:49 AM		2000	200	0.3087	7/14/2021
20.65	288	10:00 AM	24.95	2000	200	0.3163	7/15/2021
20.7	332	5:21 PM	25	2000	200	0.3199	
21.63	436	10:40 AM	25.93	2000	200	0.33	7/16/2021
	464	3:24 PM		2000	200	0.3334	
DCPD shut off during the night							
	574	9:44 AM		2000	200	0.3478	7/17/2021
	631	7:16 PM		2000	200	0.3591	
25.2	723	10:33 AM	29.5	2000	200	0.3854	7/18/2021
	843	8:47 AM		2000	200		7/19/2021

A.12 Specimen TB-VER1-2 (CCG)

CCG, 600°C,							
a (mm)	cycles	time	caliper (mm)	Pmax (lbs)	Pmin (lbs)	DCPD (mV)	date
20	N/A	7:30 AM	25.3	2000	N/A	0.3159	9/8/2021
20	N/A	4:36 PM	25.3	2001	N/A	0.3171	
20	N/A	7:17 AM	25.3	2002	N/A	0.3178	9/9/2021
20	N/A	11:01 AM	25.3	2003	N/A	0.3181	9/10/2021
20	N/A	1:19 PM	25.3	2004	N/A	0.3183	9/11/2021
No crack growth, Cycling 15 Hz							
20	0	1:28 PM	25.3	2000	200	0.332	9/11/2021

22	13501	1:43 PM	27.3	2000	200	0.3532	
Starting CCG at higher load							
22	N/A	1:47 PM	27.3	2400	N/A	0.3507	9/11/2021
23.6	N/A	9:26 AM	28.9	2401	N/A	0.3605	

A.13 Specimen TB-VER2-1 (600s hold)

600 sec hold, 600^{o}C,							
a (mm)	cycles	time	caliper (mm)	Pmax (lbs)	Pmin (lbs)	DCPD (mV)	date
20	0	8:10 AM	24.82	2000	200	0.3051	6/23/2021
20	69	7:38 PM	24.82	2000	200	0.3051	
No crack growth, cycling at 15 Hz							
20	0	7:42 PM	24.82	2000	200	0.3088	6/23/2021
20.7	9502	7:51 PM	25.52	2000	200	0.3168	
600 sec hold again							
20.7	0	8:00 PM	25.52	2000	200	0.3151	6/23/2021
20.7	73	8:08 AM	25.52	2000	200	0.3151	6/24/2021
No crack growth, cycling at 15 Hz							
20.7	0	8:26 AM	25.52	2000	200	0.3183	6/24/2021
	10005	8:36 AM	26.77	2000	200	0.3251	
600 sec hold again							
21.95	0	8:47 AM	26.77	2200	220	0.3232	6/24/2021
21.95	32	2:04 PM	26.77	2200	220	0.3232	
No crack growth, cycling at 15 Hz							
21.95	0		26.77	2000	200	0.327	6/24/2021
22.68	13457	2:23 PM	27.5	2000	200	0.34	

600 sec hold again							
22.68	0	2:33 PM	27.5	2200	220	0.3418	6/24/2021
22.68	21	5:53 PM	27.5	2200	220	0.3376	
No crack growth, cycling at 15 Hz							
22.68	0	6:00 PM	27.5	2000	200	0.3418	6/24/2021
23.93	16882	6:18 PM	28.75	2000	200	0.3635	
600 sec hold again							
23.93	0	6:23 PM	28.75	2300	230	0.3643	6/24/2021
23.93	15	8:59 PM	28.75	2300	230	0.3643	
No crack growth, cycling at 15 Hz							
23.93	0	9:05 PM	28.75	2000	200	0.366	6/24/2021
24.93	9325	9:16 PM	29.75	2000	200	0.378	
600 sec hold again							
24.93	0	9:20 PM	29.75	2500	250	0.376	6/24/2021
24.93	24	1:18 AM	29.75	2500	250	0.3766	6/25/2021
24.93	69		29.75	2500	250	0.3778	
24.93	74	9:30 AM	29.75	2500	250	0.3778	
No crack growth, cycling at 2 Hz							
24.93	0	9:30 AM	29.95	2000	200	0.3804	7/7/2021
25.43	9914	10:51	30.45	2000	200	0.3917	
600 sec hold again							
25.5	0	11:02 AM		2750	275	0.386	7/7/2021
	30	3:54 PM		2750	275	0.3884	
	129	8:27 AM		2750	275	0.3989	7/8/2021
	170	3:14 PM		2750	275	0.405	
	205	9:02		2750	275	0.4106	

	275	8:51 AM		2750	275	0.4267	7/9/2021
	276	8:52 AM		2750	275	0.427	
	325	5:02 PM		2750	275	0.4426	
	424	9:40 AM		2750	275	0.4918	7/10/2021
	449	1:51 PM		2750	275	0.5173	
	469	5:04		2750	275	0.5495	
	481	7:04		2750	275	0.5726	

A.14 Specimen TB-VER2-2 (CCG)

CCG, 600ºC,							
a (mm)	cycles	time	caliper (mm)	Pmax (lbs)	Pmin (lbs)	DCPD (mV)	date
20	N/A	8:52 AM	24.37	2000	N/A	0.3078	9/17/2021
20	N/A	11:03 AM	24.37	2001	N/A	0.307	9/18/2021
20	N/A	10:20 AM	24.37	2002	N/A	0.3061	9/19/2021
20	N/A	8:32 AM	24.37	2003	N/A	0.3052	9/20/2021
No crack growth - Cycle at 15 Hz							
20	0	10:56 AM	24.47	2000	200	0.3085	9/20/2021
21	22100	11:20 AM	25.47	2000	200	0.3277	
22	32400	11:31 AM	26.47	2000	200	0.3407	
23	44300	11:45	27.47	2000	200	0.3595	
24	55700	11:57 AM	28.47	2000	200	0.3814	
25	62000	12:04 PM	29.47	2000	200	0.397	
Starting CCG, Kmax= 40 Mpa(m^.5)							
25	N/A	12:26:00 PM	29.47	2750	N/A	0.3935	9/20/2021
25	N/A	8:14 AM	29.47	2751	N/A	0.3935	9/21/2021
25	N/A	10:21 AM	29.47	2752	N/A	0.3945	9/22/2021
25.19	N/A	7:47 AM	29.66	2753	N/A	0.3984	9/23/251
27.39	N/A	7:01 PM	31.86	2754	N/A	0.4026	
27.77	N/A	8:49	32.24	2755	N/A	0.4153	9/24/2021
29.03	N/A	5:36 PM	33.5	2756	N/A	0.4395	
30.08	N/A	8:49 PM	34.55	2757	N/A	0.4728	

31.33	N/A	11:00 PM	35.8	2758	N/A	0.5571	

A.15 Specimen TB-HOR1-1 (2 Hz)

2 Hz , 600°C,							
a (mm)	cycles	time	caliper (mm)	Pmax (lbs)	Pmin (lbs)	DCPD (mV)	date
20	0	10:35 AM	26	2000	200	0.3196	7/21/2021
20.5	3850	11:07 AM	26.5	2000	200	0.3269	
21	8120	11:42 AM	27	2000	200	0.3365	
21.2	10570	12:03 PM	27.5	2000	200	0.3426	
22	14360	12:34 PM	28	2000	200	0.3524	
22.5	16250	12:50 PM	28.5	2000	200	0.3573	
23	20200	1:23 PM	29	2000	200	0.3682	
23.5	23300	1:48	29.5	2000	200	0.3784	
24	25600	2:07 PM	30	2000	200	0.3861	
25	30300	2:46 PM	0.1	2000	200	0.404	
26	33800	3:15 PM	32	2000	200	0.4196	
27	36950	3:42 PM	33	2000	200	0.4358	
28	40000	4:07	34	2000	200	0.4526	
29	42800	4:30 PM	35	2000	200	0.4759	
30	44470	4:44	36	2000	200	0.491	
31	45900	4:56	37	2000	200	0.5086	
32	47000	5:05 PM	38	2000	200	0.5262	
33	48000	5:14	39	2000	200	0.5474	
34	48820	5:20 PM	40	2000	200	0.57	
	49540	5:27 PM		2000	200	0.601	

A.16 Specimen TB-HOR1-2 (CCG)

CCG, 600°C,							
a (mm)	cycles	time	caliper (mm)	Pmax (lbs)	Pmin (lbs)	DCPD (mV)	date

20	N/A	1:50 PM	26.09	2000	N/A	0.3085	8/16/2021
20	N/A	10:34 AM	26.09	2000	N/A	0.3123	8/17/2021
20	N/A	12:17 PM	26.09	2000	N/A	0.3123	8/18/2021
20	N/A	10:43 AM	26.09	2000	N/A	0.3123	8/20/2021
Stopped Test, no crack growth, cycling at 15 Hz							
20	0	10:39 AM	26.37	2000	200	0.3188	8/20/2021
21	16166	10:56 AM	27.37	2000	200	0.334	
Starting CCG at 2200lb Pmax							
21	N/A	11:03 AM	27.35	2200	N/A	0.331	8/20/2021
21	N/A	9:00 AM	27.35	2200	N/A	0.331	8/22/2021
21	N/A	9:06 AM	27.35	2200	N/A	0.331	8/23/2021
Stopped Test, no crack growth, cycling at 15 Hz							
21	0	9:10	27.35	2000	200	0.3409	8/23/2021
23	19310	9:30 AM	29.35	2000	200	0.3613	
Starting CCG at 2400lb Pmax							
23	N/A	9:34 AM	29.35	2400	N/A	0.3584	8/23/2021
23.26	N/A	9:57 AM	29.61	2401	N/A	0.3608	8/24/2021
23.43	N/A	9:40	29.78	2402	N/A	0.3613	8/25/2021
23.91	N/A	8:53 AM	30.26	2403	N/A	0.3627	8/26/2021
24.89	N/A	6:09 PM	31.24	2404	N/A	0.3671	8/27/2021
25.4	N/A	11:55 AM	319	2405	N/A	0.3694	8/28/2021
26.11	N/A	5:57 AM	32.67	2406	N/A	0.3743	8/29/2021
27.44	N/A	8:52 PM	34	2407	N/A	0.3816	
27.94	N/A	4:43 AM	34.5	2408	N/A	0.3877	8/30/2021

28.41	N/A	10:44 AM	34.97	2409	N/A	0.3955	
29	N/A	3:11 PM	35.56	2410	N/A	0.4036	
30	N/A	9:23 PM	36.56	2411	N/A	0.4176	
31.52	N/A	3:58 AM	38.08	2412	N/A	0.4505	8/31/2021
32.06	N/A	5:55 AM	38.62	2413	N/A	0.4734	
32.64	N/A	6:43	39.2	2414	N/A	0.4856	
33.5	N/A	7:55 AM	40.06	2415	N/A	0.5090	

A.17 Specimen TB-HOR2-1 (60s hold)

60 sec hold, 600ºC,							
a (mm)	cycles	time	caliper (mm)	Pmax (lbs)	Pmin (lbs)	DCPD (mV)	date
20	0	9:55 AM	25.13	2000	200	0.311	7/23/2021
20.37	684	9:18 PM	25.5	2000	200	0.3187	
21.09	1629	1:03 PM	26.22	2000	200	0.3298	7/24/2021
21.73	2148	9:41 PM	26.86	2000	200	0.3377	
22.37	2671	6:25 AM	27.5	2000	200	0.3475	7/25/2021
23.42	3412	6:46 PM	28.55	2000	200	0.3687	
24.43	4022	4:55 AM	29.56	2000	200	0.3916	7/26/2021
25.74	4411	11:25	30.87	2000	200	0.4096	
26.74	4617	2:51 PM	31.87	2000	200	0.424	
27.46	4789	5:43 PM	32.59	2000	200	0.4408	
29	4993	9:07 PM	34.13	2000	200	0.4719	
32.7	5244	1:18 AM	37.83	2000	200	0.5502	7/27/2021

34.5	5283	1:57	39.63	2000	200	0.578	
	5306	2:20 AM				0.6102	

A.18 Specimen TB-HOR2-2 (600s hold)

600 sec hold, 600ºC,							
a (mm)	cycles	time	caliper (mm)	Pmax (lbs)	Pmin (lbs)	DCPD (mV)	date
20	0	9:26 PM	22.75	2000	200	0.3107	7/29/2021
20.07	57	6:54 AM	22.82	2000	200	0.313	7/30/2021
21.12	264	5:21 PM	23.87	2000	200	0.3257	7/31/2021
22.17	380	12:45 PM	24.92	2000	200	0.3359	8/1/2021
22.75	418	7:05 PM	25.5	2000	200	0.3408	
23.9	501	8:47 AM	26.65	2000	200	0.355	8/2/2021
25.05	561	6:54 PM	27.8	2000	200	0.3696	
25.85	598	1:00 AM	28.6	2000	200	0.38	8/3/2021
26.92	631	6:36 AM	29.67	2000	200	0.3934	
27.75	652	10:03 AM	30.5	2000	200	0.405	
29.12	682	3:05 PM	31.87	2000	200	0.4292	
30.9	700	6:00 PM	33.65	2000	200	0.4566	
32.08	707	7:15	34.83	2000	200	0.4762	
33	712	8:02 PM	35.75	2000	200	0.4979	
34	715	8:26	36.75	2000	200	0.5185	
34.5	716	8:37	37.25	2000	200	0.5301	
	717	8:47 PM				0.543	

Appendix B. Load Shedding Procedure

B.1 C(T) specimen load shedding procedure

a_avg (mm)	alpha	Y_avg	ΔP (kN)	ΔP (kips)	Pmax (kips)	Pmin (kips)	ΔK Mpa√m	K_max Mpa√m	K_min Mpa√m
20	0.39	7.17	7.97	1.79	1.99	0.20	20	22.22	2.22
19.5	0.38	6.99	8.39	1.89	2.09	0.21	20.5	22.78	2.28
19	0.37	6.81	8.81	1.98	2.20	0.22	21	23.33	2.33
18.5	0.36	6.64	9.26	2.08	2.31	0.23	21.5	23.89	2.39
18	0.36	6.48	9.72	2.18	2.43	0.24	22	24.44	2.44
17.5	0.35	6.31	10.19	2.29	2.55	0.25	22.5	25.00	2.50
17	0.34	6.16	10.69	2.40	2.67	0.27	23	25.56	2.56
16.5	0.33	6.00	11.20	2.52	2.80	0.28	23.5	26.11	2.61
16	0.32	5.85	11.73	2.64	2.93	0.29	24	26.67	2.67
15.5	0.31	5.70	12.28	2.76	3.07	0.31	24.5	27.22	2.72
15	0.30	5.56	12.86	2.89	3.21	0.32	25	27.78	2.78
14.5	0.29	5.42	13.45	3.02	3.36	0.34	25.5	28.33	2.83
14	0.28	5.28	14.08	3.16	3.52	0.35	26	28.89	2.89
13.5	0.27	5.15	14.73	3.31	3.68	0.37	26.5	29.44	2.94
13	0.26	5.01	15.41	3.46	3.85	0.38	27	30.00	3.00
12.5	0.25	4.88	16.12	3.62	4.03	0.40	27.5	30.56	3.06
12	0.24	4.75	16.86	3.79	4.21	0.42	28	31.11	3.11
11.5	0.23	4.62	17.65	3.97	4.41	0.44	28.5	31.67	3.17
11	0.22	4.49	18.47	4.15	4.61	0.46	29	32.22	3.22
10.5	0.21	4.36	19.33	4.35	4.83	0.48	29.5	32.78	3.28
10	0.20	4.24	20.24	4.55	5.06	0.51	30	33.33	3.33